Strengthening Sequence Based on the Relative Weightage of Members in Global Damage Using Energy Dissipation Model

Thesis submitted in partial fulfilment
of the requirements for the degree of

Doctor of Philosophy in Civil Engineering

by

Niharika
20172094
niharika.talyan@research.iiit.ac.in

International Institute of Information Technology (IIIT) Hyderabad,
Hyderabad – 500032, India.
December 2023

International Institute of Information Technology, Hyderabad, India

CERTIFICATE

It is certified that the work contained in this thesis, titled "**Strengthening** s**equence based on the relative weightage of members in global damage using energy dissipation model**" by Ms. Niharika, has been carried out under my supervision and has not been submitted elsewhere for a degree.

Date

Advisor: Prof. Ramancharla Pradeep Kumar
Professor
Earthquake Engineering Research Centre
International Institute of Information Technology
Hyderabad

Dedicated to Mayank & Aadyanvi

Acknowledgement

This was a very challenging and a satisfying journey for me. I would like to express my sincere gratitude to many individuals who supported me unconditionally and motivated me throughout this journey. I am eternally grateful to my guide Prof. **Pradeep Kumar Ramancharla** for his guidance and encouragement through his words of wisdom at each stage. His willingness to share his experiences and vision has shaped me as a better engineer and as a better person. It has been a privilege to work under him. Without his support and guidance, I would not have been able to complete this thesis.

I would also like to thank my examiners **Dr. Sunitha Palissery**, **Prof. Hemant Kaushik and Prof. Dipti Ranjan Sahoo** for their valuable comments and suggestions. To my friends **Aniket, Neelima, Vyas, Pulkit, Niharika Peddaprolu** and **Bharat** for their willingness to help me, question me and for the long hour debates on the issues I faced.

I am grateful to my **parents** for their constant inspiration and motivation and to my **parents-in-law** for their enduring support throughout this journey. I am thankful to **my** a**unts, brothers, and sisters,** who supported me emotionally throughout this journey. And I would like to express my deepest gratitude to my husband, **Mayank** for his unwavering trust in my abilities and for encouraging me throughout. And a special thanks to my beloved daughter, **Aadyanvi** who joined us during this journey and adjusted to my absence to pursue my dreams, she became my source of energy.

Abstract

Damage caused by an earthquake depends not just on the intensity of an earthquake but on the engineering and construction practices of the region. Past earthquakes in Asian countries have highlighted inadequate construction practices and caused huge property and life loss, indicating the severe need to retrofit existing structures. For this, an understanding and quantification of damage are required to assess the amount of damage. Many researchers have proposed many indices; out of those, energy-based indices are chosen for this study. In literature, energy-based damage indices have progressed well but with a gap in mapping of local-to-global indices though they can be computed at local and global levels. This study bridges the gap between global and local energy-based indices using weighting factors, which further proposes sequence of strengthening. Strengthening activities shall be done first at the higher weighted members to increase the capacity of the building immediately and then to the other members. The proposed strengthening sequence is proposed to make it more economical and efficient.

This study is conducted on existing buildings, mainly on gravity load-designed buildings (Type G) and precode buildings of IS 1893 designed as per the 2002 version (Type P). These buildings represent a significant stock of RCC MRF buildings on site that should be strengthened. The members contributing significant damage are identified in existing buildings, different weights are allotted to members as per their contribution to global energy dissipation. Nonlinear static analysis is conducted to quantify the damage. The methodology adopted to compute the contribution of local damage to the exterior and interior columns is verified with

nonlinear time history analysis with eleven earthquakes. In gravity, load-designed buildings, higher weight for exterior columns is observed in the energy dissipation capacity of the building than interior columns. However, in precode buildings of IS1893, the significance of exterior and interior columns is similar.

Storey-wise weights are computed using energy dissipated by each hinge in that storey. Therefore, the highest weighted stories are identified for each type of building. Damage is distributed within stories as a parabolic curve. In type G buildings, as the height of the building increases, parabolic distribution changes from convex to concave, and the maxima location of the parabola shifts from bottom to middle stories. In type P buildings, parabolic damage distribution remains convex or like a straight line. As the height of the building increases, damage shifts to upper stories in a convex parabolic shape. An increase in the storey height of a building does not change the damage distribution pattern and the quantity of damage.

The sequence for strengthening activities is proposed as per the computed weighting factors. Strengthening activities shall be done first at the higher-weighted members to increase the capacity of the building immediately. Further, a strengthening sequence is proposed as per the weighting factor in descending order for regular RCC buildings. Therefore, proposals made in the study would increase the efficacy of strengthening activities.

…

List of Publications

Journal

- Niharika Talyan, R.K Pradeep (2004), “Strengthening sequence based on relative weightage of members in global damage for gravity load designed buildings”, *Earthquake and Structures,* **26**(2), 131-147.
  DOI: https://doi.org/10.12989/eas.2024.26.2.131
- Niharika Talyan, Pradeep Kumar Ramancharla, “Moment of Inertia as per IS Code Provisions - A Review”, *Structural Engineering Digest (SED)*, July-September 2021, 139-147. https://www.iastructe.co.in/sed.php
- Niharika Talyan, Aniket Bhalkikar and Pradeep Kumar Ramancharla, “Comparison of Building Performance with Partial Retrofitting and Full Retrofitting”, *Structural Engineering Digest (SED)*, July-September 2020, 54-59. https://www.iastructe.co.in/sed.php

Conference

- Niharika T., Pradeep, R.K. (2020). “Performance Assessment of Upper Stories in an Open Ground Storey Building with Retrofitted Ground Storey”, *17th World Conference on Earthquake Engineering*, Sendai, Japan - September 13th to 18th 2020. https://wcee.nicee.org/wcee/article/17WCEE/3g-0010.pdf

- Niharika T., R.K Pradeep (Accepted), “Path-dependent Variation of Earthquake Energy – A Case study on The Himalayan and The Hindu Kush Region Earthquakes Measured at Chandigarh”, *The 18th World Conference on Earthquake Engineering*, Milan – June 30th to July 5th 2024.

Table of Contents

LIST OF FIGURES

LIST OF TABLES

LIST OF SYMBOLS

Symbol	*Description*
c	Damping coefficient
dE	Incremental absorbed hysteretic energy
f_c'	Compressive cylindrical strength
f_{cE}'	Expected cylindrical strength of concrete
k	Tangent stiffness to the system
m	Mass of SDOF system
u	Displacement of SDOF system
$\dot{u}$	Velocity of SDOF system
$\ddot{u}$	Acceleration of SDOF system
u_{max}	Maximum deformation a structural element experienced during an earthquake
u_{equ}	Equivalent deformation capacity of the structural element
u_M	Deformation capacities of the structural elements under monotonic loading
u_C	Deformation capacities of the structural elements under cyclic loading
A_c	Area under the capacity curve
A_g	Cross-sectional area of the specimen
C_p	Control parameter which maps cumulative damage under cyclic loading between limiting damage indices
D	Damage index
D_g	Global damage index
$DI_{EC}(\delta)$	Energy capacity damage index
$DI_{k,element}$	Damage index of the kth element
Ds_k	Storey index of the kth storey
DR_d	Ratio of maximum drift ratio demand under cyclic load
DR_c	Drift ratio capacity
E_h	Hysteretic energy dissipated by an SDOF subjected to an earthquake
$E_{H,diss}$	Hysteretic energy dissipated during ground motion, demand
$E_{H,cap}$ =	Capacity of the structural element for dissipation of hysteretic energy

Symbol	*Description*
E_H	Energy demand
$E_{non-rec,y}$	Non-recoverable energy at yield
$E_{non-rec,collape}$	Non-recoverable energy at collapse under monotonic loading
$F_y =$	Calculated yield strength
I_k	Important factor for the kth story
K_f	Initial flexure member stiffness
K_r	Reduced secant stiffness
$K_{initial}$	Initial slope of the capacity curve before an earthquake
K_{final}	Final slope of the capacity curve after an earthquake
M_y	Yield moment
M_m	Maximum moment
N_{UD}	Axial Load
Q_y	Calculated yield strength
T_a	Initial time period
T_m	Maximum time period
T_f	Time period of the last interval represents a final time period
$T_{plastic}$	Time period of an existing damaged building
$T_{elastic}$	Initial time period before damage by an earthquake computed by an Iranian code
X_i	Maximum displacement in the i^{th} cycle
X_F	Final displacement
δ_y	Yield deformation
δ_u	Ultimate deformation capacity
α	Constant parameters
α_{AE}	Damage coefficients related to the initial elastic time period of the building
α_{VC}	Modification factor
β	Non-negative parameter
β_{AE}	Damage coefficients related to the initial elastic time period of the building

Symbol	***Description***
β_{PA}	Non-negative Park and Ang parameter to include the effect of cyclic loading
β_{SS}	Cumulative damage factor
β_{ws}	Cyclic loading parameter
δ_{AE}	Nonlinear fundamental period elongation
$\delta_{Critical}$	Corresponding elongation period
δ_{f_DC}	Ultimate stiffness degradation
$\delta_{\max}$	Maximum deformation under specific loading
δ_{m}	Maximum deformation under monotonic loading
δ_{M_DC}	Maximum softening index
δ_{M}	Maximum deformation under earthquake
δ_{u}	Ultimate deformation under monotonic loading
δ_{y}	Yielding deformation under monotonic loading
ε	Error in computation
η	Calibration parameter for energy functions
γ	Constant parameters
γ_{VC}	Accounts for the difference between theoretical and real hysteretic energy
λ_{1}	Constant parameters
λ_{2}	Constant parameters
$\lambda_{k,element}$	Weighting factor based on hysteretic energy
μ_{m}	Maximum ductility ratio
μ_{md}	Ratio of maximum deformation
μ_{ud}	Ratio of ultimate deformation to yielding deformation under monotonic loading
μ_{u}	Ultimate ductility ratio
ϕ_{m}	Maximum curvature of the member
ϕ_{y}	Yield curvature of the member
ϕ_{f}	Ultimate curvature of the member

Symbol	*Description*
ρ	Ratio of tension reinforcement at hinge location
$\rho^{'}$	Ratio of compression reinforcement at hinge location
ρ_t	Ratio of area of distributed transverse reinforcement to gross concrete area perpendicular to reinforcement
ρ_w	Ratio of the volume of transverse reinforcement to concrete core volume
θ	Constant
θ_c	Maximum drift ratio in an elastic SDOF
θ_m	Maximum rotation in entire loading history
θ_p	Pre capping plastic deformation capacities
θ_{pc}	Post capping plastic deformation capacities
θ_r	Recoverable rotation on unloading
θ_u	Ultimate rotation capacity

…

1 INTRODUCTION

1.1 Introduction

1.1.1 Performance of buildings during earthquakes

An earthquake is a natural phenomenon that cannot be predicted accurately or avoided. So, the best way to deal with earthquakes is to understand the response of a build-up environment to an earthquake and be prepared for it. However, earthquake is a complex phenomenon, the built-up environment of an area might respond in different ways to two different earthquakes depending upon the source and travel path of seismic waves. Also, different buildings may behave differently in the same earthquake depending upon their configuration, construction practices, and design methodology. Past earthquakes in various parts of the world have taught us how the built-up environment responds.

Significant life and property losses have been observed in many past earthquakes, as in Table 1.1.

Table 1.1: Fatalities in some of the major earthquakes.

Date	Location	Magnitude	Fatalities
15 Jan 1934	Bihar-Nepal	M 8	7253 deaths in India and 3400 in Nepal (Jain, 1998)
21 July 1956	Gujarat	M 6.1	115 deaths and 254 injuries (Kayal, 2008)
10 Dec 1967	Koyna	M 6.5	200 death and 1500 injured (Jain, 1998)
9 February 1971	San Fernando	M 6.5	60 deaths with damage of $500 million (Jennings, 1997)
19 September 1985	Mexico	M 8	10000 deaths (Popov, 1987)
21 August, 1988	Bihar-Nepal	M6.6	282 India and 722 in Nepal (Jain, 1998)
20 June 1990	Iran	M 7.4	35000 deaths (Moinfar and Naderzadeh, 1990)
20 October 1991	Uttarkashi	M 6.8	Fatalities 768 and 5066 injured (Jain, 1998)
30 September 1993	Killari (Latur)	M 6.4	Fatalities 8000 (Jain, 1998)
17 January 1995	Kobe, Japan	M6.9	5,394 deaths (Esper and Tachibana, 1998)
17 August 1999	Turkey	M 7.6	15000 deaths and 27000 injuries

			(Toksoz et al., 1999)
26 January 2001	Gujarat	M 7.7	20005 deaths and 1,66,000 injuries (Roy et al., 2002)
8 October 2005	Kashmir	M 7.6	8000 deaths and 70000 injuries (Rehman et al., 2016)
12 May 2008	Sichuan, China	M 7.9	69227 deaths (Zhao et al., 2009)
25 April 2015	Nepal, India	M 7.8	8200 deaths and 21952 injuries (Murty et al., 2016)
12 May 2015	Nepal, India	M 7.3	135 deaths and more than 2500 injuries (Murty et al., 2016)

These fatalities have been mainly due to ground shaking, movements along faults, landslides, and sliding of houses on weak soil in hilly areas. Damage caused to the built-up environment by only ground shaking due to an earthquake is being studied in this study.

San Fernando (1971) earthquake of M6.6 struck Los Angeles in the northern San Fernando Valley on 9th February. As reported in Caltech (1971) (Caltech, 1971), the intensity was not very high, but this was an important earthquake because it occurred near a densely populated area and caused damage to many important ground facilities of the city. Figure 1.1(a) highlights one such damage caused by the ground shaking in San Fernando (1971) in the New Olive View Hospital building. Huge deformation is seen in columns of an open ground storey above which the shear wall abruptly ended. Those columns were inadequate in transverse reinforcement with large tie spacing, making them nonductile, leading to shear failure. Had the intensity been stronger, there would have been a definite collapse of many buildings in the city since the design procedure did not include adequate transverse reinforcements for the ductility of frames which was later proposed in revised codes.

(a) (b)

Figure 1.1: Damage in New Olive View hospital building and Hanshin Expressway (Caltech, 1971)(Ghosh, 1995)

In 1973 Union Building Code has revised post San Fernando (1971) earthquake for stringent shear design. Similarly, in Japan, revision in the enforcement order of building standard law was made effective in 1981 after Miyagiken Oki (1978) earthquake. That included a two-phase design, one for building serviceability for frequently occurring earthquakes and the other for safety against once-in-lifetime earthquakes. In Kobe (1995) earthquake of magnitude M6.9, massive destruction was observed in old structures based on the codes before 1973 as per Ghosh (1995) (Ghosh, 1995). As shown in Figure 1.1 (b), a typical example was the failure of the Hanshin Expressway constructed in 1962. The Pier bottom failure of the Hanshin Expressway was a typical flexure and shear failure example. One segment of the elevated bridge completely collapsed. The superstructure segment changed from steel to concrete; therefore, a sudden increase in base shear led to the segment failure. Pier failed in shear at the location of the formation of a flexural hinge in the column due to premature discontinuation of longitudinal steel. However, structures based on new code performed better.

Bhuj (2001) earthquake on 26th January of magnitude M7.7 struck the city of Bhuj with an epicenter located 50 km from the Bhuj city in India. Humar et al. (2001) (Humar et al., 2001) earthquake reconnaissance highlighted poor reinforcement detailing and substandard construction practices, including inadequate transverse reinforcement. Figure 1.2(a) highlights a column failure due to flexure hinge formation and buckling of longitudinal reinforcement due to inadequate transverse reinforcement. Figure 1.2(b) highlights the flexure hinge of the column where the cover has been chipped off, exposing the reinforcement. It is visible that hooks are bent at 90° instead of 135°, capable of opening up under severe shaking, making transverse detailing ineffective. Keeping the construction joint in the column just

200-250mm below the column-beam junction is often observed, leading to improper bonds in the hinge region. Earthquake events also highlighted typical pancake failures of open-ground storey buildings, as shown in Figure 1.2(c), where an open-ground storey is crushed, bringing the rest of the floors down.

(a) (b) (c)

Figure 1.2: Column failure in Open ground stories after Bhuj (2001) earthquake (Humar et al., 2001)

(a) (b) (c)

Figure 1.3: Beam Column failures in Sumatra (2004) earthquake (Saatcioglu et al., 2005)

Sumatra (2004) earthquake of magnitude M9.3 triggered a devastating Tsunami with wave heights exceeding 20m destroying Indonesia, Malaysia, Thailand, India, and other countries surrounding the Indian Ocean. Researchers reported that no new lessons were learned from the damage caused by this earthquake's ground shaking (Saatcioglu et al., 2005). Past earthquake damage issues were observed here as well. Figure 1.3(a) highlights the lack of transverse reinforcement in beam-column joint reinforcement. Figure 1.3(b) shows a classic shear failure of the column, and Figure 1.3(c) highlights a failed beam-column connection due to a strong beam weak column. The column got damaged, and the beam remained in an elastic state.

Nepal Twin earthquakes in 2015 on 25^{th} April of M7.5 and on 12^{th} May of M7.3 struck Lamjung and Kodari areas. Though both earthquakes were almost the same magnitude, they caused different levels of damage as per the built environment near their epicenters. Ground shaking due to the long-period waves affected tall buildings more. Similar to past earthquakes, the poor performance of the open ground storey was observed again, as shown in Figure 1.4 (Rai et al., 2016). An open ground storey in Sitapalia, Kathmandu collapsed, as shown in Figure 1.4(a), and a soft storey on the 2^{nd} floor of a four-storey building in Sitapalia, Kathmandu completely collapsed, as shown in Figure 1.4(b). Reconnaissance observations concluded that structures were being built without designing. Some common violated features were huge cantilevers, lack of detailing in beam-column joints, and the practice of having open ground stories.

(a) (b)

Figure 1.4: Soft storey failure in Nepal (2015) Twin earthquakes (Rai et al., 2016)

Past earthquake reconnaissance reports show that damage in a building is dependent on the intensity of an earthquake. However, there have been cases where the intensity was not very severe; still, colossal damage was observed. Therefore, damage caused by an earthquake is dependent not just on the intensity of an earthquake but on the engineering and construction practices of the region as well. In Asian and developing countries, recent earthquakes have demonstrated damage due to the same mistakes reported in the last decade. Therefore, highlighting the fact that no strengthening of existing buildings is being taken up.

Henceforth, indicating the severe need to incorporate the lessons in constructing new buildings and, most importantly, retrofitting the old buildings as per new specifications to avoid any future damage for the same reasons. If lessons learned from past earthquakes are implemented in existing buildings, at least catastrophic failures caused by open ground stories, failure of beam-column joints, and failure of columns in strong beam weak columns can be avoided. A clear understanding of the damage caused in RCC buildings is required to start retrofitting activities on a large scale. If damage concentration and propagation pattern are known or predicted, retrofitting actions can be planned accordingly.

1.1.2 Need for damage indices

Damage quantification and information about damage concentration are required for strengthening and retrofitting activities. Damage can be quantified by assigning a numerical value to the building, known as a damage index. The damage index indicates the amount of damage caused in a building numerically or the amount of capacity left there. Therefore, the amount of repair required in a building can be associated with such indices.

Various researchers have attempted to quantify damage using damage indices. Researchers have defined damage indices on scales where lower limit indicates *no damage* and upper limit indicates *collapse of a building*. Typically it is normalized on a scale of 0-1. Any number in between defines the intermediate amount of damage. Quantitative information about the amount of intermediate damage indicates the capacity left in the building.

Damage can be computed in terms of many parameters, for example, displacement, natural period, stiffness, and energy dissipation. Further advantages and limitations of each parameter based on damage quantification are presented in the next section.

1.2 Literature Review on Damage Indices

The need for damage quantification has prompted many researchers to work on the quantification of damage. The first step is to finalize the parameter for the damage model, which can quantify the damage in a structure. In literature, damage models based on parameters such as displacement, stiffness, natural period, and energy dissipation have been proposed. Empirical or analytical formula based on these damage models, including seismic demand and structure capacity, gives an index called damage index. The damage index varies on a scale of 0-1, where 0 represents *no damage*, 1 represents *collapse*, and intermediate values indicate various damage states.

Some models proposed local damage indices of members, and some proposed global damage indices for the entire building. The objective is to capture actual damage in numbers through the damage index, reflecting locally concentrated and globally distributed damage in a building.

Many damage indices have been proposed in the literature based on the damage parameters mentioned above. Some damage models are based on one damage parameter for damage quantification, and some are based on a combination of two parameters. Different types of damage models present in the literature are reviewed below.

1.2.1 Single Parameter Model

Researchers proposed damage indices based on displacements, energy dissipation, stiffness, or natural period. Models using one physical quantity for damage measurement are called single-parameter models. Damage indices based on the single parameters for damage quantification are:

(i) Displacement-based damage models
(ii) Natural Period-based damage models
(iii) Stiffness-based damage models
(iv) Energy-based damage models

1.2.1.1 Displacement-based damage models

Damage models based on response quantities such as building displacement, inter-story drift, member deformation, or ductility give displacement-based damage indices.

Powell & Allahabadi (1988) (Powell and Allahabadi, 1988) proposed a damage index based on deformation or ductility ratio.

$$DI = \frac{\delta_{\max} - \delta_y}{\delta_u - \delta_y} \qquad \text{or} \qquad DI = \frac{\mu_m - 1}{\mu_u - 1} \tag{1.1}$$

where δ_y is yield deformation, δ_u is maximum deformation capacity, $\delta_{\max}$ is maximum deformation under specific loading. μ_m is the maximum ductility ratio and μ_u is the ultimate ductility ratio.

No experimental calibration is done for the proposed index. This ductility index does not consider the effect of repeated cycles in cyclic loading. Since the structure undergoes massive displacement in inelastic cycles under an earthquake, low-fatigue effects should be considered.

Wang and Shah (1987) (Wang and Shah, 1987) proposed a displacement-based index.

$$D = f(\beta_{ws}) = \frac{e^{n\beta_{ws}} - 1}{e^{n} - 1} \tag{1.2}$$

where β_{ws} is calculated for various values of n, determined from experimental data. For β_{ws} =0; D=0 and β_{ws} =1; D=1. Damage is dependent on maximum displacement during each cycle in which β_{ws} is the cyclic loading parameter and is given by

$$\beta_{ws} = C\sum_{i=1}^{N}\frac{X_i}{X_F} \tag{1.3}$$

where X_i is the maximum displacement in the i^{th} cycle, and X_F is the final displacement under monotonically increasing load, and C is a constant less than 1. A small-scale model of a reinforced concrete beam-column joint is used for experimental validation of the index. From the experiment, recommended values of C and n are 0.1 and 1 for well-reinforced concrete members.

The index considers the cyclic effect of earthquake loading. The value of n, dependent on the amount of reinforcement in the beam and column joint, should ideally change in all cases instead of one constant value. Hence this becomes a limitation for this index.

Bazan and Sasani (2004) (Bazan and Sasani, 2004) proposed a new index based on the drift capacity model, as the ratio of maximum drift ratio demand under cyclic load (DR_d) and drift ratio capacity (DR_c) proposed from the experiments.

$$\hat{D}I = e^{\varepsilon}\left(\frac{DR_d}{\hat{D}R_c}\right) \tag{1.4}$$

ε is the error in computation. Bazan and Sasani experimentally proved that the widely used Park and Ang model, as explained in Section 1.2.2, is biased towards dissipated energy components. Proved that considering β a constant value is incorrect and challenged Park and Ang index. Also, concluded energy may not be a reliable parameter to consider the effect of displacement history on the drift ratio capacity of an RC specimen. Experiments are performed on 159 RC specimens to derive the formula for DR_c for a reinforced concrete element

$$D\hat{R}_c = \theta\rho_w^{\alpha}\eta_o^{\gamma}\left(\lambda_1\frac{a}{d} + \lambda_2\right) \tag{1.5}$$

ρ_w is the ratio of the volume of transverse reinforcement to concrete core volume; $\eta_o = \left(P / A_g\right) f_c^{'}$ where P is applied axial load and A_g is the cross-sectional area of the specimen; $\alpha, \gamma, \lambda_1, \lambda_2$ are parameters; θ is equal to 1 for cantilever; *a/d* = aspect ratio.

The damage index considers the effect of cyclic loading, and the index proposed is derived from regression analysis of 159 RC specimens. Also, the index is proposed for an element, and its applicability to the entire building is yet to be worked upon.

Observations from Displacement-based damage indices

Some indices are non-cumulative based on maximum deformation demand, which may not work well in long-duration earthquakes. Since displacement history affects final damage, it should be considered for exact damage calculation. Though non-cumulative indices are crude and quick to get information about the amount of damage, they are not exact. Therefore, researchers tried incorporating the effect of cyclic loading by introducing relevant parameters. However, displacement-based indices cannot capture actual strength and stiffness degradation due to cyclic loading.

Also, some indices gave global damage and some local element level damage, but an accurate picture of the damage is highlighted when both are reflected in the index.

1.2.1.2 *Natural Period-based Models*

Experiments by Newmark et al. (1974) indicated that the natural frequency of a structure decreases with severe damage (Newmark and Rosenblueth, 1974). Hence, change in the structure's fundamental properties, such as natural frequency or natural period, can be used as key parameters to calculate damage. Some damage indices proposed based on the natural period are reviewed below.

DiPasquale and Cakmak (1987) (DiPasquale and Cakmak, 1987) proposed a natural period-based index that measures damage in terms of change in the fundamental period of a building caused by seismic activity. This takes into account the combined effect of stiffness degradation and plastic rotation.

$$\delta_{f\_DC} = \frac{T_f - T_a}{T_a} \tag{1.6}$$

$$\delta_{M\_DC} = 1 - \frac{T_a}{T_m} \tag{1.7}$$

The entire strong motion duration is divided into small intervals, and a time period is found for each. The time period of the first interval represents an initial time period T_a, and the time period of the last interval represents a final time period T_f and maximum time period T_m. δ_{f_DC} is the ultimate stiffness degradation, δ_{M_DC} is the maximum softening index. Six buildings experiencing the San Fernando (1971) earthquake are used to validate this index. The damage index consistently increases with the severity of the damage observed. Maximum softening and cumulative softening represent two aspects of damage. Therefore, the damage is a function of cumulative and maximum softening both.

Experimental validation with a more extensive database is needed to bring it to practical use. The stiffness degradation index is impractical to compute since digitized records are not long enough, and measuring the time period post-earthquake using instruments is not a viable solution. Ultimate stiffness degradation does not include the signature of a ground motion since it depends on only the initial and final time period values. The maximum softening index yields a value between 0-1 and includes the signature of the ground motion in the damage index. However, these damage indices could not provide information about the local damage in the elements and only provide global damage.

Ali Massumi and Ehsan Moshtagh (2013) (Massumi and Moshtagh, 2013) Correlation between Park and Ang damage Index (Park and Ang, 1985) and period elongation is shown in this paper. Effects of infill panels and distribution of damage (plastic hinges and cracks) are encompassed within DI with the addition of fundamental period elongation to the Park and Ang damage index. The correlation found encourage precise and quick assessment of existing structures by new damage pattern even when no original modal information is available. By computing $T_{plastic}$ from a field test, it can be predicted whether a structure is recoverable and what the damage is. As mentioned below, a new damage index of an RC frame building without a shear wall is proposed.

$$DI = \frac{1}{\alpha - \beta\delta_{AE}^{0.5}} \tag{1.8}$$

α, β are damage coefficients related to the initial elastic time period of the building. δ_{AE} is the nonlinear fundamental period elongation calculated from the expression as mentioned below. From the regression analysis, correlation curves between damage coefficients α, β and nonlinear fundamental period elongation δ are developed.

$$\delta = \frac{\left(T_{plastic} - T_{elastic}\right)}{T_{elastic}} \tag{1.9}$$

$T_{plastic}$ is the time period of an existing damaged building obtained by field tests experimentally; $T_{elastic}$ is the initial time period before damage by an earthquake calculated by an empirical formula given in the Iranian Code.

$$T_{elastic} = 0.07H^{(\frac{3}{4})} \tag{1.10}$$

Where H is the height of RC frames in meters. Numerical models are validated by matching experimental and numerical hysteretic curves. Once softening is observed building is irreparable, and the corresponding elongation period is called $\delta_{Critical}$. Modified damage index in terms of $\delta_{Critical}$ is

$$DI = \frac{1}{\beta(\delta_{Critical}^{0.5} - \delta^{0.5})} \tag{1.11}$$

When there is no available modal information of the original structure, DI can be calculated by computing $T_{plastic}$ from a field test. However, the index indicates only two damage states repairable and non-repairable.

Even though the building is marked irreparable, many elements will still have loading capacity remaining due to non-uniform cracks and damage distribution in the building. Some members contributing to global stability might have been damaged, indicating global instability. Though the index correctly indicates global damage but fails to highlight damage distribution at the element level. Also, values of damage coefficients α , β are limited to similar frame structures as presented in the paper, which becomes a limitation to the broad applicability of this index.

Observations from Natural Period-based indices

Natural period-based damage indices give global damage information of the structure, which incorporates the effects of cyclic loading and subsequent strength degradation. However, no local concentration of damage can be located from such indices. Calculating the change in the structure's natural period is time taking and difficult to analyze and hence becomes a significant drawback of this concept for practical purposes.

1.2.1.3 *Stiffness-based damage Models*

Dowell (1979) concluded that local stiffness degradation causes natural frequency or natural period change and hence characterizes structural damage (Dowell, 1979). Therefore, another way to capture global structural damage is by measuring the degradation of stiffness.

Banon et al. (1980) (Banon et al., 1980) proposed a flexural damage ratio (FDR) as a ratio of the initial flexural stiffness of the member to its reduced secant stiffness to measure the stiffness degradation of a member. Experimental studies done by the author to compare various damage parameters proved that FDR and energy dissipation models give better results than member ductility models, as ductility models give experimentally lesser damage values than numerical analysis. Only qualitative damage is reliable in the case of ductility parameters. Therefore, FDR proved a better option for damage calculation.

$$FDR = \frac{K_f}{K_r} \tag{1.12}$$

where K_f is initial flexure member stiffness, and K_r is reduced secant stiffness.

A better damage indicator than ductility and stiffness is calculated from the ratio of force to deformation. Therefore, it provides information about deformation and strength both in one parameter. The damage index gives member damage. However, no damage information of a building globally can be computed from this index.

Roufaiel and Meyer (1987) (Roufaiel and Meyer, 1987) proposed a modified flexural damage ratio MFDR as a member damage index.

$$MFDR = \max\left[MFDR^+; MFDR^-\right] \tag{1.13}$$

$$MFDR^+ = \frac{\frac{\phi_x^+}{M_x^+} - \frac{\phi_y^+}{M_y^+}}{\frac{\phi_m^+}{M_m^+} - \frac{\phi_y^+}{M_y^+}}; \qquad MFDR^- = \frac{\frac{\phi_x^-}{M_x^-} - \frac{\phi_y^-}{M_y^-}}{\frac{\phi_m^-}{M_m^-} - \frac{\phi_y^-}{M_y^-}} \tag{1.14}$$

M_m / ϕ_m represents secant stiffness at the onset of failure, M_y / ϕ_y represents initial elastic stiffness. When the yield moment of a member is not reached, MFDR=0, and when failure curvature is reached, MFDR=1. Damage estimation is done as per the first mode of deformation. Also, only the flexure mode of failure is considered.

Experimental validation was done with Healey and Sozen's (1978) test results for a ten-storey frame on a shake table for three ground motions.

MFDR is a local damage index, though the author also proposes the global damage index based on displacement. Based on stiffness, no global parameter is proposed. Validation is done on only one type of building; therefore, the general applicability of the index cannot be confirmed. Only the flexure mode of failure is captured, and the damage is calculated as per that.

Ghobarah et al. (1999) (Ghobarah et al., 1999) The author proposed a change in the global stiffness-based index, calculated by pushover analysis before and after an earthquake. The damage to each story, as well as the structure as a whole, can be computed from this index. $K_{initial}$ is the initial slope of the capacity curve before the earthquake and K_{final} is the initial slope of the capacity curve after an earthquake.

$$(DI)_K = 1 - \left(\frac{K_{final}}{K_{initial}} \right) \tag{1.15}$$

Similarly, it can be calculated for each storey. The storey damage index indicates which storey contributes to the damage. This index provides information on the failure sequence of elements. Therefore, a storey and global index are achieved without any weighting factor. Also, the damage index can be calculated at any loading level. This method also considers shear deformation failure.

The author has proposed a global damage index based on stiffness. Therefore, stiffness degradation is considered due to the cyclic effect. However, the calculation of this index includes much computation, each storey damage index analysis separately and a global analysis for the global index. Also, member-level damage concentration can not be predicted from this index.

Observation from Stiffness-based indices

Stiffness is considered a better damage parameter than displacement or ductility as it considers stiffness and strength deterioration in damaged members. Also, experimental and numerical models give better correlations in stiffness-based models than in ductility-based models. Compared with natural period-based indices, stiffness-based indices are easy to compute analytically. Stiffness-based models have proposed both local and global damage indices. However, it does not capture the difference between the buildings damaged by short duration and a long-duration earthquake where the final stiffness may be the same but still damage caused may be different.

1.2.1.4 Energy-based Models

The concept of energy was first proposed by Housner (1956) (Housner, 1956) at the first world conference of earthquake engineering. He proposed that the effect of ground motion on a structure depends upon the structure's capacity to dissipate or absorb energy. Within elastic limits, energy absorbed is the strain energy. As the structure exceeds its elastic stress limits in higher PGA, additional energy dissipation is through hysteretic energy because of cracking and permanent deformation. Therefore, hysteretic energy can be one more parameter for damage quantification. This theoretical concept of Housner was formulated for a building by Akiyama (1985) (Akiyama, 1985) in the book "Earthquake resistant limit state design of buildings". Further, Uang et al. (1988) (Uang and Bertero, 1988) derived energy balance equations.

Deger and Sutcu (2016) presented the distribution of earthquake input energy into different floors and structural members (Deger and Sutcu, 2017). To measure the damage potential of a building, the distribution of energy into various components, i.e., kinetic, elastic strain, hysteretic and structural damping, is observed. A four-story RCC building was tested on an E-defence shake table in Miki, Japan, and was calibrated with a numerical model in Perform 3D. It was found that the energy distribution on each floor is independent of ground motion intensity. Energy is distributed maximum on the first-floor column and then on the first-floor and second-floor beams. An increase in duration and ground motion intensity increases hysteretic energy and damage.

UCAR and Merter (2018) proposed a relationship between hysteretic energy and input energy from earthquake ground motion based on a study conducted on ground motions from 7 accelerograms (UÇAR and MERTER, 2018). Nonlinear time history analysis presents the energy distribution over the entire earthquake ground motion duration, and the ratio of hysteretic and input energy is constant. Then the result of this study was compared with already existing ratios in literature given by researchers Akiyama (1985), Fajfar & Vidic (1994), Manfredi (2001), and Khashaee (2004). However, they have already been proven over-conservative. Ratios given by the above-mentioned researchers are expressed as a function of viscous damping ratio, ductility, and hysteretic model and are not dependent on earthquake ground motion characteristics.

Akiyama and Kato (1980) proposed that damage distribution is related to the hysteretic/absorbed energy distribution in the structure (Akiyama and Kato, 1980). Therefore, hysteretic energy absorbed or dissipated is the damage potential of a structure. Using hysteretic energy dissipation as a measurable quantity for damage indexing and calculating all components of energies using energy equations, various researchers have proposed damage indices.

Anthugari and Ramancharla (2014) proposed three global energy-based models for the damage assessment of buildings (Vimala and Kumar, 2014). Damage indices from all three energy models are calculated for three types of buildings varying in height and plan. The third damage index, as presented below, is found to be in good agreement with the literature by Powell and Allahabadi (1988), Roufaiel and Meyer (1987), and Poljansek and Fajfar (2008). The computation of energy parameters is highlighted in Figure 1.5.

$$DI = \frac{(E_L - E_{NL})}{(E_{LT} - E_{NLT})} \times 100 \qquad (1.16)$$

The proposed index is a global damage index; it gives reasonable value and presents a gradual rise from no damage to slight to moderate and severe damage. This index cannot provide information about how much each member contributes to global stability since local damage information cannot be computed from this index. Models proposed do not consider damaging effects due to cyclic loading of an earthquake ground motion. They are based on monotonic loading to reduce computation efforts.

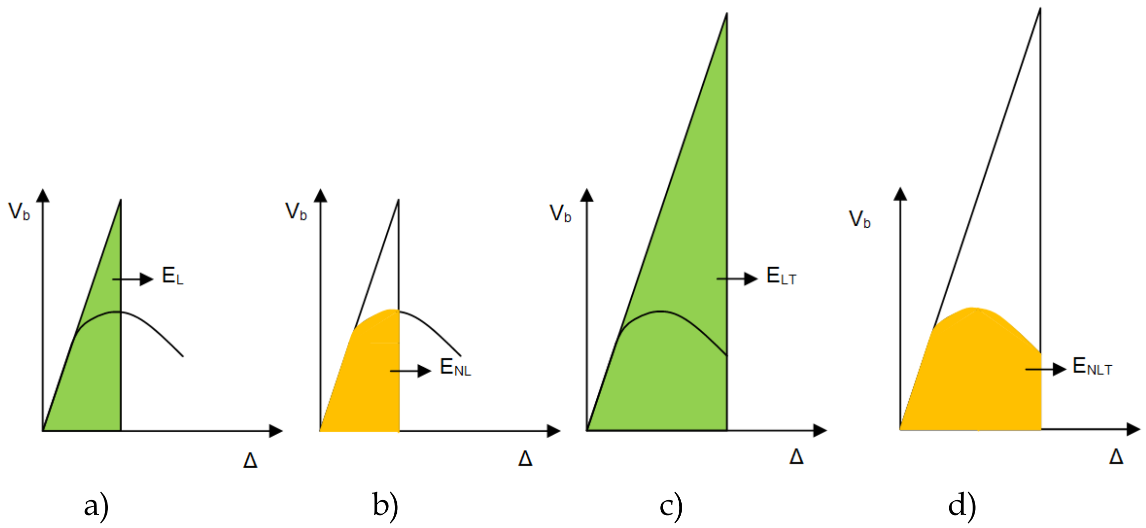

Figure 1.5: Parameters for global damage estimation based on the energy model (Reproduced) (Vimala and Kumar, 2014)

Van Cao et al. (2014) (Cao et al., 2014) proposed two energy-based damage indices, one for monotonic and the other for cyclic loading. Damage index for monotonic loading where $E_{non-rec,y}$ and $E_{non-rec,collape}$ are non-recoverable energy at yield and collapse under monotonic loading. $DI_{k,element}$ is the damage index of the kth element and $\lambda_{k,element}$ is the weighting factor based on hysteretic energy

$$DI = \left[\frac{E_{non-rec}}{E_{non-rec} + E_{rec}} \right]^{(N-i)} \tag{1.17}$$

$$DI_{structure} = \sum_{k=1}^{n} \left(\lambda_{k,element} . DI_{k,element} \right) \tag{1.18}$$

$$\lambda_{k,element} = \left[\frac{E_{non-rec,k}}{\sum E_{non-rec,k}} \right]_{element} \tag{1.19}$$

$$N = \frac{E_{non-rec,collapse}}{E_{non-rec,y}} \tag{1.20}$$

$$i = \frac{E_{non-rec}}{E_{non-rec,y}} \tag{1.21}$$

Damage index for cyclic loading

$$DI = \left[\frac{E_h}{E_h + E_{rec}} \right]^{\alpha_{VC}(N-i)} \tag{1.22}$$

$$N = \frac{E_{h,collapse}}{E_{h,1y}} = \frac{\gamma_{VC} E_{h,1collapse}}{E_{h,1y}} \tag{1.23}$$

$$i = \frac{E_h}{E_{h,1y}} \tag{1.24}$$

where α_{VC} is the modification factor describing the effect of the number of cycles. γ_{VC} accounts for the difference between theoretical and real hysteretic energy. The index for the static load on a beam/column is calibrated with Kunnath et al. (1992). The damage index for cyclic loading is validated by Park et al. (1985) damage index. The index agrees with Park and Ang at a specific α_{VC} = 0.06 value.

The energy-based index proposed is in good agreement with the literature. Though global energy dissipation in a building is well indicated in the damage index, the index does not provide element-level damage distribution information to highlight specific damaged areas.

Diaz et. al (2017) proposed an energy-based damage index for steel structures with two energy functions: Strain energy function E_{so} and energy dissipation by hysteretic function E_D (Diaz et al., 2017).

$$DI_{EC}(\delta) = \eta E_{so}(\delta) + (1-\eta)E_D(\delta) \cong DI_{PAw}(\delta) \qquad (1.25)$$

The area under the secant stiffness to the ultimate capacity point gives strain energy

$$E_{so} = \frac{(D_{ci} \times F_{ci})}{2} \qquad (1.26)$$

The area of a complete parallelogram of hysteresis depicts energy dissipated by the structure in one hysteresis cycle.

$$E_D = 4(F_y \times D_{bi} - D_y \times F_{bi}) \qquad (1.27)$$

$$F_y = K_i \times D_y \qquad (1.28)$$

$$D_y = \frac{2A_c - (F_{ci} \times D_{ci})}{(k_i \times D_{ci}) - F_{ci}} \qquad (1.29)$$

where, $DI_{EC}(\delta)$ = Energy capacity damage index; A_c is the area under the capacity curve; η = calibration parameter for both energy functions. In the energy capacity damage index, η the value should change with different types of building frames. Earthquakes with different frequency content and duration also affect the value η. The paper suggests a value of η between 0.6-0.7, a lower side for long-duration earthquakes and a higher side for near-fault short accelerograms. No experimental calibration was done for the index. However, the energy capacity damage index is validated with Park and Ang index at the element level, and globally both gave a good correlation.

Though the damage index is validated with Park and Ang index, it does not improve the current status of quantitative damage assessment. Till η is tabulated for all variations; the index cannot be used, although this energy index provides a quick and easy way to calculate damage. Until now, the usage of displacement and energy functions together was more reliable. However, this paper converts the displacement function into an energy function, making it an equivalent pure energy-based damage index, which can be easily computed with Nonlinear static analysis.

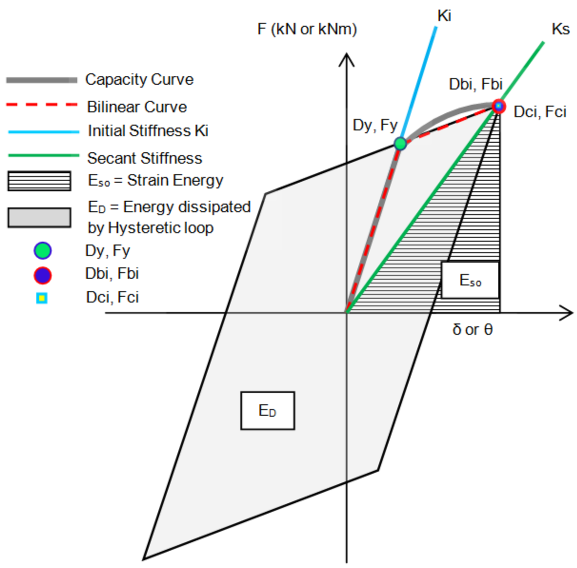

Figure 1.6: Capacity, force deformation, and hysteretic energy dissipation curve (Reproduced) (Diaz et al., 2017)

Shima Mahboubi (2019) proposed an energy-based damage index for bridge pier as a ratio of hysteretic energy and earthquake input energy (Mahboubi and Shiravand, 2019). The input energy is distributed into the structure as kinetic, strain, damping, and hysteretic energy. The author calculated hysteretic energy as the difference between earthquake input energy and other components. Since hysteretic energy calculated on the basis of energy loops may not consider the cumulative effects of pinching, stiffness degradation, inelastic deformation, low cycle fatigue, and material non-linearities. Energies are calculated from the direct integration method for a single degree of freedom system presented below.

$$DI = \frac{E_h}{E_i} = 1 - \frac{E_k + E_d + E_s}{E_i} \tag{1.30}$$

Hysteretic Energy $$E_h = E_i - E_k - E_d - E_s \tag{1.31}$$

Kinetic Energy $$E_k = \int_0^u m\ddot{u}du == \int_0^t m\ddot{u}\dot{u}dt = \frac{1}{2}m\dot{u}^2 \tag{1.32}$$

Damping Energy $$E_d = \int_0^t c\dot{u}^2 dt \tag{1.33}$$

Strain Energy $$E_s = \int_0^u k_t u du \tag{1.34}$$

Input Energy $$E_i = -\int_0^u m\ddot{u}_g du \tag{1.35}$$

where m=mass of SDOF system; u=displacement; $\dot{u}$ and $\ddot{u}$ are velocity and acceleration of SDOF system; c=damping coefficient; k=tangent stiffness to the system. The proposed damage index was compared with some well-established damage indices of literature. It performed better than all when mapped with the experiment on RC specimens with five different types of cyclic loading. The proposed index gave better results than Park and Ang in one of the experiments. The damage index proposed is easy to calculate and experimentally validated for a column member.

Maeda and Kang (2009) (Maeda and Kang, 2009) presented the fundamental idea of the Guideline for Post-Earthquake Damage Assessment of RC Buildings in Japan. The study presents a comprehensive approach to evaluate the damage to reinforced concrete buildings in the aftermath of earthquakes. The authors proposed a procedure for damage rating based on a residual capacity index (R), known as residual capacity to original capacity. The procedure was applied on low-rise buildings in Kobe 1995 earthquake, and its effectiveness and validity were discussed. The remaining seismic strength can be computed using the R index. Point A is the point of maximum response, and point B is the point during an earthquake ground motion on unloading. After unloading, η is computed as the remaining energy dissipation capacity ratio to the original capacity.

Damage levels computed for 150 school buildings were similar to the investigators' mentioned damage levels. It can be inferred that the Damage Evaluation Guideline may provide a conservative, however safe, estimation of the remaining seismic capacity for an earthquake-damaged RC building structure. Therefore, the reported damage levels of RC buildings in Kobe (1995) strong earthquakes were in good agreement with the residual capacity index.

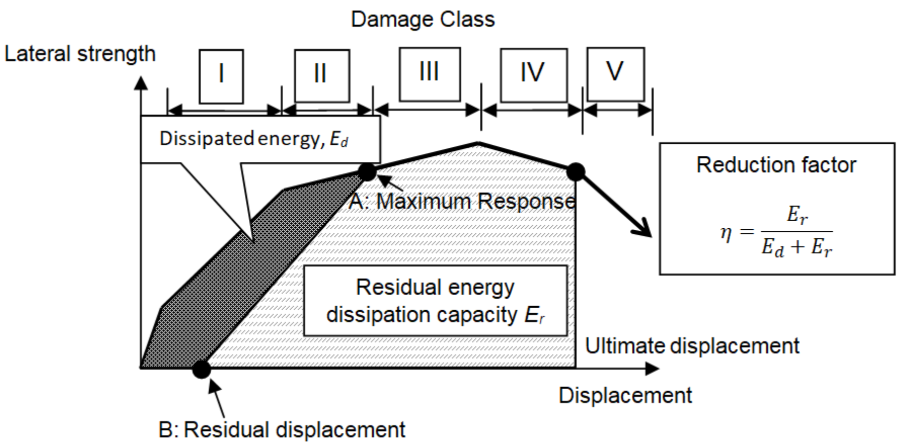

Figure 1.7: Computation of residual capacity index (Reproduced)

Observations from Energy-based indices

Another way of calculating damage is by calculating energy, which considers information of both displacement and force since energy is calculated from the area under the pushover curve or hysteresis curve depending upon the type of loading considered. The advantage of the energy parameter over the natural period is that it can be calculated at member and global levels both. Various indices have been proposed for both types of loading. Some indices incorporate damage accumulation due to cyclic effects in the energy-based method by the area under the hysteresis curve for more accuracy. However, it becomes a time taking procedure to calculate energy dissipated at every hinge location. Few authors proposed a crude and quick way to calculate energy dissipated by taking a monotonic load only. The concept of pushover capacity has been validated with the damaged buildings in real earthquakes in Japan and was concluded as a conservative but safe approach.

1.2.2 Two Parameter Model

Deformation and energy are the two most important parameters for calculating damage locally and globally. Therefore, damage models combing both parameters too were proposed in the literature.

Deformation and Energy Combined Model

Park and Ang (1985) – Authors proposed an element-level damage model comprising two components based on structural deformation and absorbed hysteretic energy (Park and Ang, 1985). Therefore, the damage index proposed is a linear function of maximum deformation and the effect of cyclic loading. Damage is represented on a scale of 0-5, with D≥1 representing total collapse.

$$D = \frac{\delta_M}{\delta_u} + \frac{\beta_{PA}}{Q_y \delta_u} \int dE \tag{1.36}$$

where, δ_M = maximum deformation under earthquake; Q_y = calculated yield strength; dE = incremental absorbed hysteretic energy; β_{PA} = non-negative parameter; δ_u = ultimate deformation under monotonic loading. This index is proposed for cyclic loading considering cumulative damage in terms of hysteretic energy, although maximum deformation is computed from monotonic loading. β_{PA} factor represented the effect of cyclic loading. The factor depended upon the shear span ratio, axial stresses, and total longitudinal and confining reinforcement. It was computed experimentally from regression analysis of a large set of 261 samples of beams and columns where failure could be located. Parameters δ_u, Q_y were also computed experimentally. The damage index was found to be log normally distributed.

Weighting factor: The author also proposed an index for a single storey and overall structure by combining element-level indices with a storey level and global index using weighting factors. The weighting factor is based on the amount of hysteretic energy dissipated by each element.

$$DI_{storey} = \sum_{i=1}^{n} \left(\lambda_{i,component} . DI_{i,component} \right) \tag{1.37}$$

$$\lambda_{i,component} = \left[\frac{E_i}{\sum_{i=1}^{n} E_i} \right]_{component} \tag{1.38}$$

$$DI_{overall} = \sum_{i=1}^{n} \left\{ \lambda_{i,storey} . DI_{i,storey} \right\} \tag{1.39}$$

$$\lambda_{i,storey} = \left[\frac{E_i}{\sum_{i=1}^{n} E_i} \right]_{storey} \tag{1.40}$$

Though it has many limitations, it is one of the most widely used indexes because of the experimental validation of well-calibrated damage states and damage index. The index gives damage value even in the elastic range where hysteretic energy dissipated is zero because of the deformation ratio though it may not be the actual damage. The upper limit of the index is more than 1, therefore, it does not satisfy the basic criteria of a damage index lying between 0-1. The methodology to determine the value of β_{PA} factor for different types of buildings is not well defined. Hence, determining β_{PA} value is one of the limitations of this damage index. The recommended value is 0.1, but it should not be constant. A combination of deformation and hysteretic energy is a nonlinear problem, but a linear combination is assumed in this index. The index has a non-normalization issue, i.e., DI>1, even when a structure is monotonically loaded since the structure dissipates some plastic energy under monotonic loading. Ideally, it should be one from the deformation component and zero from the energy component, which captures cumulative damage.

Further, many researchers worked on the same index and gave modified versions of the Park and Ang index, removing some limitations.

Kunnath et al. (1992) (Kunnath et al., 1992) proposed modifying the Park and Ang damage index by introducing moment rotation in place of the deformation ratio and ignoring the elastic recoverable part from the first term.

$$DI = \frac{\theta_m - \theta_r}{\theta_u - \theta_r} + \beta_{PA}\frac{E_h}{M_y \theta_u} \quad (1.41)$$

θ_m is maximum rotation in entire loading history; θ_u is ultimate rotation capacity; θ_r is recoverable rotation on unloading; M_y is yield moment; E_h is hysteretic energy dissipated by an SDOF subjected to an earthquake; β_{PA} factor to include the effect of cyclic loading.

This modified damage index removed the effects of recoverable or elastic rotations from the damage index, removing the limitation of the Park and Ang damage index, i.e., DI>0 even in an elastic state. This index is 0 in the elastic state though the upper limit of DI is still more than 1.

Jiang et al. (2015) (Jiang et al., 2015) proposed modifying the Park and Ang damage index. The index proposed is mentioned below.

$$D = (1-\beta)\frac{\mu_{md}}{\mu_{ud}} + \beta\frac{\int dE}{F_y \delta_y (\mu_u - 1)} \quad (1.42)$$

where μ_{md} = ratio of maximum deformation δ_m under earthquake to yielding deformation δ_y under monotonic loading; F_y = calculated yield strength; dE = incremental absorbed hysteretic energy; β = non-negative parameter different from β_{PA}; μ_{ud} = ratio of ultimate deformation to yielding deformation under monotonic loading. Since it is a combined model, β factor reflects the contribution of the deformation ratio and hysteretic energy in the damage index. 115 rectangular RC columns test results from the PEER database were extracted, which were cyclically loaded and experienced flexure dominant failure. These 13 tests of flexure dominant rectangular RC columns and beams were taken from Chen et al. (2009) (Jiang et al., 2015).

This index eliminates the non-normalization problem of the Park and Ang damage index. However, the index was primarily validated for flexure dominant columns only. For β factor, the empirical formula proposed was based on mostly experiments conducted on flexure-dominated columns only and very few beams. Therefore, it is not a universal formula to calculate β. It may give incorrect results when elements fail in shear. The limitation of this index, being a linear combination of energy and deformation, is still present though it is a nonlinear relation.

Poljanšek and Fajfar (2008) (Poljanšek and Fajfar, 2008) proposed a new damage index as the ratio of deformation quantities, where equivalent deformation capacity considers the effects of cumulative damage through the energy concept. Indirectly index considers both deformation and hysteretic energy parameters.

$$DI_{PF} = \frac{u_{\max}}{u_{equ}} \tag{1.43}$$

where u_{max} is the maximum deformation a structural element experience during an earthquake and u_{equ} is the equivalent deformation capacity of the structural element.

$$u_{equ} = u_M - \frac{E_{H,diss}}{E_{H,cap}}\left(u_M - u_C\right) \tag{1.44}$$

u_M and u_C are the deformation capacities of the structural elements under monotonic loading and cyclic loading, respectively. $E_{H,diss}$ is the hysteretic energy dissipated during ground motion, demand, and $E_{H,cap}$ is the capacity of the structural element for dissipation of hysteretic energy. The proposed index works well for cyclic loading though it requires monotonic loading deformations for computation. The author gave a nonlinear relation between deformation capacity and hysteretic energy and removes β factor from the index.

In the case of the el*astic* region, there is no energy dissipation, however, due to the elastic deformation damage index has some value. Secondly, in the case of monotonic loading, the maximum DI should be 1 when deformation demand is equal to monotonic deformation capacity. However, the equivalent deformation capacity is lower than the monotonic deformation capacity, therefore, DI would be more than 1. This does not align with the basic criteria of DI to be between 0-1. The index has not been mapped with the damage states, and experimental validation has not been attempted. The index proposed gives a global damage index, therefore, information about local damage is difficult to retrieve from this index.

Rodriguez and Padilla (2009) (Rodriguez and Padilla, 2009) Rodriguez proposed a seismic damage parameter in 1994 involving the Park and Ang damage index parameters. In addition, it included the effect of displacement history on drift ratio capacity. The proposed index value comes between 0-1.

$$I_d = \frac{E_H}{E_\lambda} \tag{1.45}$$

$$E_\lambda = k_\theta \theta_c^2 \tag{1.46}$$

$$k_\theta = kh^2 \tag{1.47}$$

E_H = Energy demand; θ_c is the maximum drift ratio in an elastic SDOF; h is the column height. The proposed damage index is calibrated using experimental results from the RC column database at failure and states preceding failure. The damage index is calibrated with the observed damage states of 21 test specimens. The damage index is also calibrated with Park and Ang damage index resulting in almost the same range however only till DI>0.6.

Though this index is experimentally validated and calibrated with damage states and gives DI between 0-1, it does not map the collapse damage state with the damage index.

Shiradhonkar and Sinha (2017) (Shiradhonkar and Sinha, 2017) developed a member damage index constituting two parts, DI_1 and DI_2. The first part marks the initiation of damage states. It is therefore defined in terms of curvature related to extreme fiber compression strain, which identifies different damage states, including crack width and spalling. Second part DI_2 represents the reduction in strength caused by damage accumulation under cyclic loading.

$$D_{proposed} = D_1 + D_2 - D_1 D_2 \tag{1.48}$$

$$D_1 = \frac{\phi_m}{\phi_f} \tag{1.49}$$

$$D_2 = \beta_{ss} \frac{\int dE}{C_p \phi_y M_y} \tag{1.50}$$

ϕ_m, ϕ_y, ϕ_f are maximum, yield, and ultimate curvature of a member. M_y is the yield moment, $\int dE$ represents dissipated hysteretic energy. C_p is the control parameter which maps cumulative damage under cyclic loading between limiting damage indices. Cumulative damage is represented by normalized hysteretic energy and β_{ss} factor. Control parameter C_p from regression analysis is computed as a function of member cross-section properties. Using strain equations from literature, extreme fiber compressive strain at significant spalling is calculated, and at other damage, states strain is calculated from IDARC-2D 7.0. These strain values are calibrated with observed damage states from the experimental PEER database. Damage quantification obtained is the element level for both beams and columns.

The index proposed is an element-level damage index that maps moderate and severe damage states with the index and is also experimentally validated.

Observations from two-parameter models

Using calibration coefficients to combine two or more parameters in the damage index limits the generalization of indices. Therefore, the preference is to have a single-parameter damage model.

1.2.3 Summary

The usage of a two-parameter model has been quite popular in literature because of the early development of experimentally validated Park and Ang (1985) damage index and its calibration with damage states. Further, many researchers tried to eliminate the limitations of that index, but still, limitations exist. In combined models, a calibration factor is always needed to decide the percentage contribution of each parameter in the total damage. These calibration factors often become limitations to their respective damage models since lots of data and a parametric study are required to give an empirical formula to fix these values.

Simultaneously, single parameters-based models such as Displacement-based, Natural-period based, Stiffness-based, and Energy-based models also evolved. Displacement-based indices could not capture strength degradation because of the cyclic loading effect. Though natural-period-based indices could effectively capture the cyclic loading effect, they gave only global damage, no local damage information could be retrieved from such indices. Stiffness-based indices could calculate local and global damage and incorporate cyclic effects. However, they could not differentiate the damage caused by short-duration and long-duration earthquakes where the final stiffness may be the same, but the damage caused could still be different. Energy-based indices were calculated from the area under the force deformation curve. Strength degradation and cumulative damage could be accurately computed for long-duration earthquakes because the area under each cycle was taken in energy computation. However, there are still some unresolved issues in energy-based indices. One is local to global mapping of energy-based damage index.

1.3 Literature Review on Weighting Factors

Two types of indices, i.e., local-level and global-level damage indices, have been proposed in the literature. Global level damage index provides information about the building's overall structural stability and remaining capacity, which, when mapped with damage states, facilitates retrofitting decisions whether a building needs retrofitting or not. If yes, how much retrofitting is required, and at what location are further questions to be answered. However, the global damage index does not provide information about damage distribution, whether the damage is locally concentrated in a few members or uniformly distributed among members. This lack of information is of paramount importance to take up retrofitting actions. Therefore, it creates the requirement for local damage indices.

Local damage indices give each member a damage index, therefore, highlights member to be retrofitted. Since both global and local damage indices are required for practical purposes, they must be related. Local damage indices of all members should combine to give the global damage index of the building.

1.3.1 Types of Weighting Factors

Appropriate weighting factors are required to map the local damage index to the global damage index. Weighting factors shall be decided such that the most crucial members should have higher importance or weighting factor as their damage would impact the global failure of the building more. Crucial members are decided considering the member type, member location, storey level, and their contribution to global stability. For example, a beam failure on the first floor might not be as damaging as a column failure on that floor for a building’s global stability. Also, a column failure on the first floor and a column failure on the top floor will have a different impact on the global stability of the building. Hence, the importance of member type and location must be appropriately weighted and accounted for in local to global damage index mapping.

Therefore, combining these local damage indices of each member using the weighting factor to get a correct global damage index depends on the concept adopted for the computation of weighting factors. Literature has three broad classifications of weighting factors in damage indices. (i) Energy-based weighting factor; (ii) Triangular shape-based weighting factor; (iii) Tributary area gravity load-based weighting factor.

1.3.1.1 *Energy-based weighting factor (EWF)*

An energy-based weighting factor was proposed by Park and Ang (1987) (Park et al., 1987). The most commonly used weighting factor in the literature to combine local damage indices to compute the global index is the energy-based weighting factor proposed by Park and Ang (1987). The authors had earlier proposed a local damage index based on the combined effect of displacement and energy (Park and Ang, 1985). A weighting factor was proposed to combine the damage indices of all building members to compute the global index. The weighting factor proposed is based on the Akiyama study, which concluded that damage distribution is closely related to the absorbed energy distribution (Akiyama and Kato, 1980). Therefore, the global index of a building D is computed from damage indices of each member D_i, weighted by their corresponding energy contribution factor λ_i as already mentioned in Equation 1.37 to 1.40.

1.3.1.2 *Triangular shape-based weighting factor (TSWF)*

A triangular shape-based weighting factor was proposed by Chung et al. (1988) (Chung et al., 1988). The author proposed a local damage index based on a modified Miner's rule and damage factors for considering the effect of loading history. A weighting factor based on a triangular shape for each storey was proposed to compute the global damage index. Storey damage index was calculated in the same way as Park and Ang damage index (Park et al., 1987). Storey indices were combined using a triangular shape with a maximum weightage at the base and a minimum at the top. This triangular distribution factor is multiplied with storey indices to compute the global damage index of the building.

$$Ds_k = \frac{\sum_{i=1}^{n} D_i^k E_i^k}{\sum_{i=1}^{n} E_i^k} \tag{1.51}$$

$$D_g = \sum_{k=1}^{N} Ds_k I_k \tag{1.52}$$

$$I_k = \frac{N+1-k}{N} \tag{1.53}$$

where D_g is the global damage index; Ds_k is the storey index of the k^th^ storey; N is the total number of stories; I_k is the important factor for the k^th^ story. The maximum damage index as per this index is 2. This weighting factor gives more importance to the lower stories than the upper stories. If a lower storey collapses, the whole building is affected, therefore, a higher global damage index. If an upper storey is affected, only a few upper stories are damaged while the rest of the building is safe, indicating a lesser global damage index. Though it has a limitation, in the same storey same weighting factor for a beam and column is assigned, though a column failure and a beam failure would have different global effects on the building.

1.3.1.3 *Tributary area Gravity load-based weighting factor (GLWF)*

A tributary area of gravity load-based weighting factor was proposed by Bracci et al. (1989) (Bracci et al., 1989). The author proposed a local damage index based on the combined effect of plastic deformation and energy dissipated through moment-curvature. The index was validated with Mander's experiments (Mander et al., 1983). To compute the global damage index weighting factor based on tributary area gravity load was proposed by Bracci et al. (1989) (Bracci et al., 1989). The authors proposed a self-weight procedure to combine local indices at the storey level.

$$(DI)_{member} = \max\{(DI)_i, (DI)_j\} \tag{1.54}$$

$$(DI)_{total} = \frac{\sum_{i=1}^{N} w_i (DI)_i^{(m+1)}}{\sum_{i=1}^{N} w_i (DI)_i^{m}} \tag{1.55}$$

$$\sum_{i=1}^{N} w_i = 1 \tag{1.56}$$

i= the component; *m*= control weighting factor for the component; w_i = importance factor for the component and is calculated as mentioned below:

w_i = (Total tributary gravity load)$_i$ / (Total tributary gravity load)$_{\text{all members}}$

Total tributary gravity load assigned importance factors to the members. As per the tributary area of gravity load, more importance is given to columns than beams and more importance to lower storey columns than upper storey columns. Almost all stories above would be affected if a column fails, but a beam failure would cause only local damage. Therefore, a higher importance factor for columns than beams leading to a higher global damage index, is justified in this method. Similarly, if a lower storey collapses, the whole building is affected, therefore, a higher global damage index. If an upper storey is affected, only a few upper stories are damaged while the rest of the building is safe, leading to a lower global damage index. For a normalized damage index, all components' importance factor sum is 1. The same procedure can be extended to the storey level. Since a storey collapse might not be reflected in the global index, it is recommended to compute both the global and storey damage indices.

1.3.2 Comparison studies on weighting factors

Rodriguez and Cakmak (1990) (Rodriguez-Gomez and Cakmak, 1990) compared the global damage index calculated from DiPasquale and Cakmak (1987) (DiPasquale and Cakmak, 1987) based on natural period parameters with the global damage index obtained from weighted averages using TSWF and EWF used on the local damage index proposed by Chung et al. (1988). The authors concluded that the global damage index from weighting factors of TSWF gave a good correlation with the numerically and experimentally found global damage index of DiPasquale and Cakmak (1987) in the first case study(Rodriguez and Padilla, 2009).

In the second case study, the report also compared the global damage index calculated numerically and experimentally from DiPasquale and Cakmak (1987) (DiPasquale and Cakmak, 1987) with the global damage index obtained from weighted averages using EWF on the local damage index of Park and Ang (1985) (Park and Ang, 1985). The comparison showed a good correlation between both indices, although damage index definitions differed in both cases. One is natural period based, and another combines deformation and energy.

EWF works well when used on Park and Ang local damage index, as the second case study proved. Since Park and Ang local damage index has deformation as one parameter, it takes care of the importance of columns which shows huge deformation in the global stability. Suppose columns dissipate less energy in comparison to beams. Even if EWF is used where column energy dissipation is less, the deformation factor in the local index makes these members considerable contributors to the global damage index. However, when EWF is used with local indices based on other parameters, this weighting factor does not give an accurate global damage index, as concluded in the first case study when EWF is used with Chung et al. (1988).

EWF is the most widely used weighting factor because of its experimental calibrations and mapping with damage states in Park et al. (1987). It can be concluded that EWF works well with Park and Ang local damage index only and might not work the same way with other parameter local indices, as shown in the study above. When used with Chung et al. (1988), a local damage index based on Minor's hypothesis did not correlate well.

Bracci et al. (1989) conducted experimental study to compare weightages (Bracci et al., 1989). A three-story two-bay RCC structure was experimentally tested until failure by Yunfei et al. (1986). The second-floor beam was severely damaged, as observed in the experiment. The same was numerically modeled in IDARC for damage calculation. One global damage index was calculated using GLWF, and another with the same importance factor was assigned to all members of all stories. In the first case, the global index was less than in the second case. Since the importance factor calculated from the gravity load tributary area was less for a beam than a column, therefore, was more important to the column than a beam. Hence, the global damage index is reduced with the usage of GLWF. Similarly, a higher global damage index is expected in the case of a building with severe column failure. This case study calculated the proposed damage index and Park and Ang index for a six-storey five-bay building. Though structural damage states were relatable, the mean proposed global index was 2.5 times the Park and Ang index. However, the proposed model gave a linear distribution between 0-1, and Park and Ang gave a nonlinear distribution with severe damage in the 0.4-0.7.

With the tributary area for gravity load as the basis for importance factor calculation, columns get a higher importance factor than beams, and lower stories get a higher distribution factor than upper stories. Therefore, a higher global damage index in the case of a column is expected than in the case of a beam failure, though energy dissipation in both members may be the same. Therefore, for local damage indices based on the energy parameter, GLWF might give a reasonable global damage index as it gives different importance factors for different members and storey levels.

Observation from comparative studies on weighting factors

Since the effectiveness of the weighting factor may change as per the type of damage index chosen. Therefore, the applicability of existing weighting factors must be checked for the local energy-based indices to compute a global energy-based index. As proved above, EWF may not work well with energy-based indices.

Existing concepts of TSWF and GLWF assume uniform or linearly decreasing distribution of weighting factors along the height of the building from bottom to top, which may not be the case in all types of buildings. The number of floors, bay width, and floor height may affect the weights. Also, the effect of with and without infill has not been included. The effect of member location within a floor is considered only in GLWF, i.e., different weighting factors for interior and exterior columns, which may be quite significant.

1.4 Literature Review on Assessment of Existing Buildings

Damages in past earthquakes have highlighted the need of mitigation. Mitigation measures include strengthening of existing buildings. An experimental study to validate and establish that the retrofitted gravity load-designed (GLD) structures have better seismic performance has been conducted. Seismic performance of reinforced concrete frames designed only for gravity loads before and after retrofitting is investigated. During excitation equal to the spectrum suggested in IS 1893:2002, cracks were observed in the ground storey. Damaged columns were retrofitted with reinforced concrete jacketing. This paper experimentally demonstrated better seismic performance of retrofitted bare frame structures as crack widths reduced in the experimental investigations on three-storied structures with single bay on 1:3 scale models on the shake table. Therefore, it emphasized the significance of retrofitting GLD buildings in India (Santhi et al., 2005). The performance of non-ductile RC moment frame buildings to demonstrate the critical need for mitigation measures worldwide was performed. The collapse risk of non-ductile RC frames buildings designed as per provisions of the Uniform Building Code 1967 and ductile RC frames designed as per the IBC 2003 building code was computed. It is found that non-ductile frames have 40 times higher results than corresponding modern code-conforming RC moment frames. Three bay two dimensional RC frame archetypes structures ranging in height from 2 to 12 stories were modeled using Opensees. The study employs nonlinear static and dynamic analyses to compare the seismic performance of non-ductile and ductile moment frames under different seismic hazard levels (Liel et al., 2011).

The vulnerability of a low-rise three-storey, four-bay RC bare frame building designed for gravity loads in seismic zone V as per the Indian standard code was assessed. Damage probability matrices were created for maximum considered earthquake (MCE) and Design basis earthquake (DBE) to compare the damage state at each hazard level. It was concluded that buildings might undergo moderate damage in DBE-level earthquakes and severe damage in MCE-level earthquakes (Halder and Paul, 2016). The seismic vulnerability of GLD buildings in seismic zones IV and V of India was carried out. Four-storey GLD buildings were analyzed and studied with a performance-based approach with fragility curves and drift hazard curves. With increasing levels of seismic hazard, the vulnerability of GLD buildings increased. For example, at 1% drift, the risk of a GLD building is twice the risk of a code-designed building in seismic zone II, and it increased to 100 times in seismic zone V. The urgent need for immediate inhabitation and mitigation measure in GLD buildings have been proposed after carrying out the seismic vulnerability of seismic zones IV and V of India (Dhir et al., 2018). Therefore, experimental and analytical studies highlighted the vulnerability of existing GLD and precode buildings and emphasized the benefits of mitigation measures.

To study the progressive collapse capacity of modern European buildings with RC frame structures, column removal case, ultimate load capacity, and maximum and residual drifts corresponding to ultimate steel strain are assessed. Two cases were analyzed; in one case, the corner column and in another case central column of the ground floor were removed. Results indicated that cases of corner column removal were more critical than the central columns with lower load capacity. Also, buildings were more sensitive to removing columns in the plan than elevation. Ground storey corner columns are critical in a five-story RCC bare frame building. This indicates that location of a column within a storey is a critical parameter which affects progressive collapse of a building (Parisi et al., 2019). The behavior of non-engineered reinforced concrete columns under cyclic loading in developing countries was examined. Experimental tests were conducted on 16 concrete columns of different dimensions and reinforcement ratios to investigate the collapse behavior of such columns. The lateral load carrying capacity of the columns with low axial load levels depends on the longitudinal reinforcement as tension failure was governing. It is observed that a tension failure governs in low rise building columns. And the number of stories affect how critical a column is (Boonmee et al., 2018). High axial load variation in bottom storey corner columns, initiated inelastic behavior at lower displacement demands and, therefore, reduced the capacity of the columns. Therefore, significance of axial load variation is demonstrated. (Rodrigues et al., 2018). The seismic response of GLD and seismic load designed (SLD) buildings built in accordance with Italian design standards in three time periods of the 1950s-60s, 1970s, and 1980s-90s were examined by De Risi et al. (2022). These were the time periods with different design provisions. The number of stories and the site hazard are some significant parameters explored. The key concerns about early seismic and non-seismic design practices were identified and modelled. The study analyzed the seismic response of the buildings, evaluated by nonlinear static and dynamic analyses, with reference to two performance levels. Three and six-story RCC bare fame buildings were selected to represent widespread buildings in four sites in Italy with increasing hazard levels. It was concluded that SLD buildings had higher displacement capacity for the same construction period. With the improvement of codes, there was no change in the results of usage prevention damage due to the 0.5% interstorey drift threshold. However, there was an improvement in performance with time in terms of the global collapse limit state. (De Risi et al., 2022).

Observation

Assessment of existing buildings is a vast area with lots of variables affecting the failure modes of a building. Some of the variables which have been discussed in the literature are geometric regularity, number of stories or axial load, design period and corresponding design codes, construction materials, modelling assumptions, different types of failures like flexure or shear or axial, location of failure initiation, country-specific construction material and design standards. Worldwide researchers have worked on assessing existing buildings and computation and mitigating risks involved. It becomes much more difficult to tackle an issue of this magnitude in countries with many unsafe buildings. Therefore, generalized solutions must be applied to widespread buildings of similar typologies. Generalized guidelines are needed to identify members and stories with the potential for huge damage.

1.5 Literature gaps

Two questions need to be addressed to carry out retrofitting activities in damaged buildings.

1. How much-retrofitting needs to be done in the building?
2. At what location would retrofitting be most effective with minimum effort?

The first question can be answered by comparing desired capacity with the base shear requirement of that region.

As understood from the literature review, the second one can be answered from the local damage indices of all members and their weighting factors. The weighting factor indicates the most critical members for the global stability of the building. Therefore, strengthening shall consider the damage distribution among members and their weighting factors. However, there are research gaps in weighting factor computations, as mentioned in the literature review.

As seen from the literature, energy-based damage indices have progressed well but with a limitation of no local to global mapping of indices. However, they can be computed at both local and global levels both. This study is proposed to map local damage to global damage using weighting factors. Each member on each floor should have a weighting factor describing how much percentage of local damage is contributed to the global building damage. Once it is established, strengthening actions can be taken up first at higher weighted members to increase the capacity of the building immediately. Moreover, such strengthening actions as per the weighting factor and local damage can be continued till the desired capacity of the building is achieved, which is computed by checking the updated capacity of the strengthened building.

Three types of weighting factors have already been proposed in the literature. It has already been proved that EWF might not hold well with all types of local damage indices. Its experimental calibration is only with Park and Ang local damage index. If more energy is dissipated in a beam than a column and EWF proposed by Park and Ang is used, then column weightage would be less than the beam. Therefore, when used with energy-based damage indices, the accurate global damage index might not be captured by otherwise popular EWF.

Existing concepts of TSWF and GLWF assume uniform or linearly decreasing distribution of weighting factors along the height of the building from bottom to top, which may not be the case in all types of buildings. Researchers have highlighted that low-rise buildings experience extensive damage in the ground storey with negligible damage in upper stories. Therefore, storey-wise weighting factors need further research where the axial load on columns significantly affects capacity and damage. The effect of member location within a floor is considered only in GLWF, i.e., higher weighting factors for the interior, which may be quite significant. However, from the literature on the progressive collapse of buildings, it is understood that corner and façade columns are the critical members. Therefore, weighting factors for columns within a storey needs further research.

1.6 Problem statement

From the gaps identified in the Literature, the need to assess existing buildings to strengthen them for the expected earthquake ground motion is evident. Upon looking at the history of design and construction practices in India, it was common to construct buildings without seismic design and without consulting a design engineer. It continued even after the introduction of seismic ductile detailing codes in 1992. These buildings are termed *Gravity load designed buildings* denoted as *Type G*. The massive stock of RCC buildings constructed with no seismic design is still in use in seismic-prone areas. Another widespread deficient typology is the buildings constructed with IS 1893:2002, i.e., between 2002 to 2016, termed *precode buildings of IS1893,* denoted as *Type P*.

Weighting factors have been identified as the key tool to assist in strengthening activities in deficient buildings. However, further research is needed to address the key limitations of existing weighting factors. The first is the computation of weighting factors for columns within the storey, and the second is the storey-wise weighting factors. The axial load of the columns may significantly impact weights. Therefore, the number of stories shall be taken as one of the parameters for the study.

1.7 Scope of study

Weighting factors to combine energy-based local and global damage indices shall be proposed, which shall assist in strengthening decisions. Nonlinear static analysis is chosen for quick and simple analysis. However, typical results are verified with non-linear time history analysis. Building types considered should be able to represent mass buildings. Therefore, two categories of buildings, Type P and Type G, are chosen for the study, representing widespread existing buildings. To simplify the problem and reduce the complexities due to many variables, the bare frame configuration is adopted to model regular RC frame buildings in 2D in SAP2000. The parametric variation with the number of stories and storey heights is taken up in this study. In future studies, more variables can be included to bring results closer to the real problem.

1.8 Objectives

Relative weightage of local damage to global damage using the energy dissipation model shall be computed. A sequence of members as per the decreasing weights shall be assigned from computed relative weights. To achieve this work is divided into the following objectives.

i) To compute the contribution of damage of exterior and interior columns to global damage in gravity load-designed buildings.

ii) To compute the contribution of damage of exterior and interior columns to global damage in buildings designed as per previous code IS 1893-2002.

iii) To compute the contribution of damage by each storey in global damage of gravity load designed building.

iv) To compute the contribution of damage by each storey in global damage of buildings designed as per previous code IS 1893-2002.

Buildings considered for the study shall include variations of 1) Axial load and 2) storey height.

1.9 Organization of thesis

Chapter 1 introduces the problem faced by the existing buildings. The literature review is divided into three sections: damage indices, weighting factors, and critical issues identified by the assessment of existing buildings. In the end, the problem statement, scope, and objectives are defined.

Chapter 2 presents details of buildings considered for the study. It starts with the geometric details and describes the analytical modelling of the buildings and the analysis details used in the study.

In *Chapter 3,* weighting factors are computed for exterior and interior columns within a storey in Type G buildings for two parameters, i.e., axial load variation and storey height variation. Validation for the methodology used in the computation of weighting factors is presented.

In *Chapter 4,* the weighting factors are computed for exterior and interior columns within a storey in Type P buildings for axial load variation.

In *Chapter 5*, storey-wise weighting factors of Type G buildings are computed for two parametric variations, i.e., variable axial load on columns and storey height variation.

In *Chapter 6*, storey-wise weighting factors of Type P buildings are computed for the same parametric variation.

Chapter 7 presents the proposal for the sequence of weighting factors to assist in strengthening activities.

Chapter 8 summarizes the study findings and recalls the key conclusions. Potential areas for future work are outlined.

2 STRUCTURAL MODELLING

2.1 Overview

To meet the objectives outlined in the previous chapter, the types of buildings considered in the study are presented in this chapter. Geometric details of the buildings and analytical modelling and analysis details are also presented in the subsections.

2.2 Building details

A substantial amount of buildings in India are designed for only gravity loading with no seismic provisions mentioned as *Type G* buildings. Another significant set of buildings constitutes *Type P* buildings constructed before the revision of earthquake loading and ductile detailing codes in 2016. These are called Precode buildings of IS 1893, termed Type P buildings. Hence, most of the RCC MRF building stock constructed before 2016 falls in either Type G or Type P buildings, and they all need strengthening. This study is being undertaken to identify significant damage contributing members in both types of buildings to propose different weights as per their contribution.

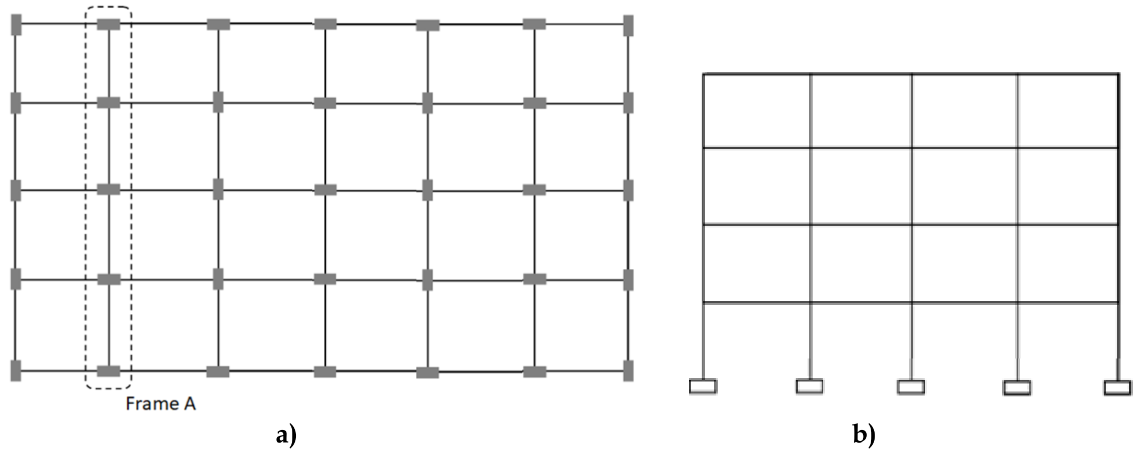

Figure 2.1: Typical Plan and elevation of four-storey type G and type P buildings.

The buildings studied are RC MRF buildings constructed in two different years and designed with different IS code editions in the same city in zone V. Building type P was built in the year 2003. During that time, IS 1893- 2002 was in practice, along with provisions of ductile detailing in beams and columns from IS 13920 : 1993. The typical plan and elevation of a 4-storey building are presented in Figure 2.1. Building type G was constructed in 1992 and was designed only for gravity loads with no earthquake loading and ductile detailing provisions for seismic loads. Building type G had key detailing issues like low confinement levels, inadequate anchorage of rebars, and inadequate lap splice length, creating a potential hinge location with a possible brittle failure (IITM and SERC, 2005).

Table 2.1: Section sizes of all type G and type P buildings with transverse reinforcement details

S.No	**Time Period (sec)**	**Column size (ext, int) (mm)**	**Column ρ_t (ext, int)**	**Column stirrup spacing (ext, int) (mm)**	**Beam size (mm)**	**Beam ρ (ρ′)**	**Beam stirrup spacing (mm)**	**Curtailment**
G4 / G4SH3	1.6	230x230, 250x300	0.00123, 0.00094	200, 200	230x350	0.0122 (0.0078)	200	-
G6 / G6SH3	2.2	230x270, 280x390	0.00123, 0.00145	200, 200	250x360	0.0103 (0.0076)	125	-
G8 / G8SH3	2.7	250x320, 300x500	0.00157, 0.00101	225, 225	250x350	0.0092 (0.0072)	125	@ 6th Storey
G10 / G10SH3	3.2	280x380, 380x500	0.00112, 0.00101	200, 225	280x330	0.0106 (0.0068)	150	@ 8th Storey
P4 / P4SH3	0.99	250x470, 300x500	0.01114, 0.00838	60, 75	250x470	0.0107 (0.0088)	100	-
P6 / P6SH3	1.3	270x450, 330x540	0.01074, 0.00727	65, 80	270x470	0.0124 (0.0081)	100	-
P8 / P8SH3	1.8	300x480, 340x560	0.00436, 0.00660	75, 85	300x450	0.0116 (0.0114)	100	@ 6th Storey
P10 / P10SH3	2.1	330x500, 360x580	0.00673, 0.00580	70, 70	330x475	0.0124 (0.0055)	100	@8th Storey
G6SH3.5	2.7	230x290, 280x400	0.00097, 0.00141	200, 200	230x360	0.0103 (0.0076)	125	-
G6SH4	3.2	230x290, 290x410	0.00097, 0.00138	200, 200	230x360	0.0103 (0.0076)	125	-
G6SH4.5	3.6	230x300, 300x420	0.00094, 0.00135	200, 200	230x360	0.0124 (0.0076)	150	-
P6SH3.5	1.6	290x470, 340x560	0.00955, 0.00660	70, 85	270x480	0.0124 (0.0097)	100	-
P6SH4	1.8	330x470, 350x570	0.00836, 0.00648	80, 85	330x500	0.0117 (0.0076)	100	-
P6SH4.5	2	340x500, 370x580	0.00785, 0.00637	80, 85	340x500	0.0113 (0.0111)	100	-

Member sizes for RC MRF buildings with variable building height and variable storey height are mentioned in Table 2.1. Building nomenclature consists of strings and numbers where G represents the Gravity load designed building, P represents the previous code designed building, and SH represents storey height. G4SH3 indicates the building is a 4-storey gravity load-designed building with a storey height of 3m. P6SH4 represents a 6-storey precode-designed building with a storey height of 4m.

2.3 Modelling

Buildings are represented as the 2-dimensional multi-degree of freedom system. A bare frame modelling approach is adopted, and this modelling is done through building analysis software SAP2000 v23.3.1 (CSI, 2016). The concrete and reinforcing steel grades used in the study are M30 and Fe-415. The Mander model (Mander et al., 1988) is used for concrete material modelling. Cracked section properties are derived from IS 15988 (2013) (IS 15988:2013, 2013). Members are modelled as elastic frame members with lumped plasticity approach by modelling concentrated nonlinearity at both member ends. Lumped plasticity models exhibit strength degradation behaviour due to bond slip, bar buckling and shear failure leading to strain softening (Haselton and Deierlein, 2007; Liel et al., 2011). In the lumped plasticity approach, an element's force deformation behavior is defined by a backbone curve. This study uses hinge backbone parameters from ASCE 41-17 to represent nonlinearity (ASCE/SEI 41-17, 2017). A more gentle slope compared to ASCE 41-17 has been provided to join points C and E in post-peak behaviour to avoid numerical stability issues, as shown in Figure 2.2 (Ibarra and Krawinkler, 2005; FEMA, 2018). Moment rotation of typical structural members of one of the models, i.e., 6 storey building, are listed in Table 2.2. Flexural hinges (M3) and interacting hinges (P-M3) are modelled at beam and column ends, respectively. User-defined hinges were a better alternative in the case of the existing precode building of Turkey in numerical analysis for better nonlinear analysis (Inel and Ozmen, 2006). Therefore, user-defined flexural hinges are used for modelling hinges. Column user-defined hinges are calculated for five axial load values for each column and given as input in SAP2000 to form a 3D envelope. For the axial load coming on each column in each combination, the software further interpolates user-defined hinge values from that envelope. Shear hinges are modelled as force-controlled brittle hinges.

As stated earlier, the Type G building has key detailing issues. Low confinement levels are simulated by transverse confinement reinforcement at the potential hinge location, $\rho_{t,}$ as per ASCE 41-17 in hinge parameters calculations (ASCE/SEI 41-17, 2017). During the construction of Type G buildings, lap splices might have been provided as per design compressive forces experienced due to gravity load. However, tensile forces act on the column during an earthquake, which renders existing lap splice length insufficient. This issue is also considered in hinge modelling parameters for a column controlled by inadequate development or splicing along clear height in Table 10-8 of ASCE 41-17. Typical transverse reinforcement provided throughout is 6Φ-200/225mm c/c spacing. For beam hinge modelling, parameters assume non-conforming transverse reinforcement to simulate low confinement levels.

Table 2.2: Plastic rotation capacities of typical members of 6 storey Type G building with a storey height of 3m.

Member	$\mathbf{N_{UD}/A_g f_{cE}'}$	$\boldsymbol{\theta_p}$	$\boldsymbol{\theta_{pc}}$
Beam	0	0.0156	0.008
Column ext (1,2 floor)	0.413	0.0168	0
Column ext (3,4 floor)	0.33	0.0208	0
Column ext (5,6 floor)	0.1	0.026	0.0097
Column int (1,2 floor)	0.45	0.0148	0
Column int (3,4 floor)	0.405	0.0186	0
Column int (5,6 floor)	0.15	0.026	0.003

Note: $N_{UD}/A_g f_{cE}'$ is the axial stress ratio. Values θ_p, and θ_{pc} are pre-capping and post-capping plastic deformation capacities.

The effect of cyclic degradation of stiffness and energy dissipation capacity is modelled using the degrading hysteresis model in SAP2000. Three parameters f1, f2, and s, are required for this hysteretic modelling. These parameters were obtained from calibrated analytical hysteretic models with experimental results for ductile and non-ductile components (Surana et al., 2017). For non-conforming beams, f1=0.95, f2=0.4, and s=0.1 are utilized. A similar degrading hysteretic model cannot be used for columns in lumped plasticity modelling; hence it is not considered in this verification study. In commercial software, sometimes the solution does not converge, therefore, while dealing with the negative stiffness in the post-peak region, a further gentle slope is adopted to converge the solution. Descending branch of the pushover curve would be affected by this approximation of a gentle slope of negative stiffness (Hall, 2018). However, a strength drops up to 85% is considered.

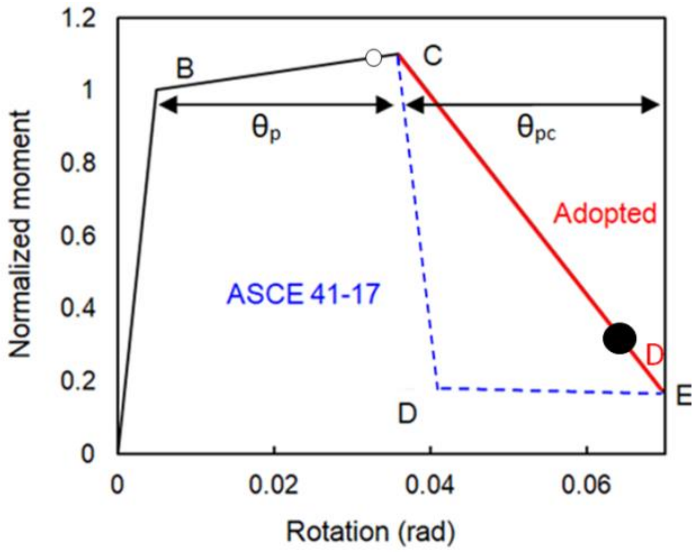

Figure 2.2: Typical backbone curve for an RC section

2.4 Analysis

The building can be analyzed through linear and nonlinear analysis both. Nonlinear analysis is closer to real structural behaviour but is complex and time-consuming. Linear analysis is quick but gives conservative results. Due to advancements in high-speed computing, researchers and engineers can deal with complex nonlinear analysis for structures more easily. Therefore, this study uses nonlinear analysis for more accurate simulation. Nonlinear analysis can be done for static and dynamic loading. The modelling procedure is the same for both analyses.

Nonlinear static analysis, known as the Pushover Analysis (POA), is done with monotonically increasing lateral load to achieve target deformation at the roof or collapse stage, which is 85% of the ultimate strength. It is a simple and quick method to observe potential damage locations in a structure and estimate its capacity. Therefore, it is a valuable tool for the damage assessment of existing structures. However, it only considers the fundamental mode and ignores higher modes. It also ignores the variation in response due to dynamic behaviour, which can be captured by only nonlinear dynamic time history analysis. However, the literature supports that pushover analysis gives a somewhat acceptable estimate of the seismic behaviour of the structure (Bosco et al., 2009; Pinho et al., 2013).

Whereas in Nonlinear dynamic analysis, earthquake ground motion is the loading. The structural response is computed at each time interval of the ground motion. Therefore, this is a more accurate analysis; however, the response will differ for different ground motions. ASCE 7 (Kircher et al., 2006) recommends performing nonlinear analysis for eleven earthquakes to cover responses for different types of earthquakes expected in that region. The analysis takes much time to run as the response is computed at each time step of an earthquake ground motion. Due to these reasons, nonlinear time history analysis is more time-consuming than nonlinear static analysis.

In this study, nonlinear static analysis is performed. However, the methodology is verified for effectiveness with the nonlinear time history analysis in subsequent chapters.

3 WEIGHTING FACTORS FOR EXTERIOR AND INTERIOR COLUMNS OF TYPE G BUILDINGS

3.1 Methodology for exterior and interior column damage contribution

This study is being carried out by pushover analysis. The area under the pushover curve gives the energy dissipation capacity of the building (Maeda and Kang, 2009; Vimala and Kumar, 2014). The study is based on this concept of energy dissipation calculation to understand the importance of exterior and interior columns in the global energy dissipation capacity of the building.

The exterior and interior columns are replaced with reduced column sections, which have a 50% yield moment of the original section, this would affect stiffness of the section as well. In the first case, the exterior left column is replaced with the reduced column section size and termed *Reduced Exterior Column Left* (RECL). In the second case, a similar replacement is done in the exterior right column, and this case is termed *Reduced Exterior Column Right* (RECR). In the third case, the interior center column is replaced with the reduced column section termed the *Reduced Interior Centre Column* (RICC). Pushover analysis is performed for all three cases to obtain the capacity curves. To calculate energy dissipation capacity, a triangle with initial elastic stiffness from the last point of pushover analysis is subtracted from the area under the curve to indicate recovery of elastic energy, as shown in Figure 3.2. Four capacity curves are obtained for every building, i.e., one original capacity curve and three reduced section capacity curves for RECL, RECR, and RICC. The energy dissipation capacity of all three reduced cases is subtracted from the original building energy dissipation capacity, as shown in Figure 3.2. Reduction in the energy dissipation capacity of the building due to the reduced sections is computed. If a member with a reduced section causes more reduction in energy dissipation capacity, it has a higher contribution and hence a higher weighting factor. This way, the contribution of exterior and interior columns is calculated for GLD buildings.

Non-linear time history analysis is also performed using eleven earthquakes to establish this methodology firmly. GLD building is strengthened at exterior columns in one case and interior columns in another. Their non-linear time history analysis compared the behavior of the original GLD building and strengthened buildings.

3.2 Effect of Axial Load

3.2.1 Gravity load designed building of 4 Storey (G4)

The hinge mechanism of a G4 building at 85% strength drop in PoA is presented in Figure 3.1. It is observed that the ground floor's exterior and interior columns got damaged and crossed peak point 'C' of the backbone curve (Figure 2.2). Upper-storey beams and columns have also yielded; however, they are in the backbone curve's B-C range (Figure 2.2).

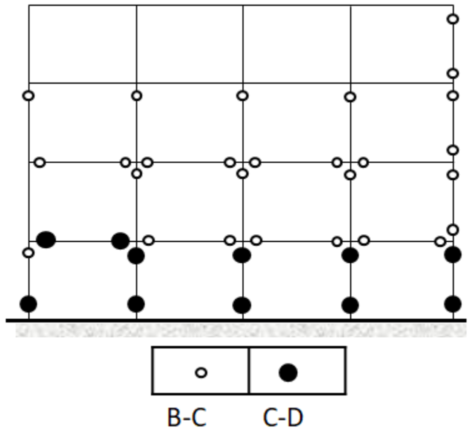

Figure 3.1: Hinge mechanism of G4 building at the pushover step corresponding to 85% strength drop.

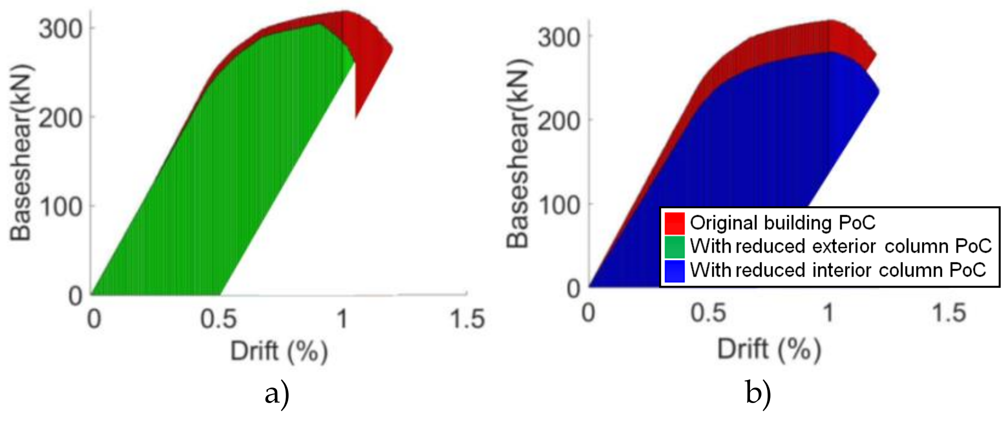

Figure 3.2: a) Comparison of G4 building capacity curve with another capacity curve of 4 storey building with a) reduced exterior column b) reduced interior column

The capacity curve from NSA of RECL is plotted in Figure 3.2 a) in green colour, and its area under the curve is reduced from the area under the original building capacity curve plotted in red. It is observed that the energy dissipation capacity of the building is reduced by 23.6% in the RECL case, as tabulated in Table 3.1. Whereas in the case of the RICC section, the capacity curve is plotted in blue

Figure 3.2 b) and compared with the original building capacity curve plotted in red. The energy dissipation capacity of the building is reduced by 8.3%.

The green capacity curve for RECL shows that strength drop is at lower drift, and more reduction in energy dissipation occurs when the exterior column is reduced in size. Therefore, exterior columns have a higher weighting factor in the building's global stability and energy dissipation capacity.

Table 3.1: Reduction in energy dissipation capacity of type G buildings with increasing axial load

Building Name	**Exterior Column Left (%)**	**Interior Column Centre (%)**	**Exterior Column Right (%)**
G4	**23.6** ↑	8.3	4.8
G6	**4.1**	-1	**8.2** ↑
G8	**7** ↑	4.8	-1.3
G10	0.1	-2.4	-20

3.2.2 Gravity load designed building of 6 Storey (G6)

The hinge mechanism of the G6 building is presented in Figure 3.3, which highlights beam mechanism formation on the first and second storey where beams lie between points 'C' and 'D' (Figure 2.2) of the hinge backbone curve. Therefore, dissipating huge amounts of energy. Exterior columns yielded in almost all stories, and interior columns yielded in the first and third storey. Hence, energy dissipation capacity is shared by both beams and columns.

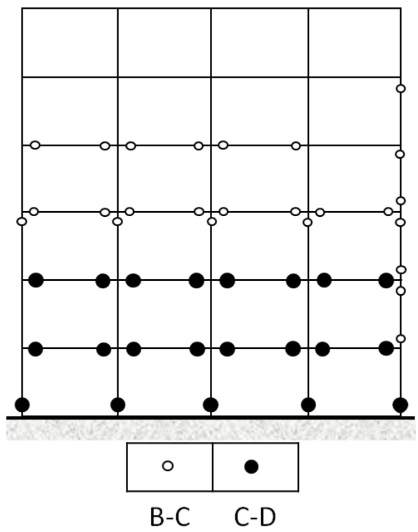

Figure 3.3: Hinge mechanism of G6 building at the pushover step corresponding to 85% strength drop.

Nonlinear static analysis for three reduced cases is performed further to study its division between exterior and interior columns. Subtraction of reduced section energy dissipation capacity from original building energy dissipation capacity gives 8.2% contribution for exterior and negligible for interior columns calculated from Figure 3.4 a) and b) and is tabulated in Table 3.1. Again computed contribution of exterior and interior columns in the energy dissipation capacity of the building follows the same trend, i.e., more contribution from exterior columns than interior columns. However, the overall contribution is significantly less from columns, and the same is plotted in Figure 3.9.

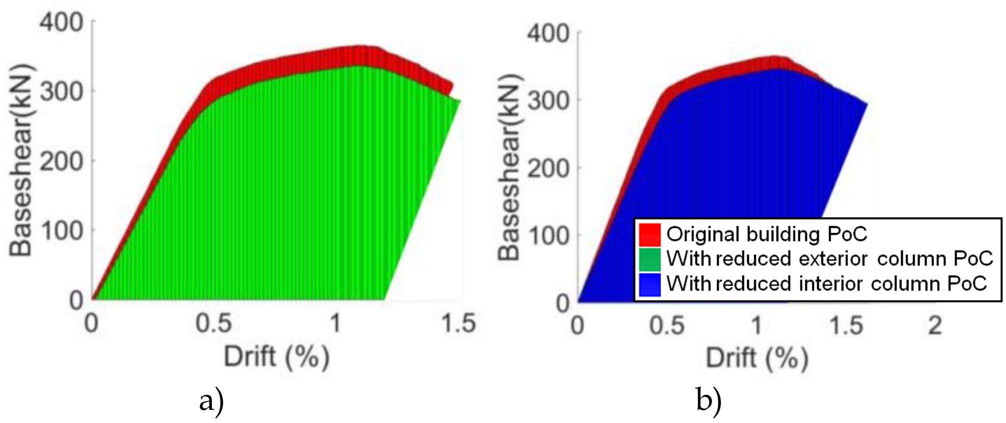

Figure 3.4: a) Comparison of G6 building capacity curve with another capacity curve of 6 storey building with a) reduced exterior column b) reduced interior column

3.2.3 Gravity load designed building of 8 Storey (G8)

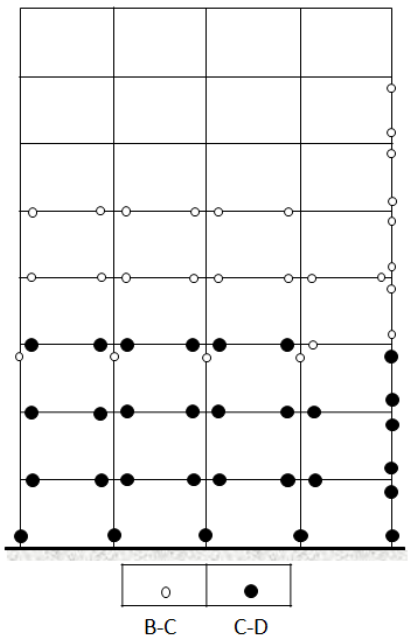

Figure 3.5: Hinge mechanism of G8 building at the pushover step corresponding to 85% strength drop.

The hinge mechanism for the G8 building is shown in Figure 3.5. All the beams up to the third storey are damaged. They lie between points 'C' and 'D' (Figure 2.2), exhibiting strength degradation after utilizing their entire ductility and dissipating huge energy. The first storey columns and the exterior columns up to the third storey have yielded and are in the strength degradation zone of the backbone curve, hence dissipating huge energy. Both columns and beams share energy dissipation.

Nonlinear static analysis of buildings with reduced exterior and interior columns is performed, and capacity curves are plotted in Figure 3.6. The contribution of the exterior column is computed from the subtraction of the capacity curve of the RECL from the capacity curve of the original building. Similarly, the contribution of the interior column is also computed. It is observed that the exterior column contributes 7% energy dissipation, while interior columns contribute 4.8% energy dissipation, as tabulated in Table 3.1. The higher contribution of exterior columns reduced to 7% in G8 as the number of stories increased. However, the weightage of the exterior columns is still higher in G8, the contribution of the exterior and interior columns is comparable and plotted in Figure 3.9.

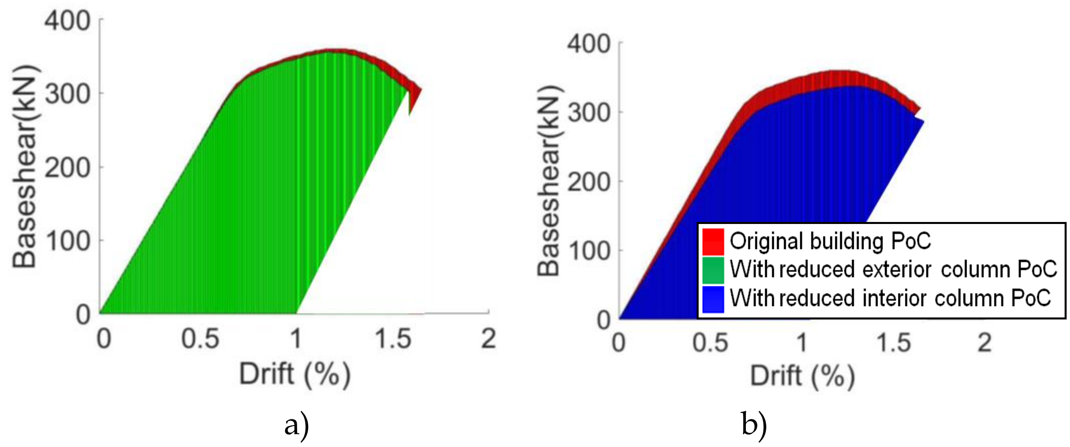

Figure 3.6: Comparison of G8 building capacity curve with another capacity curve of 8 storey building with a) reduced exterior column b) reduced interior column

3.2.4 Gravity load designed building of 10 Storey (G10)

In the G10 building, eighth storey columns just yielded, as shown in Figure 3.7. The drop in capacity curve obtained from pushover analysis is mainly because of the beam hinges in the second to sixth storey beams, which lie between points 'C' and 'D' in the hinge backbone curve (Figure 2.2). Till 85% of strength drop in POC, participation of columns in energy dissipation capacity is less.

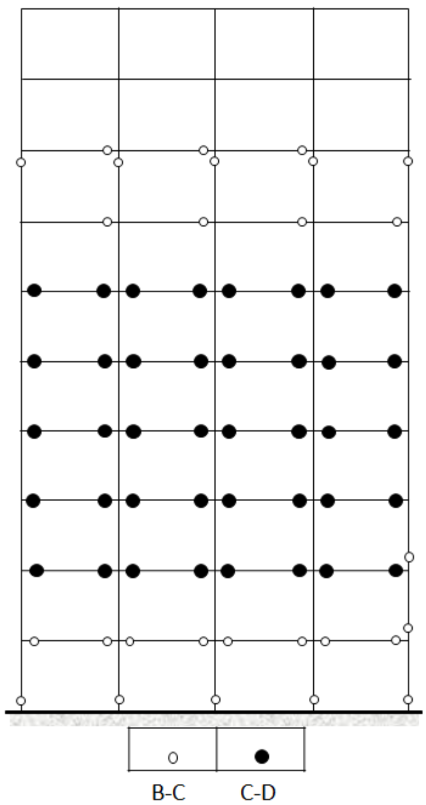

Figure 3.7: Hinge mechanism of G10 building at pushover step corresponding to 85% strength drop.

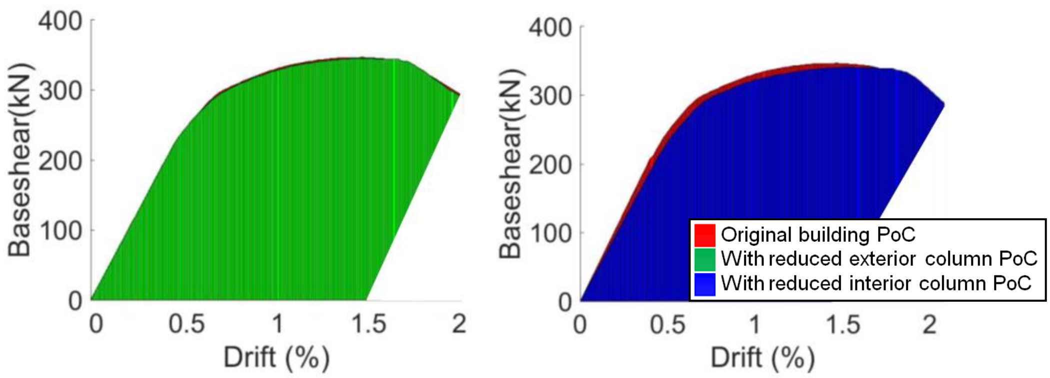

Figure 3.8: Comparison of 10 storey building capacity curve with another capacity curve of 10 storey building with a) reduced exterior column b) reduced interior column

The buildings' energy dissipation capacity reductions in three cases calculated from Figure 3.8 are tabulated in Table 3.1. The percentage contribution is significantly less. 90% of energy is dissipated via beams and only 10% of energy is dissipated via columns. As energy dissipation capacity is coming from beams, this method cannot be used to calculate exterior and interior column weights in the case of G10.

3.2.5 Discussions

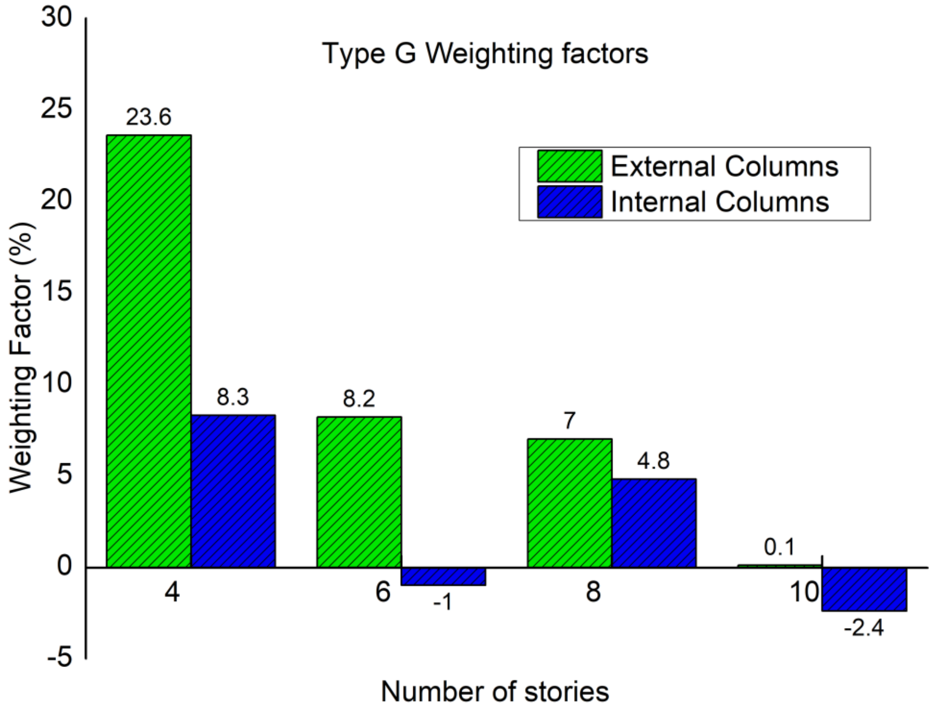

Figure 3.9: Weightage of exterior and interior columns in type G buildings

In gravity load-designed buildings with a storey height of 3m, it is observed that the exterior columns have higher weightage in energy dissipation capacity of the building than interior columns in G4, G6, and G8 buildings, as shown in Figure 3.9. The exterior columns of these buildings were designed for almost half the vertical load of interior columns. However, they are subjected to lateral load, which puts exterior columns under huge axial stress. Therefore, the higher weightage of exterior columns in gravity-load-designed buildings is justified theoretically also. However, in G10, almost the entire energy dissipation capacity happened via beams. Therefore, the same cannot be concluded for G10 from this methodology.

3.3 Effect of Storey Height

The effect of storey height is studied on the weights of interior and exterior columns. The storey height of a G6 storey building is varied from 3m to 4.5m to observe the change in the contribution of exterior and interior columns. Four G6 buildings are designed and analyzed with storey heights of 3m, 3.5m, 4m, and 4.5m.

3.3.1 G6 with 3m storey height (G6-SH3)

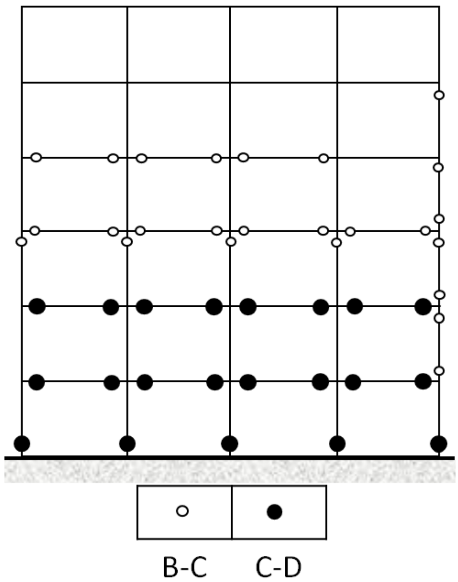

Figure 3.10: Hinge mechanism of G6-SH3 building at the pushover step corresponding to 85% strength drop.

The hinge mechanism of a 6-storey G6 building is presented in Figure 3.10. Beams up to the second storey have crossed post-peak strength. Exterior and interior columns are yielded up to the fifth storey. However, they are in the backbone curve's B-C range (Figure 2.2).

The capacity curve obtained from the PoA of RECR is plotted in green in Figure 3.11. Its area under the curve is computed and subtracted from the original building capacity curve area plotted in red. This subtraction gives an energy dissipation capacity of 8.2% due to the reduced exterior column section, as tabulated in Table 3.2. Whereas in the case of the RICC section, the capacity curve is plotted in blue, subtracted from the original building capacity curve in red, and tabulated in Table 3.2. The first row of Table 3.2 highlights more weightage of exterior columns when the storey height is 3m.

Table 3.2: Reduction in energy dissipation capacity of type G buildings with increasing storey height

Building with a variable storey height	Exterior Column Left (%)	Interior Column Centre (%)	Exterior Column Right (%)
G6SH3	4.1	-1	**8.2**
G5SH3.5	4.3	-0.5	**7.1**
G5SH4	**6.5**	**4.9**	5.6
G5SH4.5	3	2.5	**8**

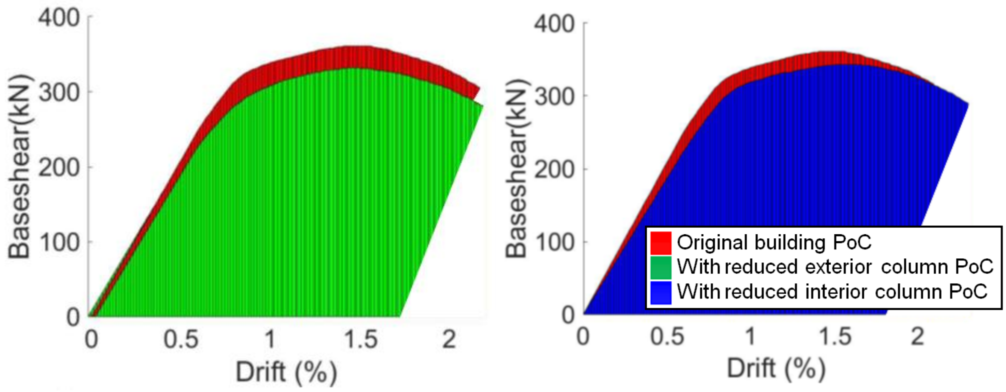

(a) (b)

Figure 3.11: Comparison of G6SH3 building capacity curve with another capacity curve of 6 storey building with (a) reduced exterior column (b) reduced interior column

3.3.2 G6 with 3.5 m storey height (G6SH3.5)

The hinge mechanism of a 6-storey G6 building with a storey height of 3.5 m is presented in Figure 3.12. Most of the beams up to the third storey are in their post-peak strength region. Exterior and interior columns up to the third storey are yielded. However, they are in the backbone curve's B-C range (Figure 2.2).

The capacity curve obtained from NSA of RECR is plotted in green colour along with the red colour pushover curve of the original building in Figure 3.13. 7.1 % reduction in area under the curve gives energy dissipation capacity due to reduced exterior column section as tabulated in Table 3.2. Similarly, the reduction in energy dissipation capacity due to the reduced interior section is tabulated in the second row of Table 3.2. It is observed that the weightage of exterior columns is higher than interior columns even when the storey height is increased to 3.5m.

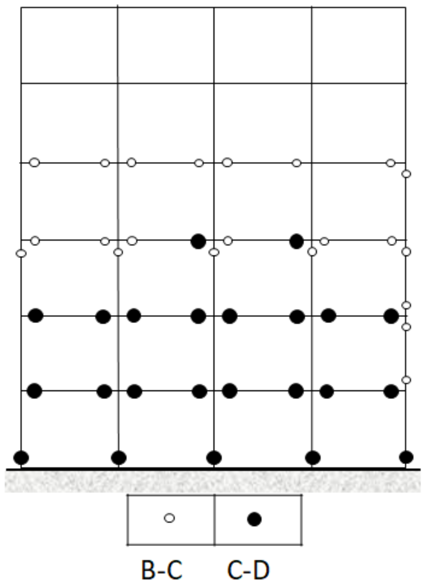

Figure 3.12: Hinge mechanism of G6-SH3.5 building at the pushover step corresponding to 85% strength drop

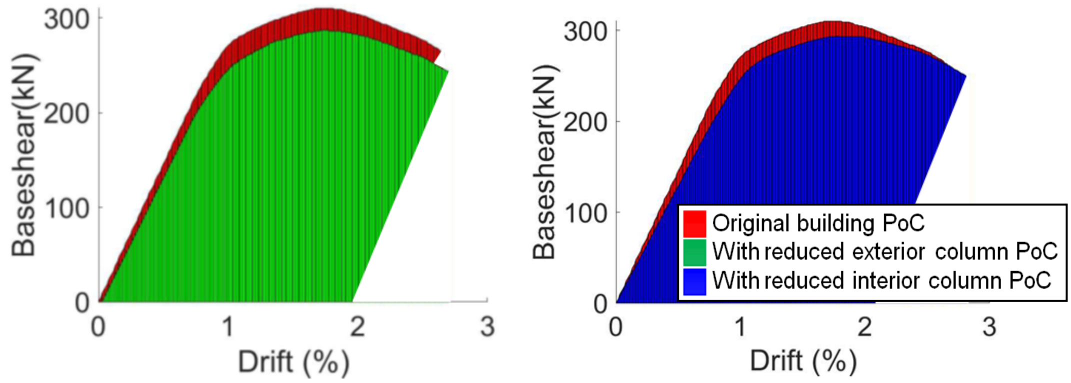

Figure 3.13: Comparison of G6-SH3.5 building capacity curve with another capacity curve of 6 storey building with (i) reduced exterior column, (ii) reduced interior column

3.3.3 G6 with 4m storey height (G6SH4)

The hinge mechanism of a 6-storey G6 building with a storey height of 4m is presented in Figure 3.14. Beams up to the third storey have crossed post-peak strength. Exterior and interior columns are yielded up to a third storey. However, they are in the backbone curve's B-C range (Figure 2.2).

The capacity curves for RECL and the original building are plotted in Figure 3.15. The difference in the area under the curve is 6.5% indicating energy dissipation capacity due to the reduced exterior column section. Capacity curves for RICC and the original building are also plotted in Figure 3.15b. The difference in the area under the curve is 4.9%, and the same values are tabulated in Table 3.2. It is observed that both exterior and interior columns contribute in a similar range. Due to the increase in height of columns, they are more flexible and attract lesser moments. Exterior columns were significantly deficient; however, the deficiency was reduced due to lesser demands in exterior columns. This may have reduced exterior columns' significance in global stability. Therefore, both exterior and interior columns share similar weightage in global stability.

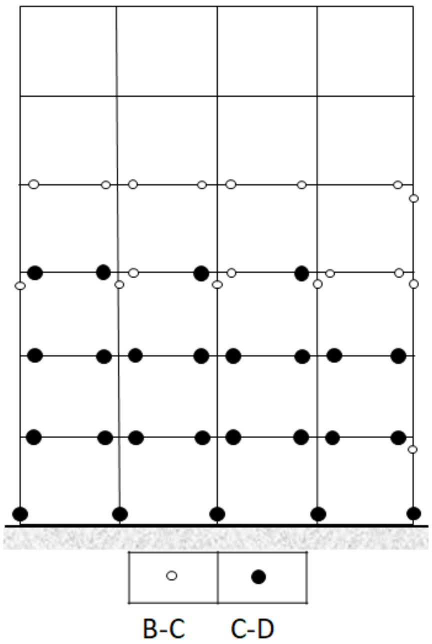

Figure 3.14: Hinge mechanism of G6SH4 building at the pushover step corresponding to 85% strength drop

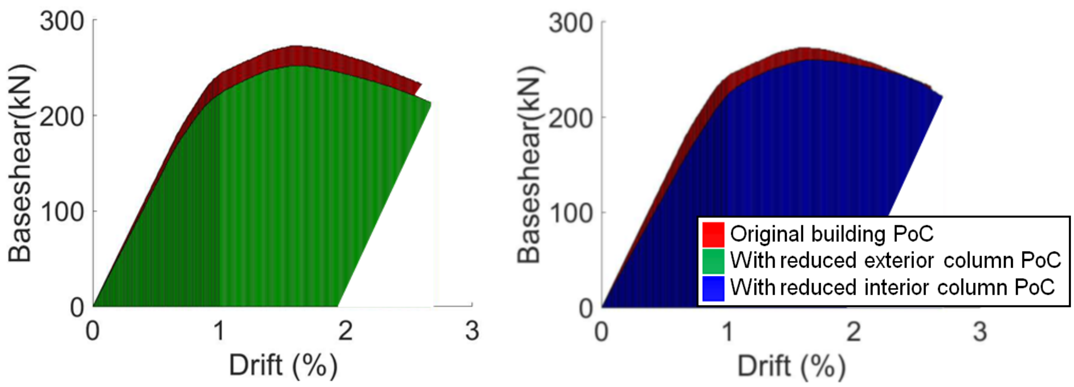

Figure 3.15: Comparison of G6SH4 building capacity curve with another capacity curve of 6 storey building with (i) reduced exterior column (ii) reduced interior column

3.3.4 G6 with 4.5m storey height (G6SH4.5)

The hinge mechanism of a 4.5m storey height of the G6 building is presented in Figure 3.16. Similar to lower-storey height buildings, extensive damage upto third storey beams is observed where beams are in the peak strength range of the backbone curve. Furthermore, columns have yielded up to the third storey.

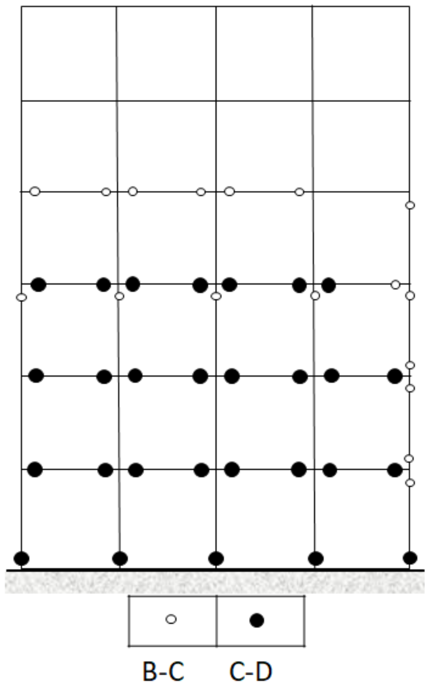

Figure 3.16: Hinge mechanism of G6SH4.5 building at the pushover step corresponding to 85% strength drop

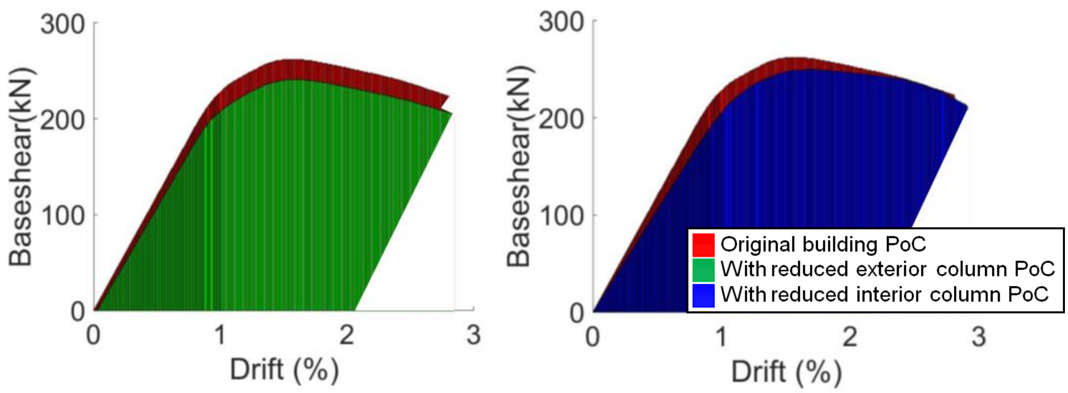

Figure 3.17: Comparison of G6SH4.5 building capacity curve with another capacity curve of 6 storey building with (i) reduced exterior column, (ii) reduced interior column

The capacity curves for RECL and the original building are plotted in Figure 3.17. The difference in the area under the curve is 8%, indicating energy dissipation capacity due to the reduced exterior column section. Capacity curves for RICC and the original building are also plotted in Figure 3.17 (ii). The difference in areas under the curve is 2.5%, and the same values are tabulated in Table 3.2. It is observed that both exterior and interior columns contribute in a similar range. As stated in the previous section, due to flexible columns, fewer moments are attracted to columns. Exterior columns have become less deficient due to reduced demands. However, the significance of exterior columns is reduced; it is still higher than interior columns.

3.3.5 Discussions

The G6 building is analyzed with 3, 3.5, 4, and 4.5m storey heights to understand the effect of increasing story height. Damage contribution of exterior and interior columns in all cases are plotted in Figure 3.18. It is observed that exterior weightage is significantly higher for 3m and 3.5m storey heights. As the storey height increased to 4 and 4.5m, the difference in weightage between exterior columns and interior columns reduced; however, exterior columns still hold higher weights than interior columns. Hence, it is concluded that as storey height increases, exterior columns continue to be higher weighted members; however, quantitative significance is reduced due to flexible columns attracting lesser moments.

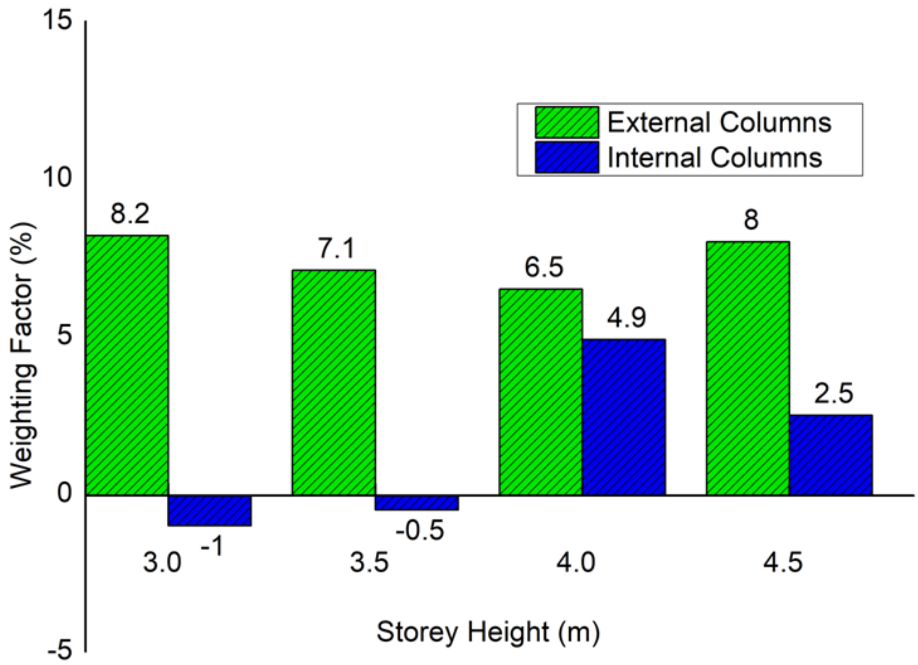

Figure 3.18: Weightage of exterior and interior columns of G6 building with increasing storey height.

3.4 Validation of methodology - Non-Linear Time History Analysis

GLD building is strengthened at exterior columns in one case and interior columns in another, denoted as '*ECS*' and '*ICS*'. The third case is the original GLD building. Strengthening is done by concrete jacketing of columns. At least 100 mm is increased on all four sides of the section, as recommended in IS 15988:2013 (IS 15988:2013, 2013). Sizes of strengthened buildings *ECS* and *ICS* are given in Table 3.3. Non-linear time history analysis of strengthened and original buildings is attempted to understand the effectiveness of concrete jacketing of exterior columns. Eleven earthquake ground motions are selected as per the guidelines in ASCE 7 (ASCE/SEI-7-16, 2017) for the non-linear time history analysis. The time history and Fast Fourier transforms of these ground motions are shown in Figure 3.19 a)~k). Earthquakes are selected such that building fundamental frequency lies in the predominant frequency range of earthquake ground motions, as shown in Figure 3.19. The PGA of earthquakes selected ranges from 0.016g to 0.57g. For Non-linear time history analysis, PGA is scaled to 0.36g to match zone V as per IS 1893:2016. However, it was observed that further scaling is required in Northridge and Chichi to observe damage in the building. Therefore, as per the latest PGA proposal for the Himalayan region by Sreejah et al. (2022), scaling is done till 0.6g (Sreejaya et al., 2022).

When a scaled ground motion is subjected to the building, seismic energy is fed into the structure. Seismic energy has various components, i.e., kinetic energy, elastic strain energy, hysteretic energy, and structural damping energy. Hysteretic energy is also a parameter for measuring the damage potential of a building (Akiyama, 1985). Further energy balance equations have been derived using different types of energies (Uang and Bertero, 1988). Hysteretic energy can be calculated by computing the area under the hysteresis loops in each cycle of seismic loading. However, it is a tedious and complex process to compute for the entire building subjected to the earthquake ground motion. Therefore, this study calculates hysteretic energy as the difference between the earthquake input energy and the other components.

Table 3.3: Section sizes and reinforcement details of strengthened buildings

G6	Original Column Section sizes (mm)	Original Column r/f (%) (1,2)(3,4)(5,6) storey levels	Column stirrup r/f	Strengthened Column Section sizes (mm)	Strengthened Column r/f (%) (1,2)(3,4)(5,6) storey levels	Column stirrup r/f
Exterior Column	230x270	(3.2)(3.2)(2)	6Φ 170mm c/c	430x470	(1.6)(1.6)(1.3)	8Φ 100mm c/c
Interior Column	280x390	(3.5)(2.3)(1.4)	6Φ 200mm c/c	480x590	(1.8)(1.3)(1.1)	8 Φ 100mm c/c

Energies can be calculated from the direct integration method. For a single degree of freedom system, energy equations are presented below.

Hysteretic Energy $$E_h = E_i - E_k - E_d - E_s \tag{3.1}$$

Kinetic Energy $$E_k = \int_0^u m\ddot{u}du = = \int_0^t m\ddot{u}\dot{u}dt = \frac{1}{2}m\dot{u}^2 \tag{3.2}$$

Damping Energy $$E_d = \int_0^t c\dot{u}^2dt \tag{3.3}$$

Strain Energy $$E_s = \int_0^u k_t u du \tag{3.4}$$

Input Energy $$E_i = -\int_0^u m\ddot{u}_g du \tag{3.5}$$

where m =mass of SDOF system; u =displacement; $\dot{u}$ and $\ddot{u}$ are velocity and acceleration of SDOF system; c =damping coefficient; k =tangent stiffness to the system.

A comparison of all three cases of Type G building is made by computing hysteretic energy from the method mentioned above using SAP2000 v23.3.1. The plot of hysteretic energy dissipated in the original building GLD, ICS, and ECS buildings at every time step in each earthquake time history is plotted in Figure 3.20 & Figure 3.21 a). Jumps in the horizontal line of hysteretic energy indicate energy dissipation in the formation of hinges in beams and columns as shown in Figure 3.20 & Figure 3.21 b), c) & d) corresponding to each earthquake ground motion.

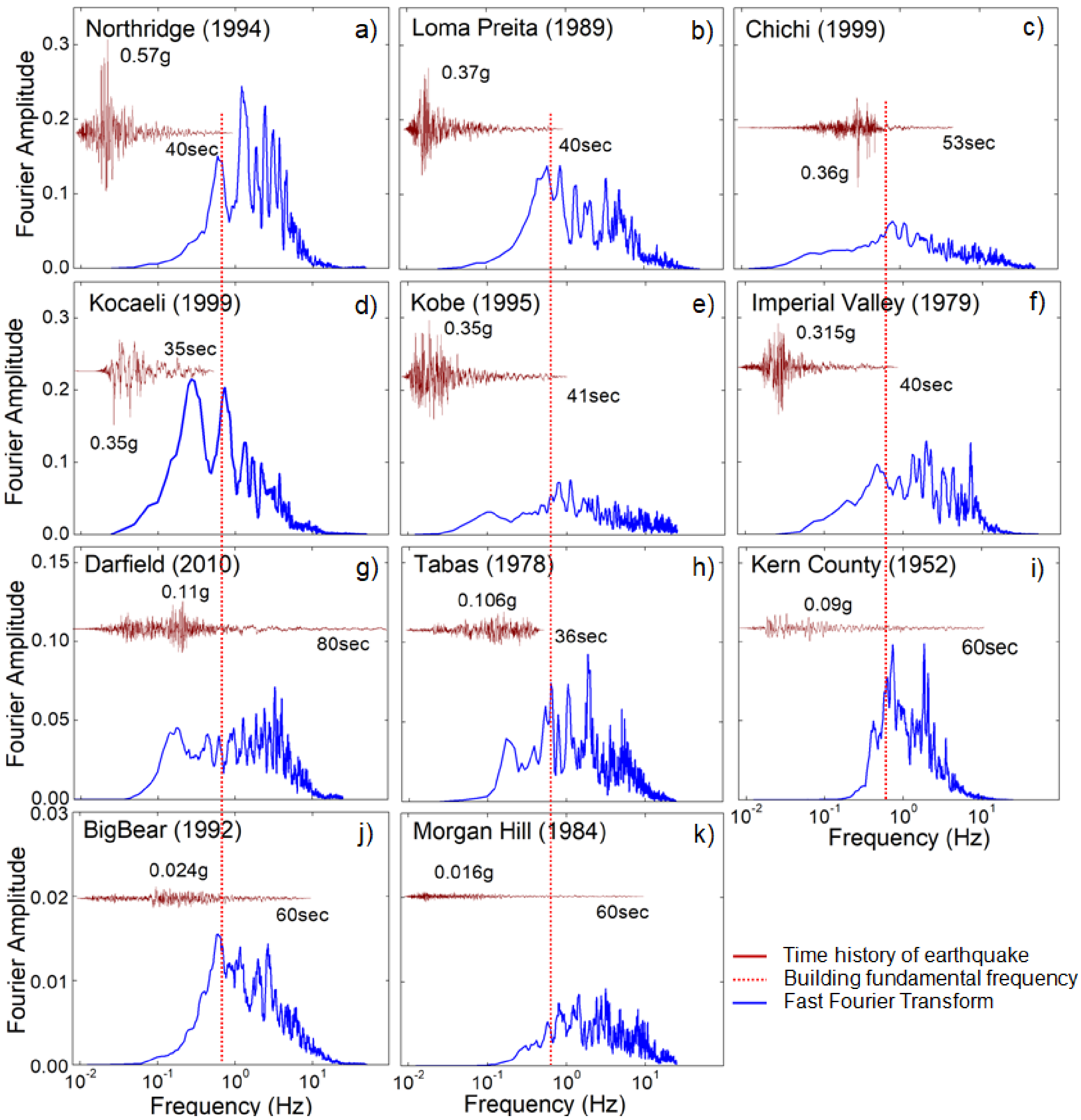

Figure 3.19: Fast Fourier Transform of earthquakes

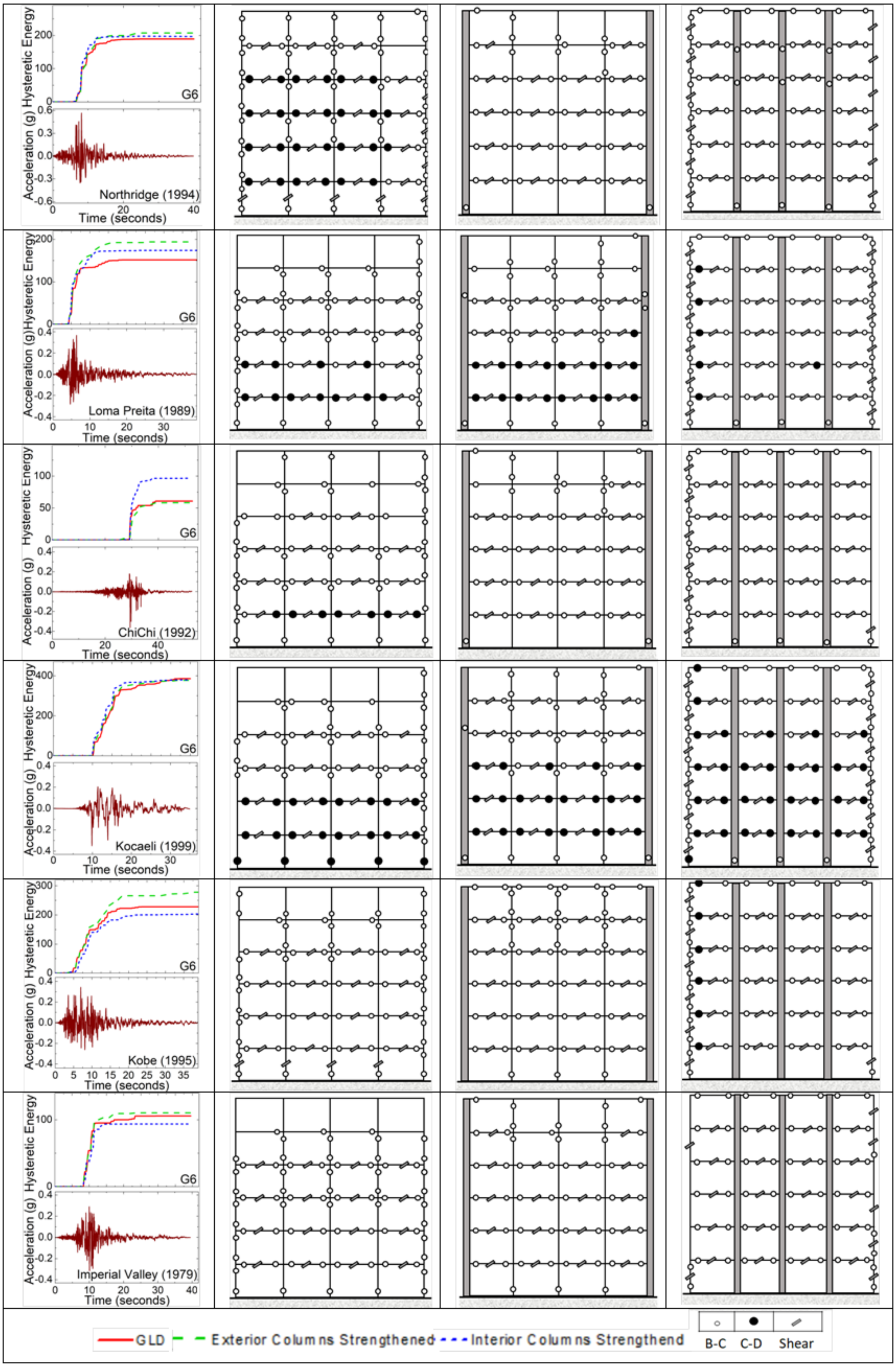
Hysteretic Energy
Acceleration (g)
Time (seconds)
G6
Northridge (1994)
Loma Preita (1989)
ChiChi (1992)
Kocaeli (1999)
Kobe (1995)
Imperial Valley (1979)
GLD
Exterior Columns Strengthened
Interior Columns Strengthend
B-C
C-D
Shear

a) b) c) d)

Figure 3.20: a) Hysteretic Energy dissipation and time history of six earthquake ground motions. Hinge mechanism of b) GLD c) Interior Column Strengthened d) Exterior Column Strengthened type G buildings when subjected to earthquakes

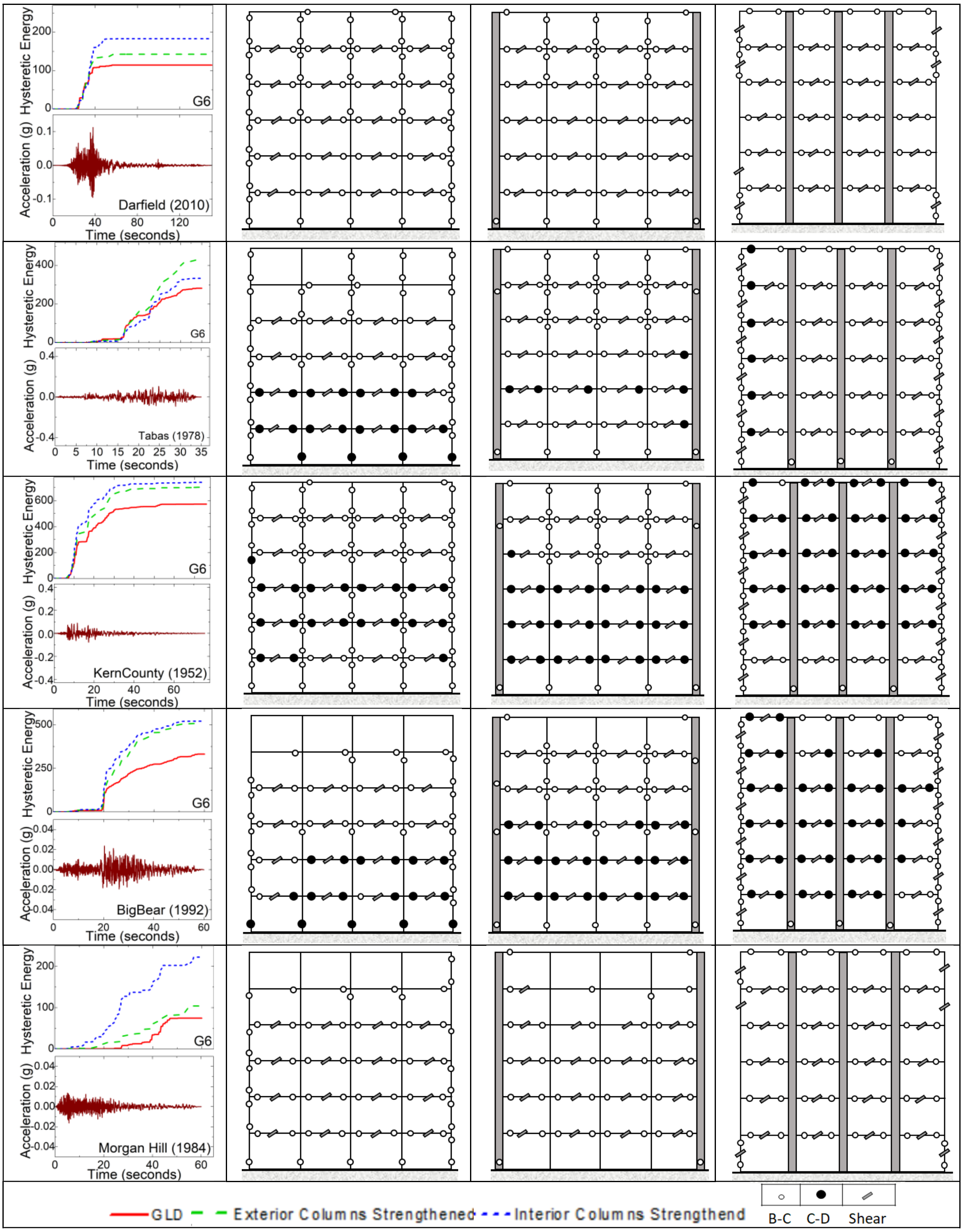

a) b) c) d)

Figure 3.21: a) Hysteretic Energy dissipation and time history of five earthquake ground motions. Hinge mechanism of b) GLD c) Interior Column

Strengthened d) Exterior Column Strengthened Type G buildings when subjected to earthquakes

When the original building is subjected to the Northridge (1994), Chichi (1999), Kocaeli (1999), and Morgan Hill (1984) earthquake, flexure hinges formed in exterior and interior columns. After exterior column strengthening, however, hysteretic energy remained almost the same but hinges redistributed to beams and interior columns along with yielding of some exterior columns as shown in Figure 3.20 and Figure 3.21c). This is a seismically desirable behavior. After interior column strengthening, either there is some increment or no change in hysteretic energy, however in all cases exterior columns failed in shear, indicating this is not a preferable strengthening solution. Therefore, due to the redistribution of hinges in beams, ECS is a preferred strengthening scheme to start with and exterior columns are given higher weightage.

When the original building is subjected to Loma Preita (1989), Kobe (1995), Imperial Valley (1959), Darfield (2010), Tabas (1988), Kern County (1952) and Big Bear (1992) earthquake, flexure hinges are formed in all exterior and some interior columns. In the ECS building, hysteretic energy increased as hinges shifted from exterior columns to beams. This is a seismically good behavior where beam capacity is utilized prior to columns, and more hysteretic energy dissipation is observed as plotted in Figure 3.20 a) and Figure 3.21 a). In the ICS building, in some cases, hysteretic energy increased, and in some cases, it decreased; however, both are not desirable as there is shear hinge formation in exterior columns. Therefore, ECS is a better option to quickly upgrade the seismic safety of the building by redistributing the damage to beams. Therefore, this reinforces the proposal of higher weightage of exterior columns.

It is observed that strengthening redistributed the damage and utilized the redundant non-linear capacity of beams prior to the columns. This is the desired seismic behavior of a building, and in many cases, ECS dissipates higher hysteretic energy. Hence, exterior columns shall be given higher weightage in the strengthening sequence. This observation from non-linear time history analysis supports the higher weightage of exterior columns than the interior columns, as concluded in Section 3.2 with the proposed methodology from NSA.

3.5 Summary

This case study is conducted to study the weightage of interior and exterior columns of regular gravity load-designed buildings. The structural members shall be strengthened in a sequence of higher weightage with the idea of strengthening the most crucial member first. With this philosophy, NSA is performed to compute the energy dissipation capacity of the building for weightage calculation. To establish results firmly, non-linear time history analysis is performed on the original and strengthened building to observe the behaviour in a real earthquake. Parametric variation is done by increasing axial loads due to increasing building height and by increasing storey height. It is observed how the weights of exterior and interior columns are affected.

1. The effect of axial load on the weightage of interior and exterior columns is studied by changing the number of stories, i.e., G4, G6, G8, G10. For G4, G6 and G8 buildings, exterior columns have higher weightage in the energy dissipation capacity of the building. Axial stress distribution on exterior columns is more due to lateral load. Therefore, in Type G buildings where exterior columns are significantly under-designed for lateral forces, strengthening them increases the overall strength of the building. However, in the G10 building, the weights of columns could not be computed as significant energy dissipation was due to beams.

2. The effect of increasing storey height is also studied where G6 building is analyzed with 3, 3.5, 4, and 4.5m storey heights. It is observed and concluded that, as storey height increases, quantitatively weightage of exterior columns reduces as the difference between the weights of exterior and interior columns reduces. However, exterior weightage is still higher as they demonstrate a huge deficiency. Therefore, the exterior column shall be strengthened first to start strengthening sequentially, irrespective of the storey height.

3. For verification of NSA methodology, non-linear time history analysis is performed for eleven earthquakes. The building is strengthened at the exterior and interior columns separately. Because of a seismically desirable behavior of redistribution of damage to beams in the case of strengthened exterior columns, it is concluded that exterior columns have a higher weightage. Also, beam damage prompted higher hysteretic energy dissipation in many cases. Therefore, the results supporting higher weightage for exterior columns obtained from the proposed NSA methodology hold good.

4 WEIGHTING FACTORS FOR EXTERIOR AND INTERIOR COLUMNS OF TYPE P BUILDINGS

The methodology to compute weights of exterior and interior columns remains the same as proposed for Type G buildings. For each precode building of IS 1893, four capacity curves are obtained, i.e., one original capacity curve and three reduced section capacity curves for RECL, RECR, and RICC. The energy dissipation capacity of all three reduced cases is subtracted from the original building energy dissipation capacity. Reduction in energy dissipation capacity of the building is observed due to reduced exterior and interior columns. The higher the reduction in energy due to the reduced section, the higher its contribution and hence a higher weighting factor. Weighting factors of exterior and interior columns may vary as the axial load on columns increase with an increasing number of stories and may also get affected by an increase in the storey height of the building.

4.1 Effect of Axial Load P1

Three buildings of 4, 6, and 8 stories termed P4, P6, and P8 are designed and analyzed to study the effect of increasing the axial load on columns with increasing stories. Nonlinear static pushover analysis is performed to obtain the capacity curve of the original buildings. Further exterior and interior columns are reduced in sections, respectively, to obtain capacity curves of RECL, RECR, and RICC. With the computed capacity curves, weights for exterior and interior columns are computed in the following sections.

4.1.1 Precode building of IS 1893 – 4 storey (P4)

On nonlinear static analysis of a 4-storey precode building, it is observed that first, second, and third-storey columns and beams are damaged, as shown in Figure 4.1. At the pushover step corresponding to 85% strength drop, columns are nearby peak point ‘C’ (Figure 2.2), represented in green colour in the hinge backbone curve. Whereas first storey beams are in the strength degradation zone between C and D. Rest of the energy is dissipated through second and third storey columns and beams. In this building, energy is getting dissipated through beams and columns both. To compute the contribution of exterior and interior columns in the energy dissipating capacity of the building, exterior and interior columns are reduced, respectively. As described previously, three more nonlinear static analyses are performed with reduced column sections of the exterior left, right, and interior center column termed RECL, RECR, and RICC. The building's energy dissipation capacities are calculated by calculating the area under the curves. Capacity curves of RECL, RECR, and RICC are subtracted from the original building capacity curves to compute the effect of exterior and interior columns separately.

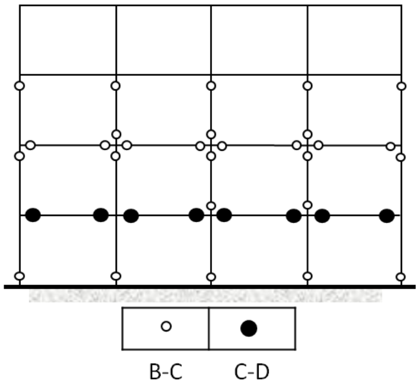

Figure 4.1: Hinge mechanism of P4 building at the pushover step corresponding to 85% strength drop

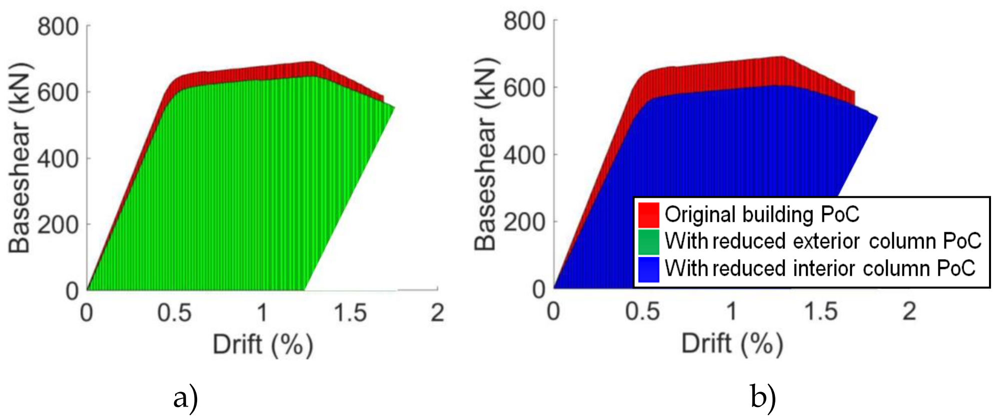

Figure 4.2: Comparison of P4 building capacity curve with another capacity curve of 4 storey building with a) reduced exterior column b) reduced interior column

It is observed that the energy dissipation capacity of the building is marginally affected by 1.4% when the exterior left column is intentionally reduced by 50% in yield strength in the case of RECL. The capacity curve for RECL is plotted in Figure 4.2 a) in green colour and is compared with the original curve plotted in red in Figure 4.2 a) and b). Similarly, in the case of the RICC section, the energy dissipation capacity of the building is reduced by 4.6% by the interior column is reduced intentionally. The capacity curve is plotted in blue (Figure 4.2 b) and compared with the original building capacity curve plotted in red. In both cases, it is observed that the capacity of the building reduced, but ductility increased. Therefore, energy dissipation capacity, i.e., the area under the PoA curve, remained almost the same. Reductions in the energy-dissipating capacity of the building obtained from subtracting area under the curves from Figure 4.2 a) and b) are tabulated in Table 4.1. The energy dissipation capacity of the building is reduced less than 5% with a reduction in interior and exterior column sizes. Minimal contribution indicates that this methodology can not be used for weightage calculation.

Table 4.1: Reduction in energy dissipation capacity of type P buildings with increasing axial load

Building Name	Exterior Column Left (%)	Interior Column Centre (%)	Exterior Column Right (%)
P4	0.1	4.3	1.4
P6	4	-3	0.1
P8	1.1	-5	0.4

4.1.2 Precode building of IS 1893 - 6 Storey (P6)

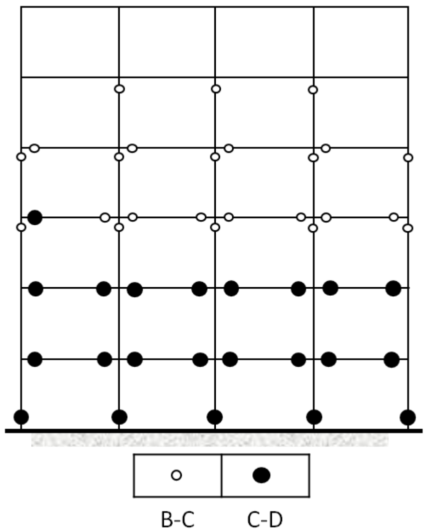

Figure 4.3: Hinge mechanism of P6 building at the pushover step corresponding to 85% strength drop.

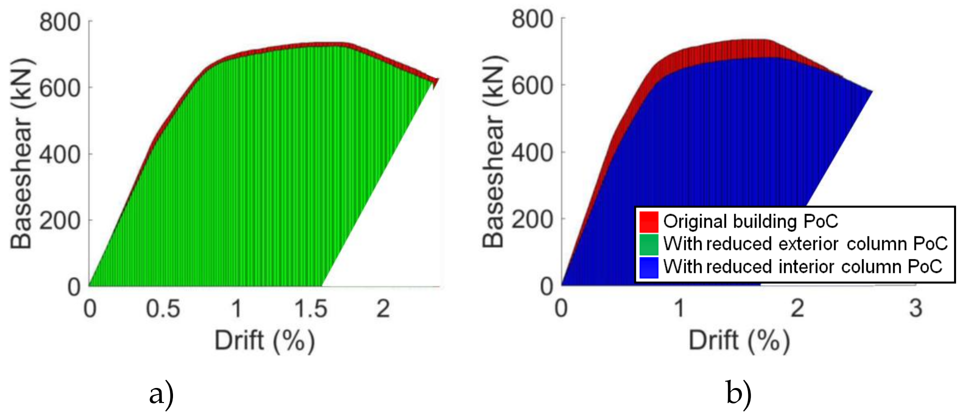

Figure 4.4: Comparison of P6 building capacity curve with another capacity curve of 6 storey building with a) reduced exterior column b) reduced interior column

In this case, the first storey columns are in the strength degradation zone, and the third, fourth, and fifth are between 'B' and 'C'. At the last point of PoA, which is 85% strength drop, the first and second-storey beams exhibit strength degradation behaviour as they lie between points C and D in the hinge backbone curve. Hinges of third and fourth storey beams lie between points B and C. Both beams and columns share the energy dissipation capacity in this case. To further study its division between exterior and interior columns similar study of reduced exterior and interior column section sizes is done.

Nonlinear static analysis for three cases, RECL, RECR, and RICC, as described earlier, is carried out. In the case of RECL, the 4% contribution of exterior columns in the energy dissipation capacity of the building is calculated from Figure 4.4 a) and tabulated in Table 4.1. It is observed that in this case, the effect of exterior and interior columns is negligible on the global energy dissipating capacity of the building. A small contribution of less than 5% indicates that this methodology can not be used for weight computation.

4.1.3 Precode building of IS 1893 - 8 Storey (P8)

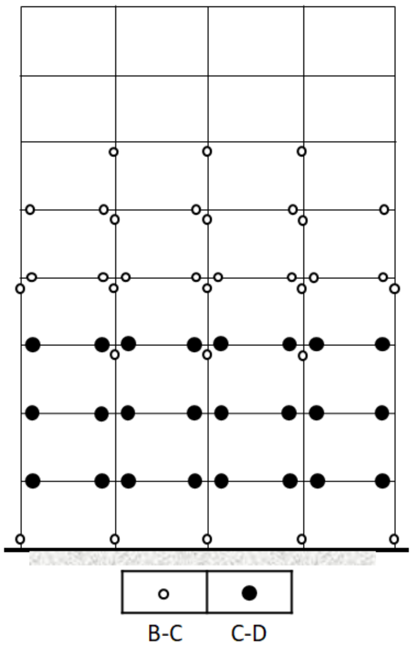

Figure 4.5: Hinge mechanism of P8 building along with M-θ of the beam and exterior columns, respectively.

In 8 storey building of type P, first, fourth, fifth, and sixth-storey columns yielded. Beam hinges in the 1st, 2nd, 3rd, and 4rth storey lie between points C and D in the hinge backbone curve, indicating severe damage and huge energy dissipation. Nonlinear static analysis for three reduced-size cases of exterior and interior columns termed RECL, RECR, and RICC is carried out. The reductions in energy dissipation capacity of the buildings in three cases calculated from Figure 4.6 are less than 5% and are tabulated in Table 4.1. It is observed that there is energy dissipation from beams and columns. However, their failure does not have an impact on the global stability of the building. Minimal contribution indicates that this methodology can not be used for weight compuation.

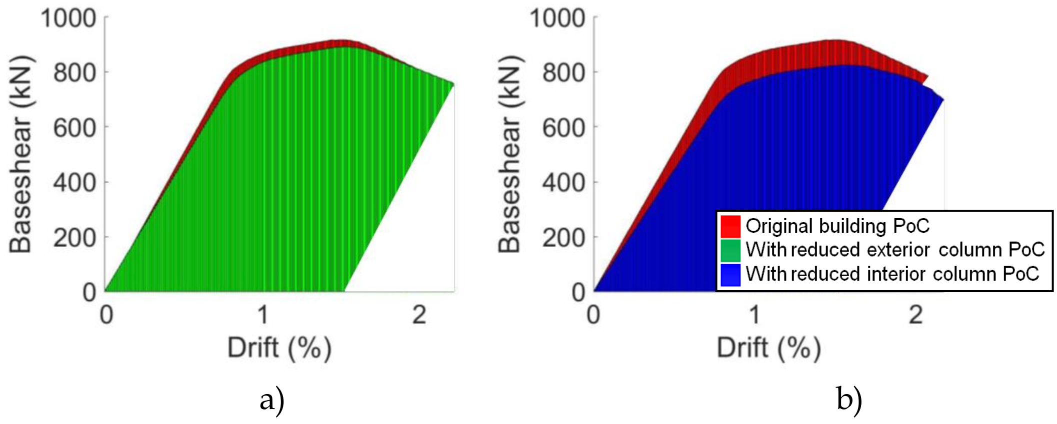

Figure 4.6: Comparison of P8 building capacity curve with another capacity curve of 8 storey building with a) reduced exterior column b) reduced interior column

4.1.4 Discussions

Less reduction in global energy due to damage of columns may be because no energy is dissipated via that particular member or maybe because there is no highly deficient member like exterior columns in Type G buildings, all load paths are mobilized, and redundancy of the building is being utilized properly. Due to this reason, even if a column is damaged, immediate collapse is not observed. Alternatively, it may be because of lesser energy dissipation locally by that particular member. Therefore, the local energy dissipated by each member is computed by calculating the area under the moment rotation curve of each hinge in the beam and column.

The computation of energy dissipation at the local level shows that the column to beam energy ratio is 1:0.96 for P4, 1:2.2 for P6, and 1:3.6 for P8 buildings. In P4, the amount of energy dissipated in columns is more than the beam. As the height of the building increases, i.e., in P8, more energy dissipation is in beams. Therefore, it is demonstrated that even though some amount of energy is dissipated via columns in 4 storey building, their damage does not impact the global damage index much. This indicates that precode buildings can use different load paths due to redundancy, unlike GLD buildings, as there were highly deficient exterior columns for seismic loading.

4.2 Summary

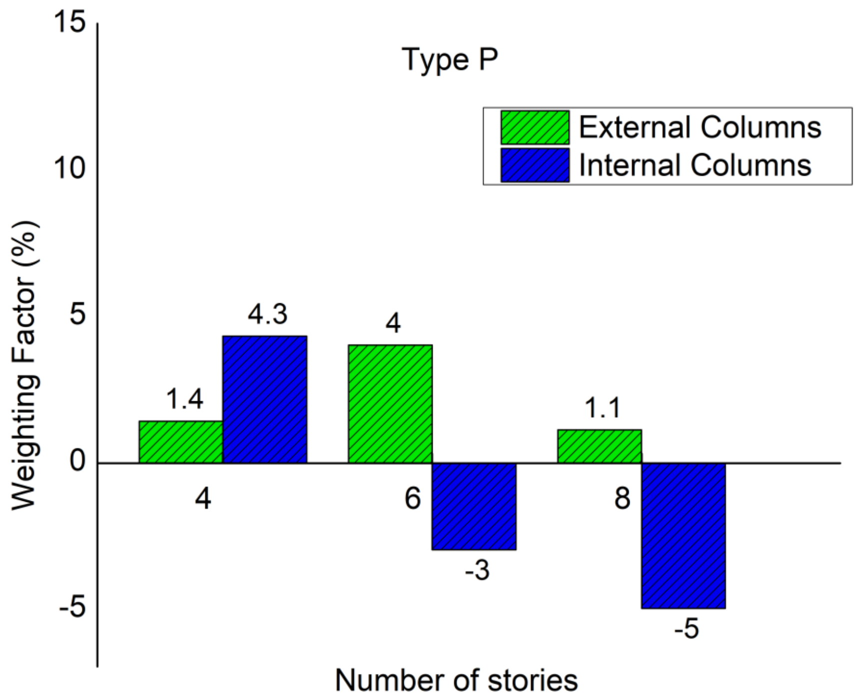

Figure 4.7: Exterior and Interior column weighting factors with the increasing number of stories

Exterior and interior column weighting factors are computed with the same methodology using non-linear static analysis as proposed in section 3.1 and verified with non-linear time history analysis in section 3.4. Weights computed for P4, P6, and P8 buildings are plotted in Figure 4.7. Since weights are less than 5%, it is concluded that numbers are quite less to compute the significant contribution of either the exterior or interior column. When columns are intentionally damaged, no impact on the global damage index of the building is observed. Redundancy is being utilized better in Type P buildings as there is no extremely deficient member like exterior columns in Type G buildings, hence all loads paths can be mobilized. Due to this, global weightage numbers are less than 5%. Therefore, damage to exterior or interior columns had negligible impact on the global damage of the building. Weights could not be computed from this methodology.

5 STOREY-WISE DAMAGE CONTRIBUTION FOR TYPE G BUILDINGS

Each storey contributes to global damage; however, contribution may vary depending upon its location and the type of building. To study the damage contribution of each storey of Type G building, two parameters, i.e., variable number of stories and variable storey height, have been chosen. Non-linear static analysis is performed to observe the hinge mechanism in each storey for lateral loading. The hinge mechanism indicates the damage progression in the building. Since energy is chosen as the damage quantification parameter, energy dissipated in each hinge of a storey is computed to quantify the contribution of a storey.

5.1 Methodology for storey-wise damage contribution

The area under the moment rotation curve of a hinge gives energy dissipated in the formation of that hinge. This calculation is done for the hinges formed in beams and columns of each storey to calculate the storey damage via energy dissipation. Similarly, damage in the whole building can be calculated. The ratio of storey damage to the entire building damage computes the contribution of each storey. The contribution of each storey is computed at five stages till the last step of the pushover curve to understand the progress of damage. Three main stages are at steps where (i) yielding starts, (ii) ultimate strength is achieved (iii) at the last step of POA. Two intermediate stages are defined to understand the progress of damage to the ultimate and last steps of POA, respectively. These five stages, denoted with letters A to E, are shown in Figure 5.1.

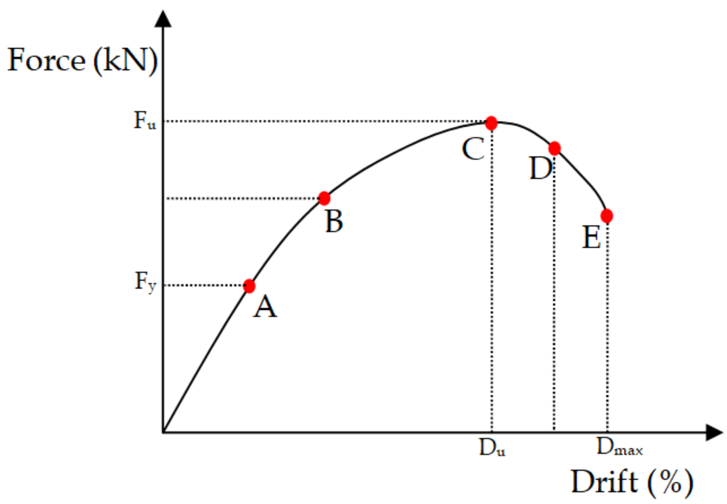

Figure 5.1: Different stages considered for weights computation in the pushover curve

Stage A marks the initiation of yielding, stage C marks the ultimate strength of the building, and stage E marks the last step of pushover analysis. Stage B marks the middle point of yielding strength and ultimate strength. Stage D marks the middle point of deformation corresponding to the ultimate strength and maximum deformation. The contribution of each storey (E_s) in damage is calculated by the ratio of energy dissipated by each storey divided by the total dissipated energy (EB) of the building.

Contribution of nth storey = E_{sn}/ E_B

5.2 Effect of Axial load

The effect of increasing the axial load on the storey weightage is captured by considering buildings with an increasing number of stories. Four buildings of different heights, 4, 6, 8, and 10 storey, are considered in this study. Storey weights are computed in all cases to understand how storey weights changed as the building height increased. Each storey comprises columns and the beams on top of those columns. The area under the moment rotation curve is computed for all members of the storey to compute the storey damage. Total damage in the building is computed by computation of the percentage damage contribution of each storey. Damage contribution of each storey in each building is computed at B, C, D & E, considering damage at E as 100% and at A as just started with the first hinge. Table 5.1 summarizes each story's damage contribution in four buildings at stage B and indicates less than 10% damage in all buildings. As pushover progress to stage C, which is the ultimate strength stage, it is observed that there is more than 50% damage in G4 and G10; however, less than 50% in G6 and G8 (Table 5.2). Damage in all buildings at stage D increased to more than 70%. The contribution of each storey is tabulated in Table 5.3. The last step of pushover analysis which is at 85% strength drop, is assumed to be 100% damage. The contribution of each storey in 100% damage is tabulated in Table 5.4.

Table 5.1: Storey-wise comparison of damage in type G buildings with increasing axial load at stage 'B' in the capacity curve.

Storey Height	**G4** **5%**	**G6** **3%**	**G8** **3.5%**	**G10** **6.6%**
Tenth Storey				-
Ninth Storey				-
Eight storey			-	-
Seventh Storey			-	-
Sixth storey		-	-	0.4
Fifth Storey		-	-	1

Fourth Storey	-	-	-	1.5
Third Storey	0	0.8	0.6	1.7
Second Storey	0	1.5	0.4	1.5
First Storey	4	1	0.1	0.4

Table 5.2: Storey-wise comparison of damage in type G buildings with increasing axial load at stage 'C' in the capacity curve.

Storey Height	**G4** **73%**	**G6** **48%**	**G8** **49%**	**G10** **65%**
Tenth Storey				-
Ninth Storey				-
Eight Storey			-	0
Seventh Storey			-	2
Sixth storey		-	-	7
Fifth Storey		-	1	11
Fourth Storey	0	2	7	14
Third Storey	5	8	12	15
Second Storey	14	18	14	13
First Storey	53	21	15	12.8

Table 5.3: Storey-wise comparison of damage in type G buildings with increasing axial load at stage 'D' in the capacity curve.

Storey Height	**G4** **88%**	**G6** **79%**	**G8** **74%**	**G10** **90%**
Tenth Storey				-
Ninth Storey				-
Eight Storey			-	1.7
Seventh Storey			-	2
Sixth storey		-	-	12
Fifth Storey		-	1	14
Fourth Storey	2	2	6	16
Third Storey	15	15	17	16
Second Storey	14	26	22	14
First Storey	69	36	28	14

Table 5.4: Storey-wise comparison of damage in type G buildings with increasing axial load at stage 'E' in the capacity curve.

Storey Height	G4 100%	G6 100%	G8 100%	G10 100%
Tenth Storey				-
Ninth Storey				-
Eight Storey			-	8
Seventh Storey			-	1
Sixth storey		-	0	18
Fifth Storey		-	1	17
Fourth Storey	1	1	7	17
Third Storey	4	18	20	15
Second Storey	13	30	28	12
First Storey	83	51	43	13

From stage E, it is observed that damage is concentrated at the ground storey in G4 building up to 83% (Table 5.4). In G6, the maximum damage is in the ground storey up to 50%; in G8, the maximum damage in a storey is 43%. In the G10 building, the maximum damage in a storey is 18%. Therefore, it is observed that as building height increases, damage concentration in a single storey is reduced from 83% to 18% as it is distributed to more stories in higher buildings. The trend stays the same in all stages.

To understand why damage is progressing to upper stories in G10 building and not concentrated on the ground floor like in G4, G6 and G8, storey weights are rearranged stage-wise for each building. Damage progression and distribution are studied in buildings of variable height.

5.2.1 Storey-wise damage progression in G4

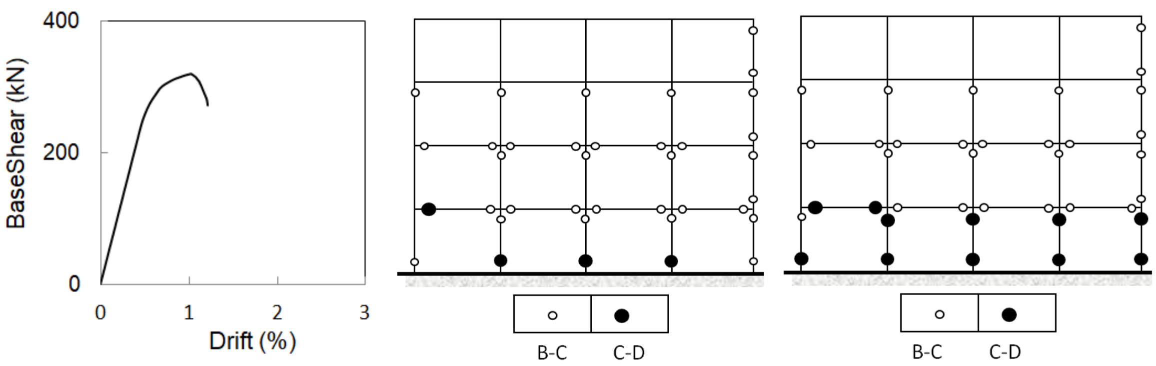

a) b) c)

Figure 5.2: Pushover curve for G4 building along with hinge states at C and E, respectively

Storey weights computed in the previous section are rearranged stagewise for the G4 building and are tabulated in Table 5.5. The first story is observed to be damaged more than 50% at stage C, and damage increased to 83% in stage E. Second storey is damaged up to 13% in stage E. Therefore, almost the entire damage is concentrated in the first storey.

Table 5.5: Damage contribution of each storey in each stage of the pushover curve of the G4 building

Damage	**A 0.001%**	**B 5%**	**C 73%**	**D 88%**	**E 100%**
Fourth Storey	-	0	0	2	1
Third Storey	-	0	5	5	4
Second Storey	0.001	1	14	14	13
First Storey	-	4	**53**	**69**	**83**

The transition of damage from B to C is observed to understand the progression of damage. It is reported that there is a sudden damage increment from 5% to 73% in the building at this stage. On further distribution, it is observed that 30% contribution is from first storey columns and 23% is from first storey beams, and rest 15% is divided to the upper storey. Therefore, a huge damage contribution is from first-story columns. Since the Mc/Mb ratio is 0.4-0.5 for exterior and 0.6-0.9 for interior columns, columns are the first to get damaged. Therefore, the building could not use redundancy due to beams, and damage is concentrated.

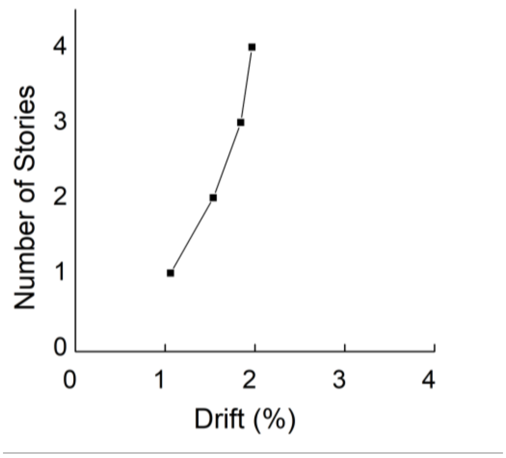

Figure 5.3: Storey deflection of G4 building

Building deflection is plotted in Figure 5.3 to compute interstorey drifts (ISD). To understand why weights are concentrated more in the first storey. ISD at stages A, C, and E are plotted along with the demand capacity ratio (DCR) of exterior columns and weighting factors in Figure 5.4. As the pushover curve progresses from the stage of the first yield point to ultimate capacity, i.e., A to C, it is observed that ISD increases in the first, second, and third storey at stage C (Figure 5.4). However, the maximum increment in ISD is observed in the first storey. The first storey columns at the bottom yielded and initiated redistribution of moments to the top of the first storey columns. The effect of this high ISD in the first storey is reflected in the damage contribution of the first storey, which is 50% at stage C.

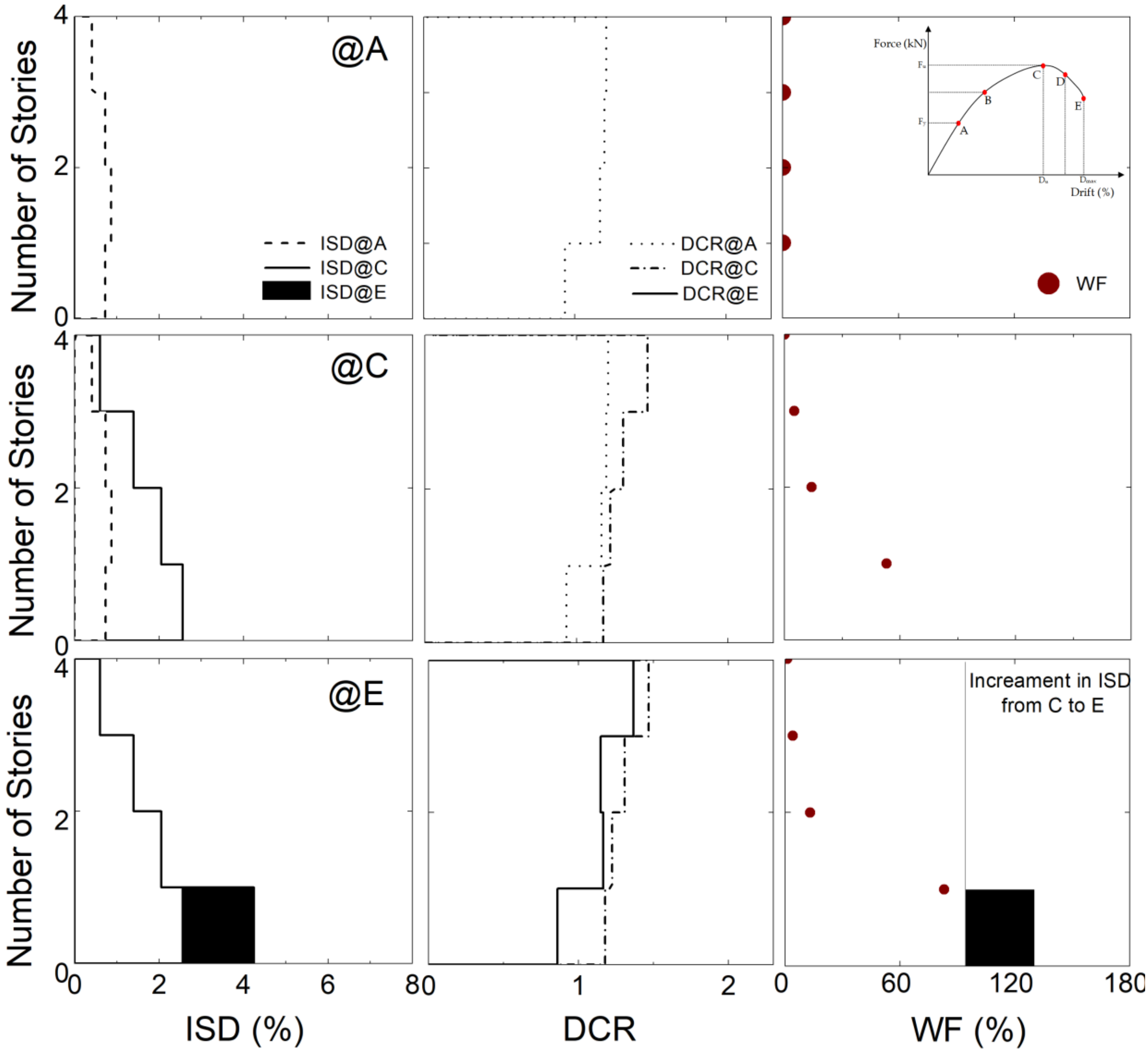

Figure 5.4: Interstorey drift, demand capacity ratio, and weighting factors at different stages of the Pushover curve in the G4 building

Increment in ISD from stage C to stage E is limited to the first storey. The demand capacity ratio (DCR) is reduced in the corresponding storey column at the bottom. This indicates that the column started utilizing nonlinear capacity by deforming more with lesser demands, leading to more damage in the first storey. This demand is redistributed to the top of the first storey column, which crosses the post-peak strength of the column at the top in stage E, as shown in Figure 5.2 (c). In addition, beams of the first storey also crossed post-peak strength and are in the strength degradation zone of the backbone curve, as shown in Figure 5.2 b) and c). They provide less restraint to first storey columns, making them more flexible. Therefore, more damage is observed in the first storey due to flexible columns and their nonlinear behaviour.

An increment in ISD from stage C to stage E in the first storey is observed to trigger an increment in damage contribution in the same storey (shaded in black in Figure 5.4@E). Parabolic damage distribution is observed from the damage percentage of each storey at stage E with maxima of the convex parabola at the bottom storey, as shown in Figure 5.4. Therefore, it is observed that P4 building has parabolic damage distribution with maximum damage at the first storey, as highlighted with a blue trend line in Figure 5.5. The damage contribution of each storey is the damage weightage of that storey. The highest weighting factor is for the first storey, which significantly affects the health of the building.

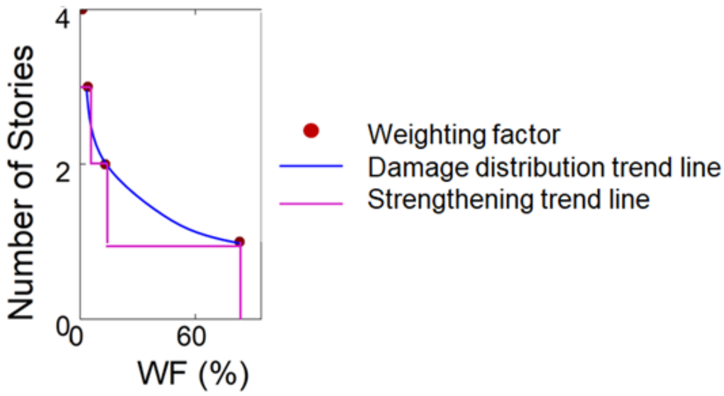

Figure 5.5: Storey weights and proposed strengthening scheme for the G4 building

Therefore, zone-wise strengthening activities shall be proposed in line with the storey weights. Zone 1 is defined as the first storey till one storey above the mid-height of the building. Stepped strengthening is proposed in zone 1, with the maximum at the bottom and the minimum at one storey above the mid-height of the building. The strengthening proposal is shown with a pink line in Figure 5.5. Stepped strengthening shall be done sequentially as per the base shear requirement of that region. After strengthening at the first storey, updated capacity shall be computed. If the updated capacity is less than the base shear, strengthening shall be done at the next storey (Niharika and Ramancharla, 2020).

5.2.2 Storey-wise damage progression in G6

Storey weights are rearranged stage-wise and are tabulated in Table 5.6. It is observed that there is a sudden damage increment of 45% from stage B to stage C. At stage E, more than 50% damage is concentrated in the ground storey, and the rest of the stories get 30% and 18% damage. Hence, the entire damage is distributed in three stories with a 2:1 distribution ratio among beams and columns.

Figure 5.7 presents the deflection profile of the building to compute ISD. To understand the reasoning behind the damage distribution in each storey at each state, ISD, DCR of exterior columns, and damage weights are computed and plotted (Figure 5.8).

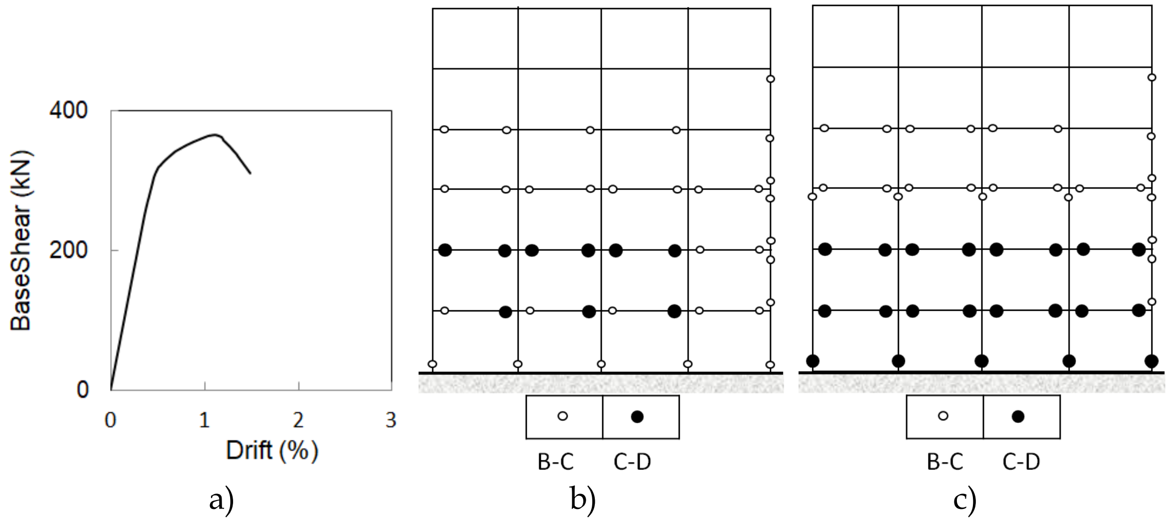

Figure 5.6: Pushover curve for G6 building along with hinge states at C and E, respectively.

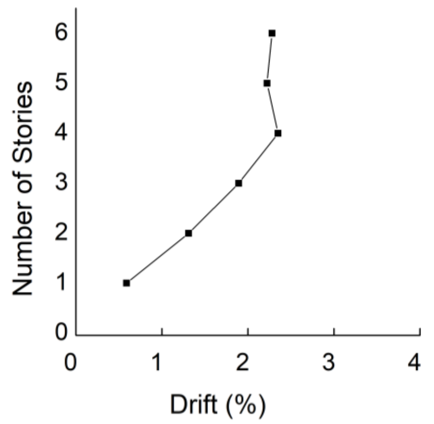

Figure 5.7: Storey deflection of G6 building

Table 5.6: Damage contribution of each storey in each stage of the pushover curve of the G6 building.

Damage	A 0.001%	B 3%	C 48%	D 79%	E 100%
Sixth Storey	-	-	-	-	-
Fifth Storey	-	-	-	-	-

Fourth Storey			2	2	1
Third Storey	-	0.8	8	15	18
Second Storey	0.001	1.5	18	26	30
First Storey	-	1	21	36	51

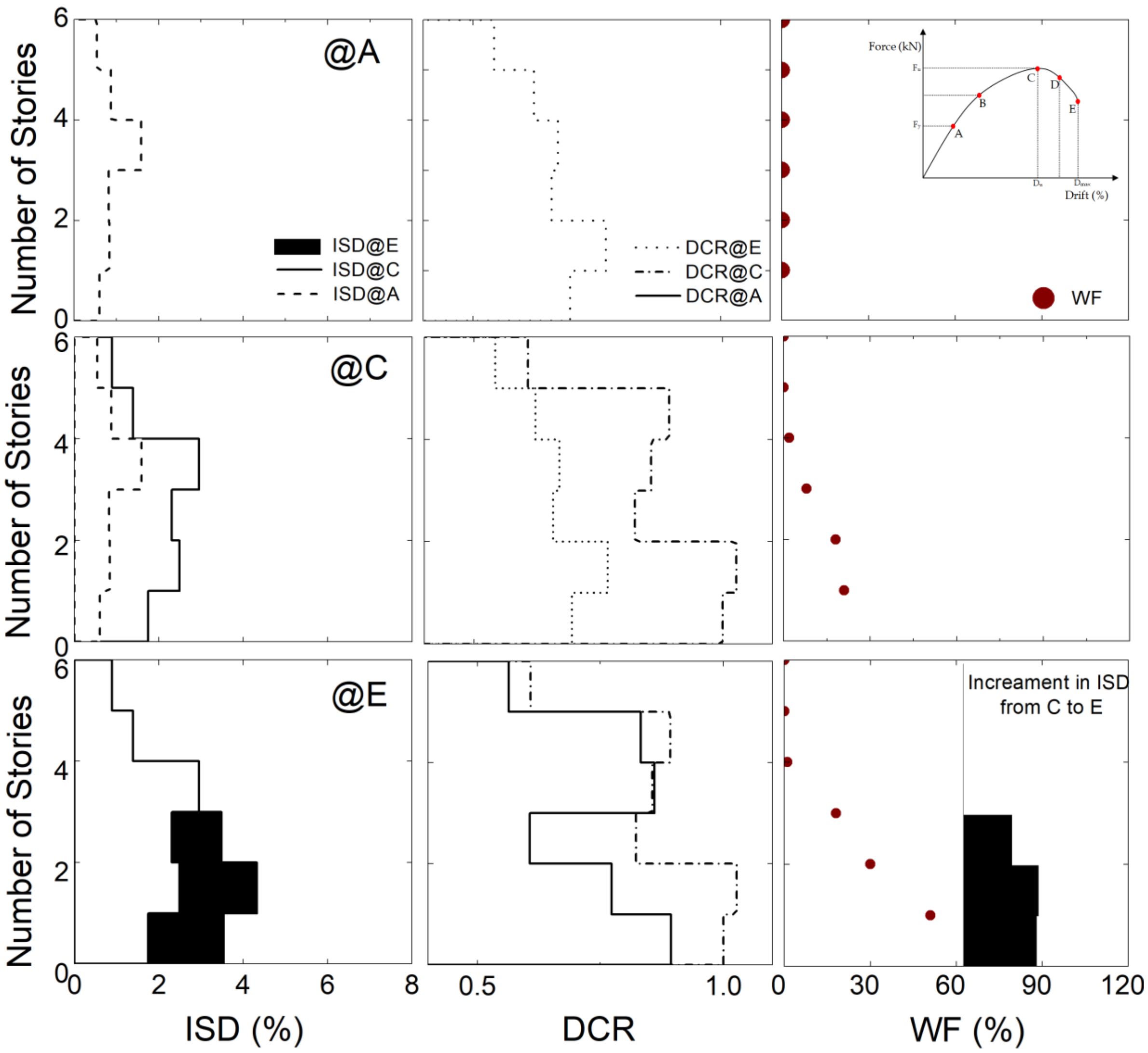

Figure 5.8: Interstorey drift, demand capacity ratio, and weighting factors at different stages of the Pushover curve in the G6 building

As the pushover analysis progresses from stage A to C, it is observed that ISD and DCR increase in all stories due to increasing lateral loads. However, the damage is only observed in the first, second, and third stories.

As the pushover curve progresses from C to E, the increment in ISD is huge in the first three stories. DCR reduced in the same stories in stage E (Figure 5.8). Due to damaged first and second-storey beams, less restraint is provided to columns (Figure 5.6 c)). Flexible columns attract lesser moments, reducing DCR in the bottom two stories. In addition, third-storey columns hinged, increasing the flexibility of columns up to the third-storey. Therefore, the DCR of third-story columns is also reduced. Due to the flexibility of the bottom three storey columns and the nonlinear behaviour of columns, ISD in the bottom three stories is huge. And due to beam damage in the first and second storey and column hinge mechanism in the third storey. Damage weights are high in the bottom three stories. This indicates that members utilize nonlinear capacity by deforming more with the reduced moments, leading to more damage in the first three stories.

As the increment in ISD from stage C to stage E is limited to the bottom three stories (shaded black in Figure 5.8 @E), the damage is also observed in the same stories. The damage is distributed in a parabolic shape with maxima at the bottom storey and minimum significant damage at the mid-height of the building, as shown in Figure 5.8@E. Damage contribution is the damage weighting factor of each storey. Therefore, it is observed that the G6 building distributes damage in a shape similar to a straight line in the transition of a convex parabola to a concave parabola with maximum weightage of damage at the first storey, as highlighted in Figure 5.9.

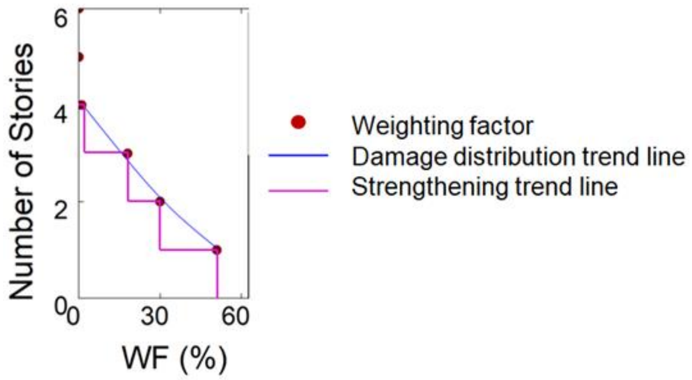

Figure 5.9: Storey weights and proposed strengthening scheme for the G6 building

Hence, strengthening activities shall be proposed zone-wise as per the damage weights. Zone 1 is defined as the first storey till one storey above the mid-height of the building. Therefore, stepped strengthening shall be done in zone 1 with a maximum at the bottom and a minimum at one storey above the mid-height of the building, as shown with the pink line in Figure 5.9. Stepped strengthening shall be done in a sequential manner as per the base shear requirement of that region. If the updated capacity after the first storey strengthening is less than the base shear, this shall be done at the next storey with the reduced amount of strengthening.

5.2.3 Storey-wise damage progression in G8

Storey weights are rearranged in Table 5.7 to understand the damage progression stagewise in the G8 building. It is observed that there is a sudden damage increment of 48% from stage B to stage C. At stage E, around 43% damage is concentrated in the ground storey, and the upper two stories get 28% and 20%

damage. The entire damage is distributed in three stories with a 2:1 distribution ratio among beams and columns. The building deflection profile is plotted in Figure 5.11 to compute ISD. The ISD and DCR of exterior columns are plotted in Figure 5.12 to understand how damage gets distributed to the stories.

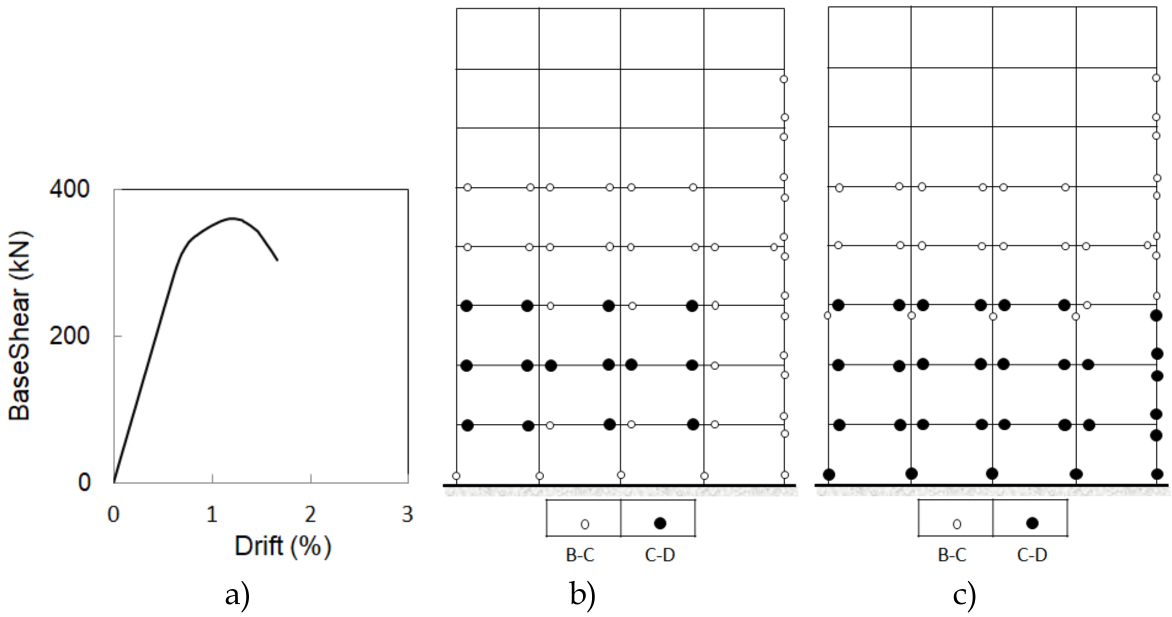

Figure 5.10: Pushover curve for G8 building along with hinge states at C and E

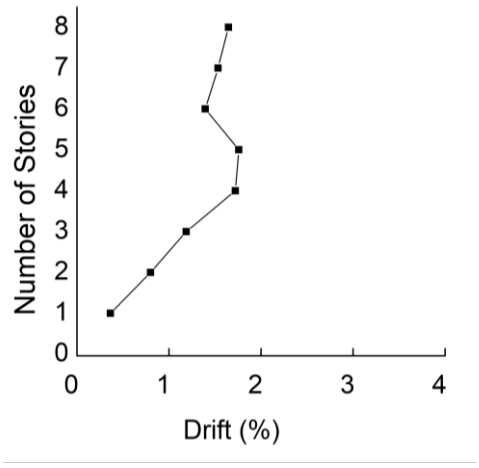

Figure 5.11: Storey deflection of G8 building

Table 5.7: Damage contribution of each storey in each stage of the pushover curve of the G8 building

Damage	A 0.001%	B 1.2%	C 49%	D 74%	E 100%
Eight storey	-	-	-	-	-
Seventh Storey	-	-	-	-	-

Sixth storey	-	0.1	0	0	0
Fifth Storey	-	0	1	1	1
Fourth Storey	-	0	7	6	7
Third Storey	-	0.6	12	17	20
Second Storey	-	0.4	14	22	28
First Storey	-	0.1	15	28	43

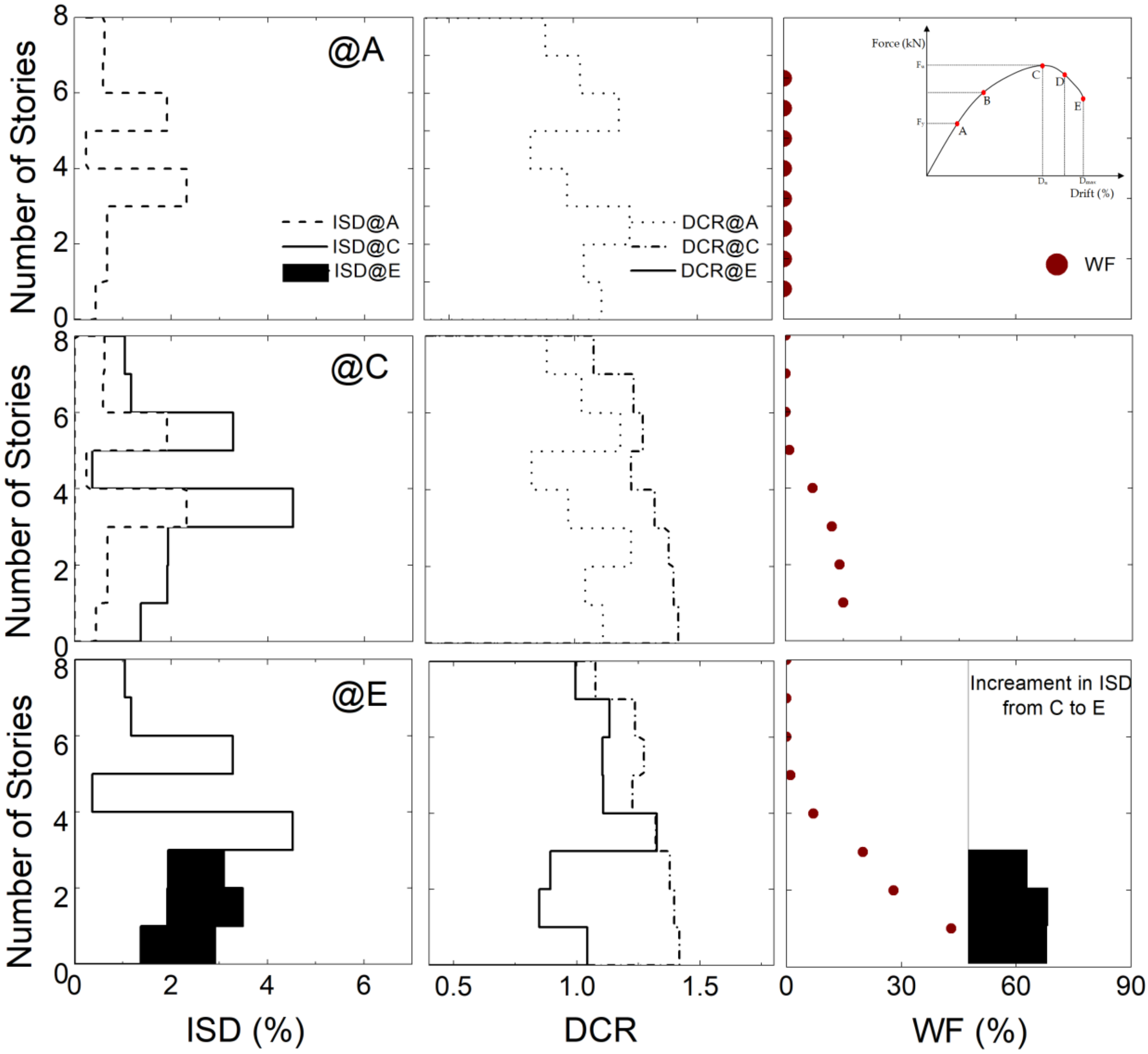

Figure 5.12: Interstorey drift, demand capacity ratio, and weighting factors at different stages of the Pushover curve in the G8 building

As pushover progresses from stage A to stage C, an increment in ISD is observed in all stories, with a maximum in the fourth storey. This led to damage in the first four stories plotted as the damage contribution of each storey (Figure 5.12).

As pushover progresses from stage C to stage E, the DCR substantially reduces in the first three stories. Due to the damaged beams in the bottom three stories, less restraint is provided to the columns leading to flexible columns (Figure

5.10 c)). Due to flexible columns and damaged beams, fewer demand moments are attracted to bottom stories, and hence, DCR in the bottom three stories reduced. DCR reduction is accompanied by the huge increment in ISD from C to E in the bottom four stories shaded in black (Figure 5.12@E). Therefore, damage in the bottom three stories increased further in this stage, with a major concentration in the first storey.

Damage contribution is from the bottom stories with maxima at the bottom storey and minima at the mid-height of the building. Damage distribution is similar to a straight line transitioning from a convex parabola to a concave parabola. The damage distribution pattern is plotted in the blue trend line in Figure 5.13. Damage contribution is the damage weighting factor, and the first storey has the highest weighting factor and hence affects the health of the building more.

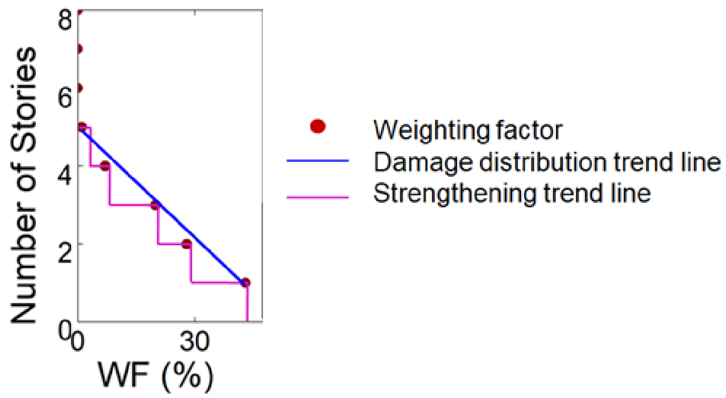

Figure 5.13: Weighting factors and proposed strengthening scheme for the G8 building

Strengthening activities are proposed zone-wise as per the damage weights. Zone 1 is defined as the first storey till one storey above the mid-height of the building. The stepped strengthening in zone 1, as shown with the pink line in Figure 5.13, is proposed. The strengthening is done sequentially as per the base shear requirement of a city.

5.2.4 Storey-wise damage progression in G10

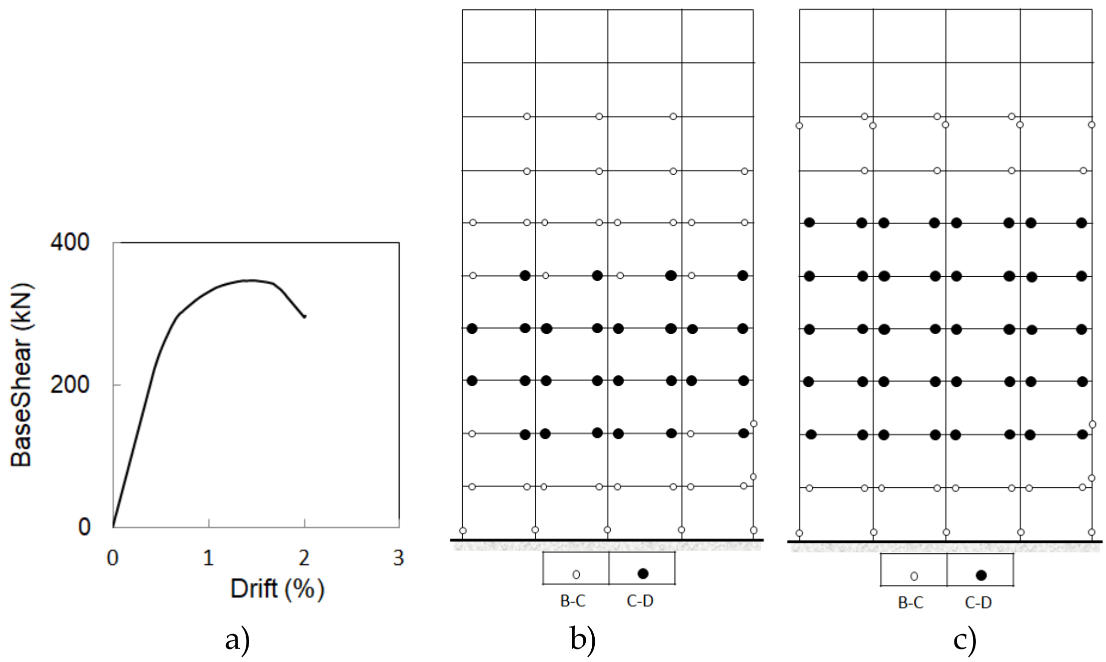

Figure 5.14: Pushover curve for G10 building along with hinge states at C and E

Storey weights are rearranged stagewise for G10 and are tabulated in Table 5.8 to understand the damage progression in each storey. Up to the sixth story, it is observed that up to 20% of damage is distributed in each storey. As building height increases, damage concentration is reduced, and damage gets distributed to upper stories. The building deflection profile is plotted in Figure 5.15 to compute ISD. ISD and the DCR of exterior columns are plotted in Figure 5.16 to understand how damage gets distributed to upper stories.

Table 5.8: Damage contribution of each storey in each stage of the pushover curve of the G10 building.

Damage	A 0.001%	B 6.6%	C 65%	D 90%	E 100%
Tenth Storey	-	-	-	-	-
Nineth Storey	-	-	-	-	-
Eight storey	-	-	0	1.7	8
Seventh Storey	-	-	2	2	1
Sixth storey	-	0.4	7	12	18
Fifth Storey	-	1	11	14	17
Fourth Storey	-	1.5	14	16	17
Third Storey	-	1.7	15	16	15
Second Storey	-	1.5	13	14	12
First Storey	-	0.4	12.8	14	13

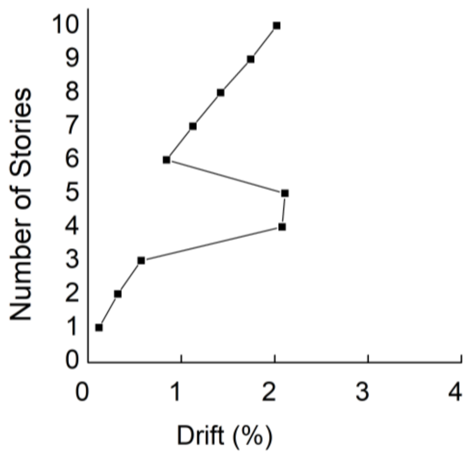

Figure 5.15: Storey deflection of a G10 building

Most of the beams up to the sixth storey are in the strength degradation zone of the backbone curve, providing lesser restraint to columns, as shown in Figure 5.14 c). Flexible columns of bottom stories attract lesser moments and redistribute them to upper stories. It is observed that moments have been redistributed to the eighth storey in stage E. Due to redistributed moments in eight storey, columns yielded, and storey mechanism is observed. In stories at mid-height of the building, ISD increased, as shaded in black in Figure 5.16, because of the increased flexibility of columns, and corresponding damage increased because of beams in the strength degradation zone. At the seventh storey, little increment in ISD and a considerable reduction in the DCR plot are observed. Because of this reduced demand, the area under the moment rotation curve is reduced; therefore, negligible damage weightage is observed at stage E. The reduced moment of the seventh storey shifted to the eighth storey, as seen in the DCR plot, hence causing damage at the eighth storey indicated in the plot of damage contribution at stage E (Figure 5.16).

In the G10 building, the peak damage contribution is in the middle stories and is distributed in a parabolic shape, as highlighted by the blue trend line in Figure 5.16. In this case, damage contribution and weighting factors are different. Since the maximum damage contribution is at mid-height, the weightage of the stories below shall be considered same as the maximum weightage at mid-height. Therefore, the proposed relative weighting factors are marked with double circles in Figure 5.17. Furthermore, the highest weighted stories are all the stories from first up to one storey above the mid-height of the building, which significantly impacts the health of the building.

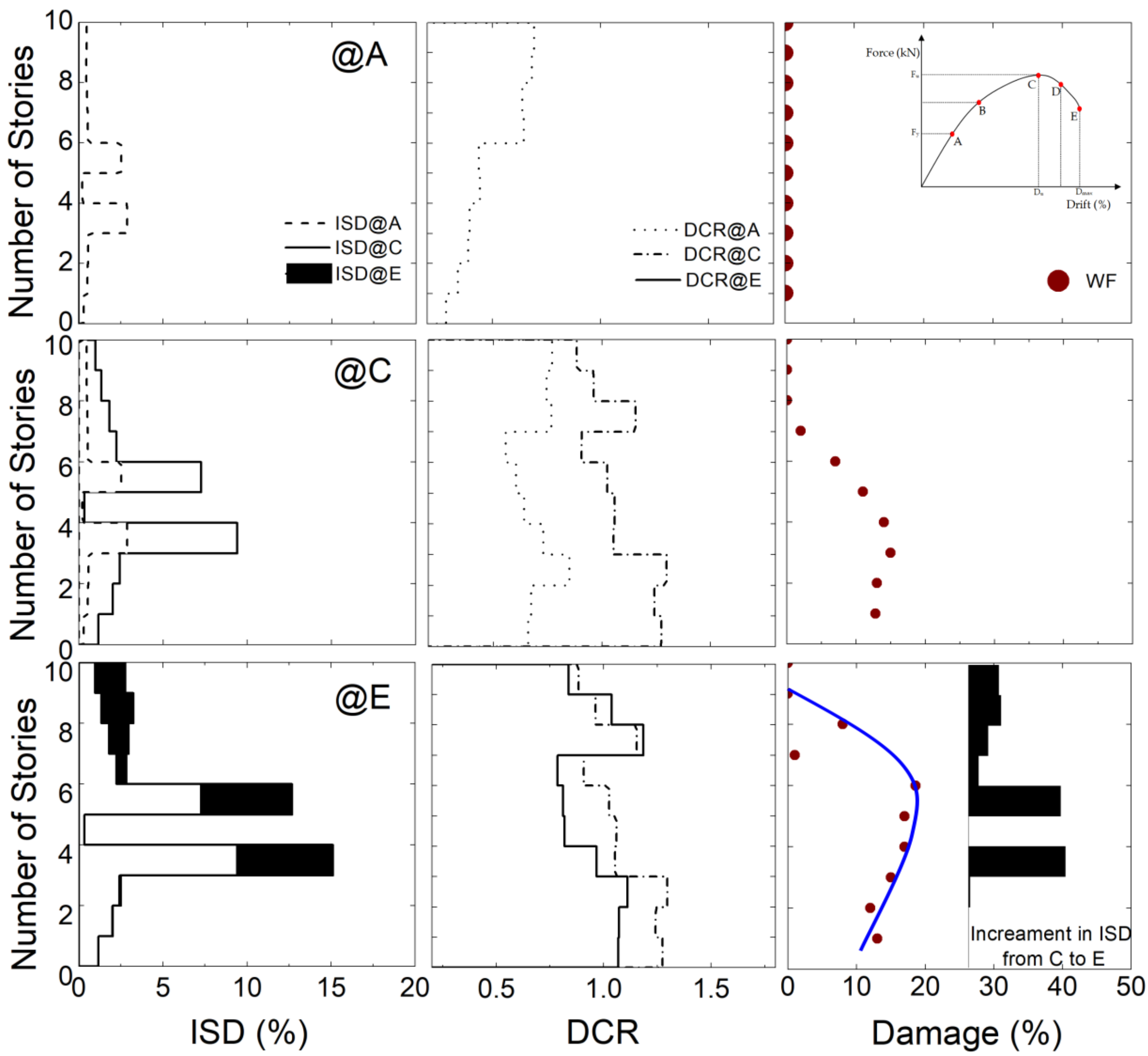

Figure 5.16: Interstorey drift, demand capacity ratio, and damage contribution at different stages of the Pushover curve in the G10 building

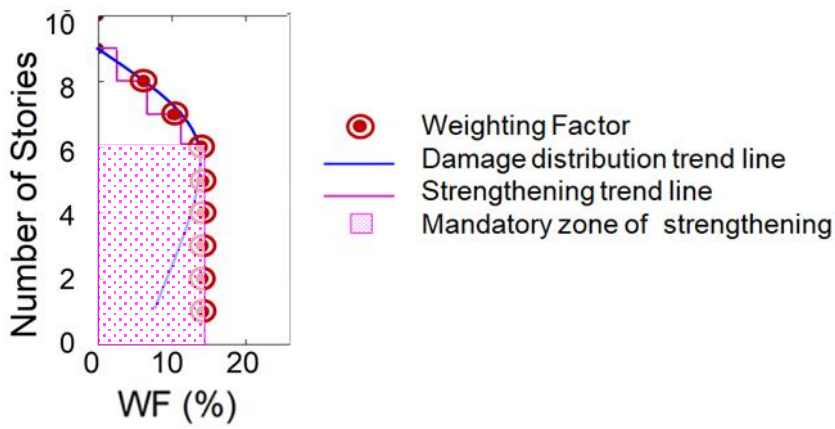

Figure 5.17: Storey weights and proposed strengthening scheme for the G10 building

Therefore, strengthening activities are proposed zone-wise as per the damage weights of each storey. Zone 1 is defined as the first storey till one storey above the mid-height of the building (shaded in pink in Figure 5.17), and zone 2 is for upper stories up to 90% height of the building. The same amount of strengthening is proposed in Zone 1, and stepped strengthening is proposed in Zone 2, as shown with the pink line in Figure 5.17. Zone 1 same amount of strengthening is mandatory in a single step, and zone 2 stepped strengthening is done in a sequential manner as per the base shear requirement of a city.

5.2.5 Discussions

Modal participation factors are tabulated in Table 5.9. The contribution of the first mode is 86% in 4-storey buildings and 79% in 10-storey buildings. The contribution of higher modes increased from 14% to 20% as the height of the building increased from G4 to G10. Therefore, validating that damage shifted to the upper stories as building height increased.

Table 5.9: Modal participation ratios for type G buildings

	G4	G6	G8	G10
Mode 1	**86.437**	**83.078**	**80.646**	**79.207**
Mode 2	**9.541**	**9.756**	**10.056**	**9.918**
Mode 3	2.813	3.639	3.948	**4.160**
Mode 4	0.680	1.867	1.898	2.135
Mode 5		0.931	1.419	1.484
Mode 6		0.274	0.620	1.049
Mode 7			0.739	0.623
Mode 8			0.221	0.690

It has been understood that damage distribution cannot be associated with a single trend of uniform, triangular, and nonlinear distribution along the height. The distribution pattern is parabolic, and the shape and location of the parabola changes with an increase in building height.

5.3 Effect of Storey Height

The G6 building is analyzed with varying storey heights from 3m, 3.5m, 4m, and 4.5m to study the effect of storey height. Damage contribution of each storey is computed in all four buildings at each stages A, B, C, D, and E. Damage contribution at yielding stage A is tabulated in Table 5.10 and indicates that damage started on the same floor in all buildings. Damage contribution at stage B is mentioned in Figure 5.11 highlights similar damage in three stories. Table 5.12 presents storey weights at stage C, i.e., at the ultimate strength of the buildings. It is observed that the total damage in the building is reduced; however, the difference is not huge. Damage distribution in several stories remains the same. Table 5.13 & Table 5.14 present storey weights at stages D & E, and it is observed that damage distribution remains the same even in later stages of pushover analysis. Damage distribution and the quantity of damage remain almost the same. Therefore, damage contribution is not affected by different storey heights in the buildings.

Table 5.10: Damage contribution at stage A in the G6 building with increasing storey height

Damage	**3m 0.001%**	**3.5m 0.001%**	**4m 0.001%**	**4.5m 0.001%**
Sixth Storey	-	-	-	-
Fifth Storey	-	-	-	-
Fourth Storey	-	-	-	-
Third Storey	-	-	-	-
Second Storey	0.001	0.001	0.001	0.001
First Storey	-	-	-	-

Table 5.11: Damage contribution at stage B in the G6 building with increasing storey height

Damage	**3m 3.3%**	**3.5m 3%**	**4m 2.9%**	**4.5m 2.7%**
Sixth Storey	-	-	-	-
Fifth Storey	-	-	-	-
Fourth Storey	-	-	-	-
Third Storey	0.8	0.7	0.7	0.7
Second Storey	1.5	1.4	1.3	1.2
First Storey	1	1	0.9	0.8

Table 5.12: Damage contribution at stage C in the G6 building with increasing storey height

Damage	**3m 49%**	**3.5m 40%**	**4m 40%**	**4.5m 30%**
Sixth storey	-	-	-	-
Fifth Storey	-	-	-	-
Fourth Storey	2	1	2	0.5
Third Storey	8	10	10	7

Second Storey	18	16	16	14
First Storey	21	13	12	9

Table 5.13: Damage contribution at stage D in the G6 building with increasing storey height

Damage	**3m 79%**	**3.5m 78%**	**4m 74%**	**4.5m 73%**
Sixth storey	-	-	-	-
Fifth Storey	-	-	-	-
Fourth Storey	2	2	3	1
Third Storey	15	15	16	16
Second Storey	26	26	25	27
First Storey	36	35	30	29

Table 5.14: Damage contribution at stage E in the G6 building with increasing storey height

Storey Height	**3m 100%**	**3.5m 100%**	**4m 100%**	**4.5m 100%**
Sixth storey	-	-	-	-
Fifth Storey	-	-	-	-
Fourth Storey	1	2	3	1
Third Storey	18	18	22	21
Second Storey	30	34	29	32
First Storey	51	46	46	46

5.4 Summary

The damage contribution of each storey is computed by calculating the energy dissipation of each member by using the area under the moment rotation curve. The effect of increasing the axial load on columns and increasing storey height on storey weights is studied. Four buildings with increasing floors, G4, G6, G8, and G10, are studied to study variable axial load on columns. In G4, G6 and G8 buildings, the maximum increment in interstorey drift from C to E stage is in the bottom stories. This led to the peak damage in the bottom stories with maxima in the first storey. The last storey with some damage is near the mid-height of the building. Therefore, in such cases, the highest weighted storey is the first storey, and weightage reduces as per the parabolic curve as we go up till the midheight of the building. A stepped strengthening is proposed in zone 1, which is done in a sequential manner as per the base shear requirement of that area.

However, as the number of stories increases in G10, peak damage is observed at the storey with maximum increment in interstorey drift from C to E, which lies nearby the midheight of the building. In this case, the damage is distributed to several floors avoiding local concentration of damage. However, the middle storey has the highest damage. All stories below are allotted the same weighting factor as the middle storey with maximum damage. Strengthening is proposed zone-wise in two zones as per the damage weights. The same amount of strengthening is proposed in Zone 1, and stepped strengthening is proposed in Zone 2. Zone 1 same amount of strengthening is mandatory, and zone 2 stepped strengthening is done in a sequential manner as per the base shear requirement of that area.

Four buildings with variable storey heights (3m, 3.5m, 4m & 4.5m) are analyzed to study the effect of storey height on the damage distribution and strengthening proposal. It is observed that the same number of stories are damaged when the storey height of the building is increased. The quantity of the damage remains almost the same. Therefore, damage distribution and highest weightage storey label are not affected by varying storey height of gravity load designed buildings.

Therefore, it has been demonstrated that low-rise buildings have convex parabolic damage distribution with the highest weighting factor for the first storey. However, damage distribution changed as building height increased. It is observed that parabolic damage distribution shifts to upper stories and is concave in shape, with the highest weighting factor for all the stories from the ground up to one storey above the mid-height of the building. Therefore, the shape of the parabola shifted from convex in G4 to concave in G10, with G6 and G8 in transition as a straight line. Stepped strengthening in buildings up to 8 stories is proposed in Zone 1 in a sequential manner. In G10 building with concave damage distribution, the same amount of strengthening in zone 1 is mandatory in a single step, and in zone 2, sequential stepped strengthening is proposed.

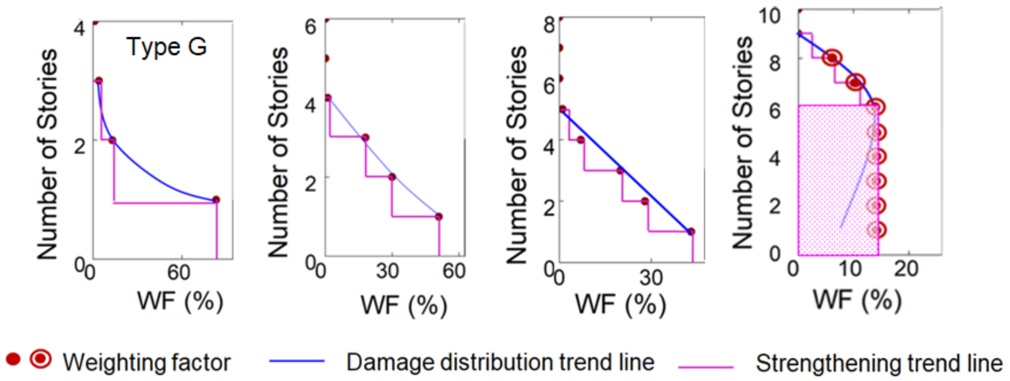

Figure 5.18: Summary of storey weights distribution and proposed strengthening scheme in Type G buildings

6 STOREY-WISE DAMAGE CONTRIBUTION FOR TYPE P BUILDINGS

Storeywise damage contribution is computed for Type P buildings to understand how the damage contribution of each storey changes. To study the damage contribution of each storey in Type P building, two parameters, i.e., axial load and storey height, have been chosen. Non-linear static analysis is performed to observe the hinge mechanism in each storey for lateral loading. The hinge mechanism indicates the damage progression in the building at five stages, as mentioned in section 5.1. Since energy is chosen as the damage quantification parameter, energy dissipated in each hinge of a storey is computed to quantify the contribution of a storey. Storey weights are computed in the same manner mentioned in Section 5.1 using the computation of energy dissipated via the area under the moment rotation curve of each hinge.

6.1 Effect of Axial Load

Buildings considered to study the effect of increasing axial load are 4, 6, 8, and 10-storey buildings. Damage contribution is computed for all the buildings to understand how damage changed as the axial load on columns increased with an increasing number of stories. Each storey comprises columns and the beams on top of those columns. The area under the moment rotation curve is computed for all members of the storey to compute the storey damage. Similarly, total damage in the building is computed. The ratio of storey damage to the entire building damage computes the damage contribution of each storey. Damage contribution of each storey in each building is computed at B, C, D & E (Figure 5.1), considering damage at E as 100% and damage at A as just started. Table 6.1 summarizes each story's damage contribution in four buildings at stage B and indicates less than 5% damage in all buildings. As pushover progress to stage C, it is observed that there is more than 50% damage in P4, and it reduces as the height of the building increases; (Table 6.1). Similarly, damage at stage D in P4 is 83% and decreases as the height of the building increases. The last step of pushover analysis which is at 85% strength drop, is assumed to be 100% damage. The contribution of each storey in 100% damage is tabulated in Table 6.4.

Table 6.1: Storey-wise comparison of damage contribution in type P buildings with increasing axial load at stage 'B' in the capacity curve.

Storey Height	P4 3%	P6 3%	P8 2.5%	P10 2.8%
Tenth Storey				-
Ninth Storey				-
Eight storey			-	-
Seventh Storey			-	-
Sixth storey		-	-	0.3
Fifth Storey		-	-	0.2
Fourth Storey	-	0.1	0.1	0.4
Third Storey	-	0.8	0.8	0.6
Second Storey	-	1.2	1.4	0.7
First Storey	3	0.9	0.2	0.4

Table 6.2: Storey-wise comparison of damage contribution in type P buildings with increasing axial load at stage 'C' in the capacity curve.

Storey Height	P4 71%	P6 61%	P8 55%	P10 37%
Tenth Storey				-
Ninth Storey				-
Eight Storey			-	1
Seventh Storey			-	3
Sixth storey		-	-	3
Fifth Storey		-	1	4
Fourth Storey	-	4	8	7
Third Storey	14	13	14	8
Second Storey	15	18	15	8
First Storey	42	26	17	9

Table 6.3: Storey-wise comparison of damage contribution in type P buildings with increasing axial load at stage 'D' in the capacity curve.

Storey Height	P4 83%	P6 83%	P8 81%	P10 73%
Tenth Storey				-
Ninth Storey				-
Eight Storey			-	1
Seventh Storey			-	3
Sixth storey		-	-	3

Fifth Storey		-	1	5
Fourth Storey	-	4	11	10
Third Storey	13	17	21	14
Second Storey	20	25	22	16
First Storey	55	37	26	21

Table 6.4: Storey-wise comparison of damage contribution in type P buildings with increasing axial load at stage 'E' in the capacity curve.

Storey Height	P4 100%	P6 100%	P8 100%	P10 100%
Tenth Storey				-
Ninth Storey				-
Eight Storey			-	1
Seventh Storey			-	3
Sixth storey		-	-	3
Fifth Storey		-	1	6
Fourth Storey	-	3	14	13
Third Storey	12	21	25	19
Second Storey	24	28	26	20
First Storey	64	47	33	35

From stage E, it is observed that damage is concentrated up to 64% at the ground storey in the P4 building (Table 6.4). In P6, the maximum damage in the ground storey is around 50%; in P8, the maximum damage in a storey is 33%. In the P10 building, the maximum damage in a storey is 35%. Therefore, it is observed that as building height increases, maximum damage concentration in a storey is reduced from 64% to 35%, and it is distributed to more stories in higher buildings. The trend stays the same in all stages. To understand why damage is progressing to upper stories as the height of the building increases, damage contribution is rearranged stage-wise for each building. Damage progression and distribution are studied in buildings of variable height.

6.1.1 Storey-wise damage progression in P4

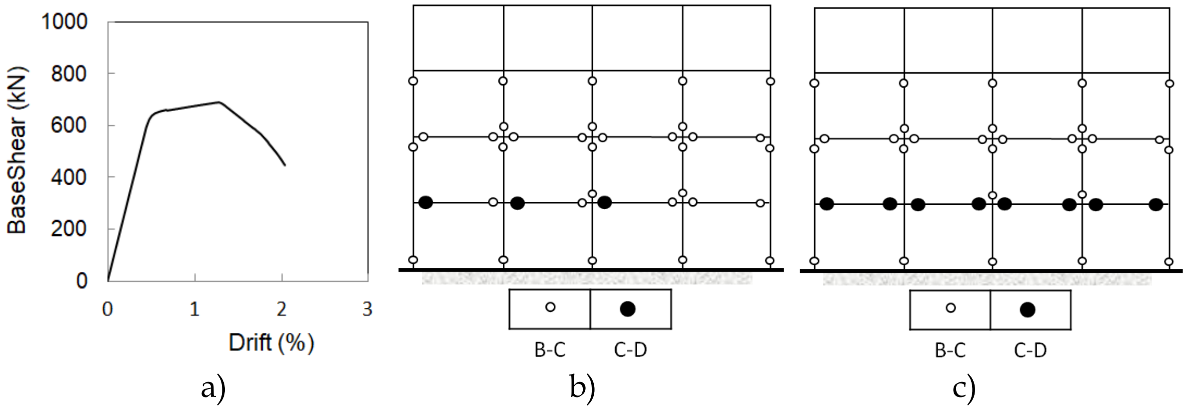

Figure 6.1: Pushover curve of P4 building along with hinge states at stages C and E

Damage contribution computed in the previous section is rearranged stagewise for the P4 building and is tabulated in Table 6.5. The first story is observed to be damaged around 42% at stage C, and damage increased to 64% in stage E. Second storey is damaged up to 24% in stage E. Therefore, more than 80% of damage is concentrated in the first and second storey.

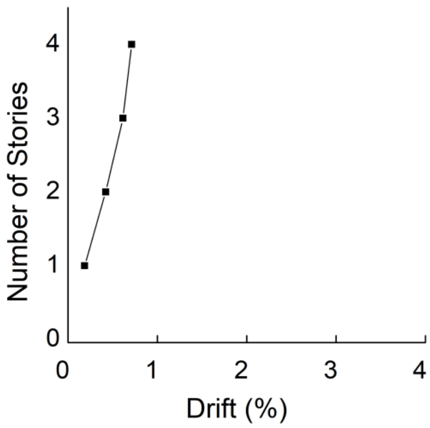

Figure 6.2: P4 building deflection profile

The transition of damage from B to C is observed to understand the progression of damage. It is reported that there is a sudden damage increment from 3% to 71% in the building at this stage. The further distribution shows that 15% contribution is from ground-storey columns and 27% is from ground-storey beams, and 29% is divided into upper-story columns and beams. Therefore, a huge damage contribution is from the ground storey, and the same trend continues till stage E. To understand why weights are concentrated more in the ground storey. The building deflection profile is plotted in Figure 6.2. Interstorey drift is computed from the deflection profile and at stages A, C, and E, along with the demand capacity ratio of exterior columns, as shown in Figure 6.3.

Table 6.5: Damage contribution of each storey in each stage of the pushover curve of the P4 building

Damage	**A** **0.001%**	**B** **3%**	**C** **71%**	**D** **83%**	**E** **100%**
Fourth Storey	-	0	0	0	0
Third Storey	-	0	14	13	12
Second Storey	0.001	0	15	20	24
First Storey	-	3	42	55	64

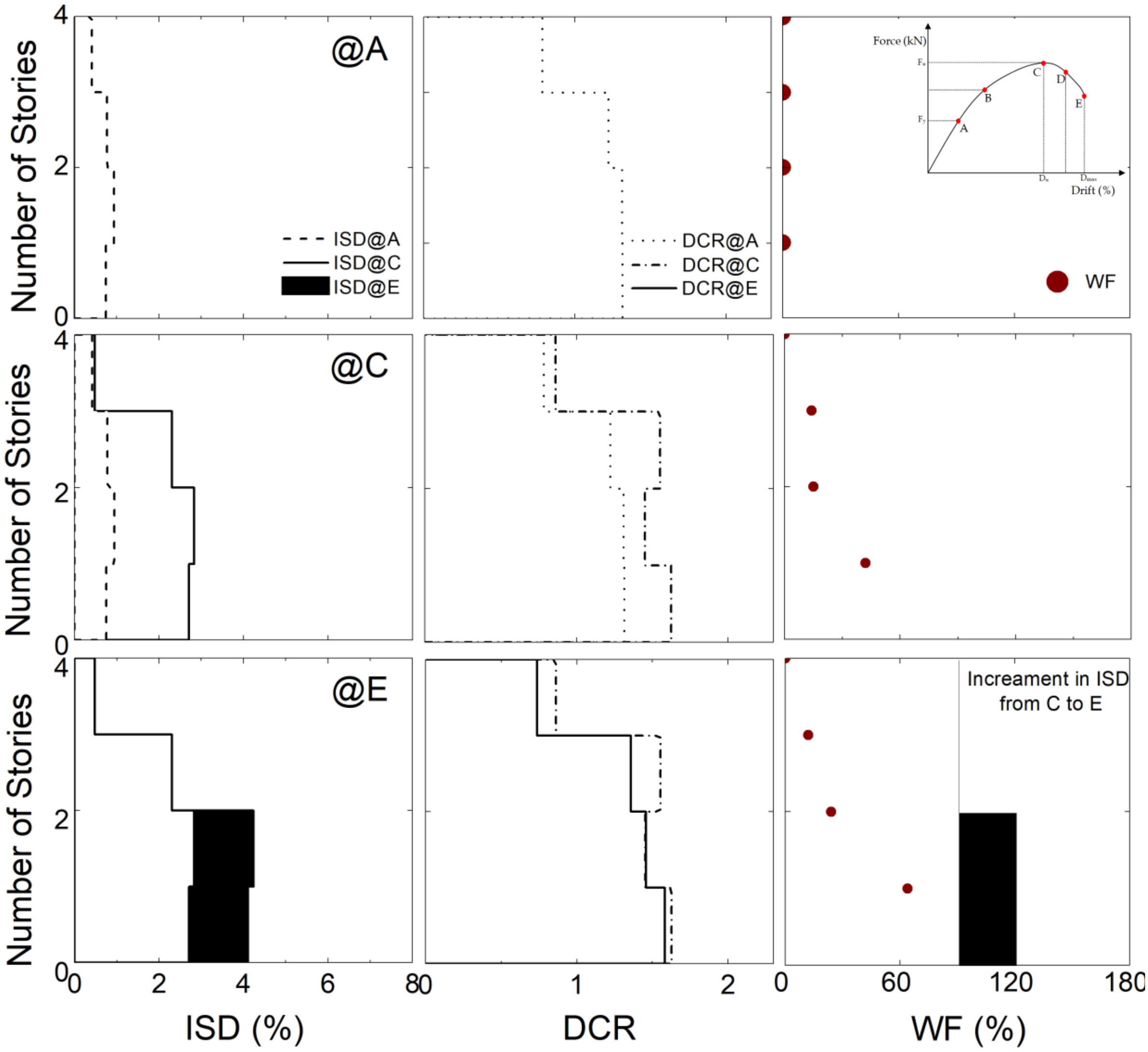

Figure 6.3: Interstorey drift, demand capacity ratio, and damage contribution at different stages of the Pushover curve in the P4 building

From stage A to C of PoA, the lateral load increases ISD in three stories due to increased DCR in the corresponding stories. This led to huge damage contribution from the bottom three stories; however, significant damage is in the first storey. This damage contribution is the weighting factor and is plotted in the third column of Figure 6.3.

Increment in ISD from stage C to stage E is limited to the bottom two stories. DCR remained the same or reduced a little in these two stories. This indicates that members utilize nonlinear capacity by deforming more with the same or less moment, leading to more damage in the first two stories. As beams of the first storey crossed post-peak strength and are in the strength degradation zone of the backbone curve as shown in Figure 6.1 b) and c). They provide less restraint to first storey columns, making them more flexible. In addition to that, the first storey columns yielded in stage C at the bottom. Due to more flexibility of columns because of damaged beams and due to the nonlinear behaviour of columns, more damage is observed in the first storey.

When an increment in ISD from stage C to stage E is limited to bottom stories, significant damage is also observed in similar stories (shaded black in Figure 6.3). Damage distribution observed is parabolic with maxima at the bottom storey, as shown in Figure 6.4. It is observed that P4 building has parabolic damage distribution with maximum damage at the first storey, as highlighted with a blue trend line in Figure 6.4. Therefore, the first storey is the highest weighted storey which affects the health of the building.

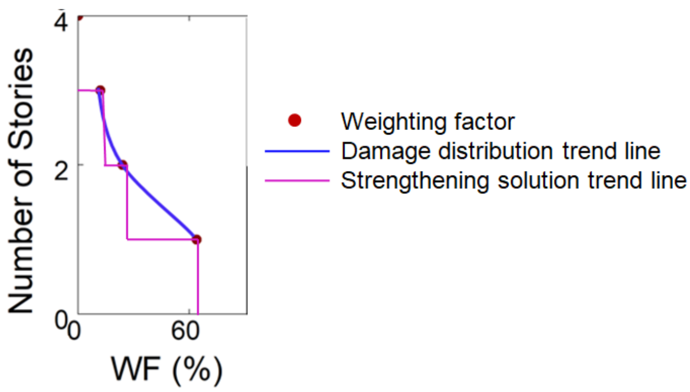

Figure 6.4: Strengthening pattern for P4 building

Hence, stepped strengthening activities are proposed zone-wise as per the damage distribution. Zone 1 is defined as the first storey till one storey above the mid-height of the building. Stepped strengthening is proposed in zone 1, with the maximum at the bottom and the minimum at one storey above the mid-height of the building, as drawn with a pink line in Figure 6.4. This shall be done in a sequential manner as per the base shear requirement of that area. If the updated capacity after the first storey strengthening is less than the base shear, strengthening shall be done at the next storey with reduced strengthening.

6.1.2 Storey-wise damage progression in P6

Damage contributions computed in the previous section are rearranged stage-wise for the P6 building and are tabulated in Table 6.6. The first story is observed to be damaged around 26% at stage C, and damage increased to 47% in stage E. Second and third storey are damaged up to 28% and 21% in stage E. Therefore, almost the entire damage is concentrated in the bottom three stories with a maximum in the first storey.

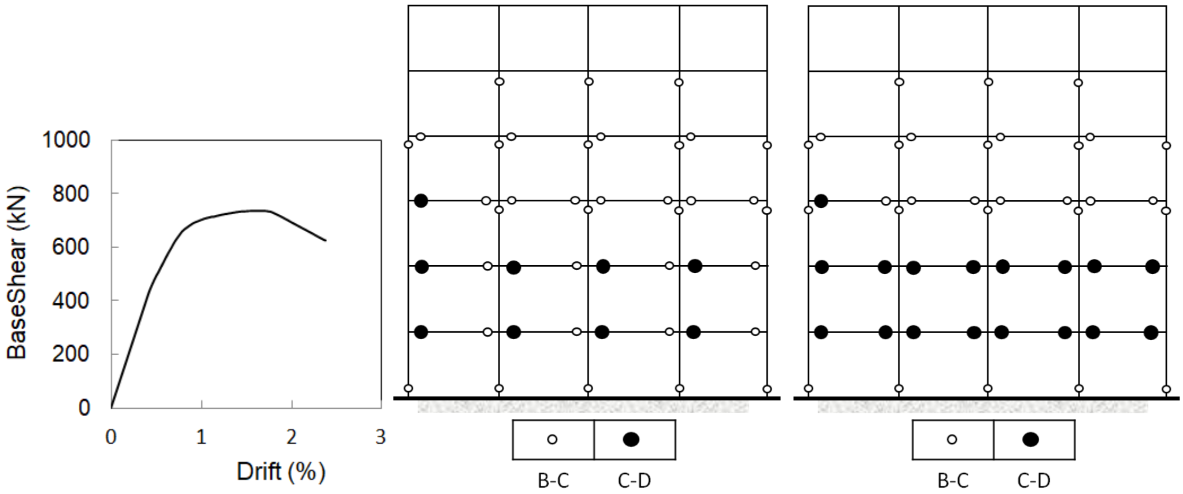

a) b) c)

Figure 6.5: Pushover curve along with hinge states at stages C and E

Table 6.6: Damage contribution of each storey in each stage of the pushover curve of the P6 building.

Damage	**A 0.001%**	**B 3%**	**C 61%**	**D 83%**	**E 100%**
Sixth Storey	-	-	-	-	-
Fifth Storey	-	-	-	-	-
Fourth Storey	-	0.1	4	4	3
Third Storey	-	0.8	13	17	21
Second Storey	-	1.2	18	25	28
First Storey	0.001	0.9	26	37	47

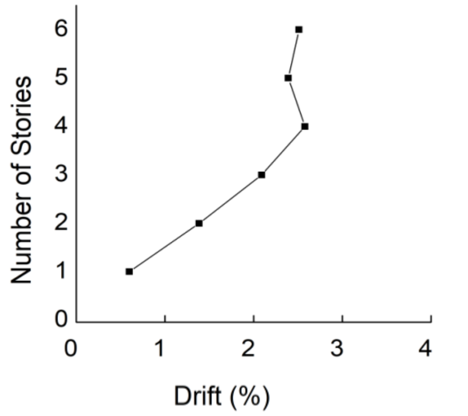

Figure 6.6: P6 building deflection profile

The building deflection profile is plotted in Figure 6.6; further ISD is computed from the building deflection profile. To understand why weights are concentrated at the ground storey, ISD at stages A, C, and E are plotted along with the DCR of exterior columns and damage contribution of each storey in Figure 6.7.

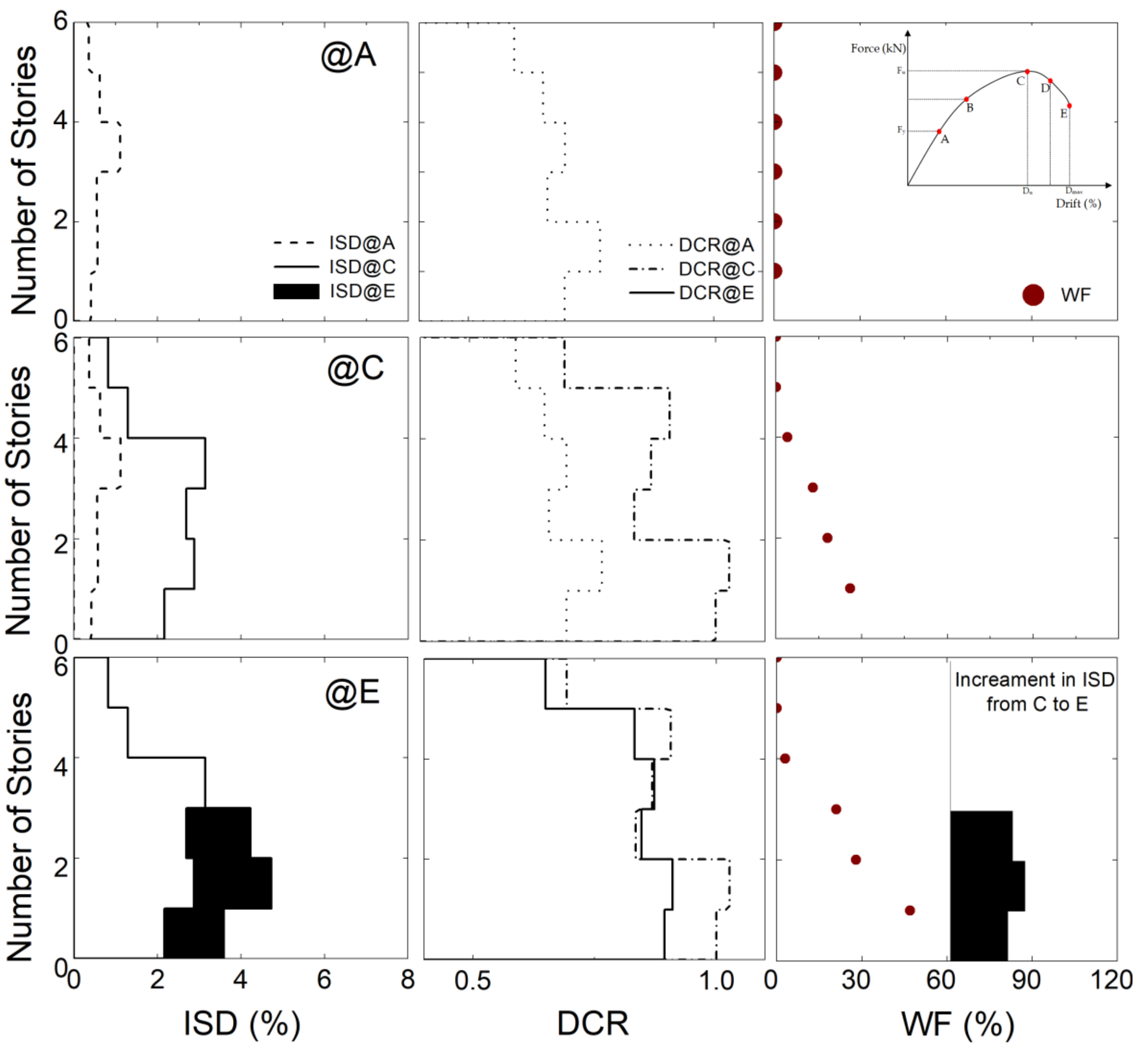

Figure 6.7: Interstorey drift, demand capacity ratio, and weighting factor at different stages of the Pushover curve in the P6 building

From stage A to C, as lateral load increases, an increment in ISD is observed in all stories, as DCR also increases in all stories. However, the increment in ISD from stage C to stage E is limited to the bottom three stories only. It is observed from DCR that demand reduced in the bottom two stories due to the damage in the beam members, as shown in Figure 6.5 b) and c). As beam members get damaged, less restraint is provided to the columns. Damaged beams increase the columns' flexibility, redirecting fewer moments to the first and second storey. Due to this, a reduction of moments in the first and second storey columns is observed. Due to damaged beams, damage contribution of the first and second storey increased. These reduced moments get redistributed to the third and fourth storey; hence, no reduction in DCR is observed there. However, due to redistributed forces, the external column gets hinged to form a storey mechanism at the third storey (Figure 6.5 c)). Due to the storey mechanism, an increase in damage contribution at the third storey is observed.

As the increment in ISD from stage C to stage E is limited to the bottom three stories (shaded black in Figure 6.7), the damage is also observed in the same stories. Damage is distributed in a parabolic shape with a maximum at the bottom storey and minimum significant damage at the mid-height of the building, as shown in Figure 6.7 @E. Damage patterns can also be related to the deflection profile of the building. In the P6 building, the weighting factor is the same as the damage contribution, as shown in Figure 6.8. Therefore, the highest weighted storey to affect the health of the building is the first storey.

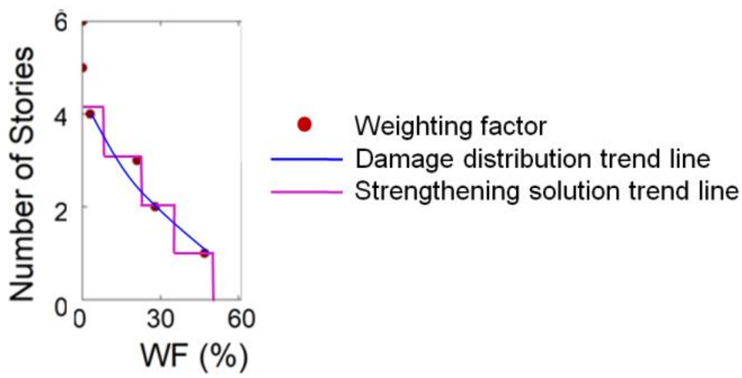

Figure 6.8: Strengthening pattern for P6 building

Hence, strengthening activities are proposed zone-wise as per the damage weights. Zone 1 is defined as stories from the bottom up to one storey above the mid-height of the building. Stepped strengthening is proposed in zone 1, as drawn with a pink line in Figure 6.8. This shall be done sequentially as per the base shear requirement of that area. If the updated capacity after the first storey strengthening is less than the base shear, strengthening shall be done at the next storey.

6.1.3 Storey-wise damage progression in P8

Damage contribution is rearranged stagewise for the P8 building and is tabulated in Table 6.7. The first story is observed to be damaged around 33% at stage E. Second and the third storey is damaged up to 26% and 25% in stage E. The entire damage is concentrated in the bottom four stories. To understand why damage is concentrated in bottom stories, building deflection, ISD, and DCR are computed. The building deflection profile is plotted in Figure 6.10. ISD at stages A, C, and E are plotted along with the DCR of exterior columns in Figure 6.11.

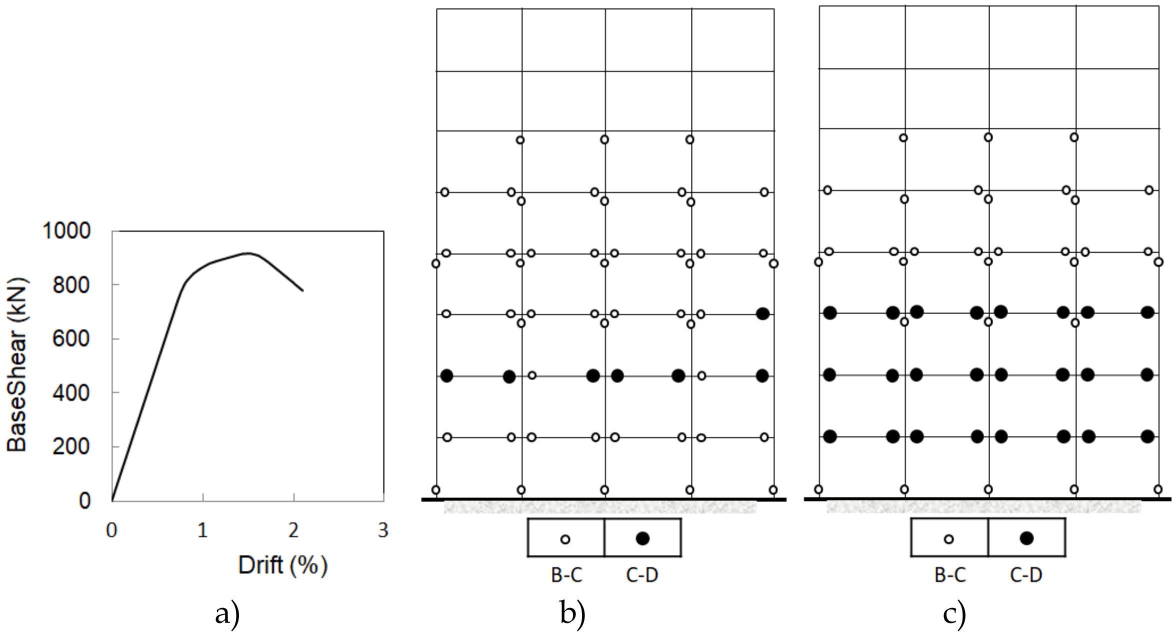

Figure 6.9: Pushover analysis of a P8 building along with hinge states at stages C and E

Table 6.7: Damage contribution of each storey in each stage of the pushover curve of the P8 building.

Damage	**A** **0.001%**	**B** **2.5%**	**C** **55%**	**D** **81%**	**E** **99%**
Eight Storey	-	-	-	-	-
Seventh Storey	-	-	-	-	-
Sixth Storey	-	-		-	-

Fifth Storey	-	-	1	1	1
Fourth Storey	-	0.1	8	11	14
Third Storey	-	0.8	14	21	25
Second Storey	-	1.4	15	22	26
First Storey	0.001	0.2	17	26	33

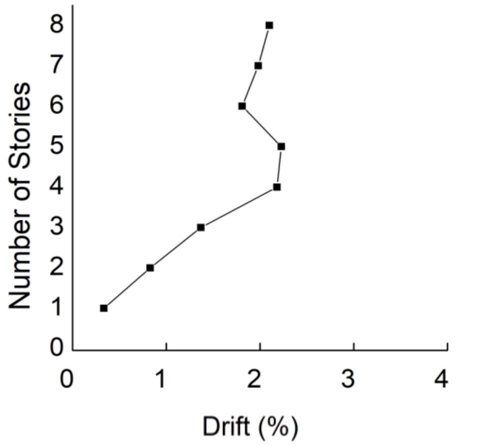

Figure 6.10: Deflection profile of P8 building

An increment in ISD in stage C is observed in almost all stories. DCR also increased in all stories; however, the damage is observed only in the bottom four stories. Increment in ISD from stage C to stage E is observed in the bottom four stories as shaded in black in stage E of Figure 6.11. From stage C to E, as lateral load increased, DCR reduced in the bottom three stories. Demands redistributed to the fourth storey (Figure 6.11 @E). Therefore, an increment in ISD from stage C to stage E is observed in the bottom four stories (shaded black in Figure 6.11), leading to damage in the same four stories. Damage distribution is parabolic, with a maximum at the bottom and minimum significant damage at the mid-height of the building, as plotted in Figure 6.12. Damage contribution is the weighting factor of the storey. Therefore, it is observed that in the P8 building, damage distribution is parabolic with maximum weightage of damage at the first storey. Therefore, the first storey is the highest weighted storey to affect the health of the building.

Strengthening activities are proposed in line with the damage weights. Zone 1 is defined as stories from the bottom up to one storey above the mid-height of the building. Stepped strengthening is proposed in zone 1, as drawn with a pink line in Figure 6.12. This shall be done sequentially as per the base shear requirement of that area. If the updated capacity after the first storey strengthening is less than the base shear, strengthening shall be done at the next storey.

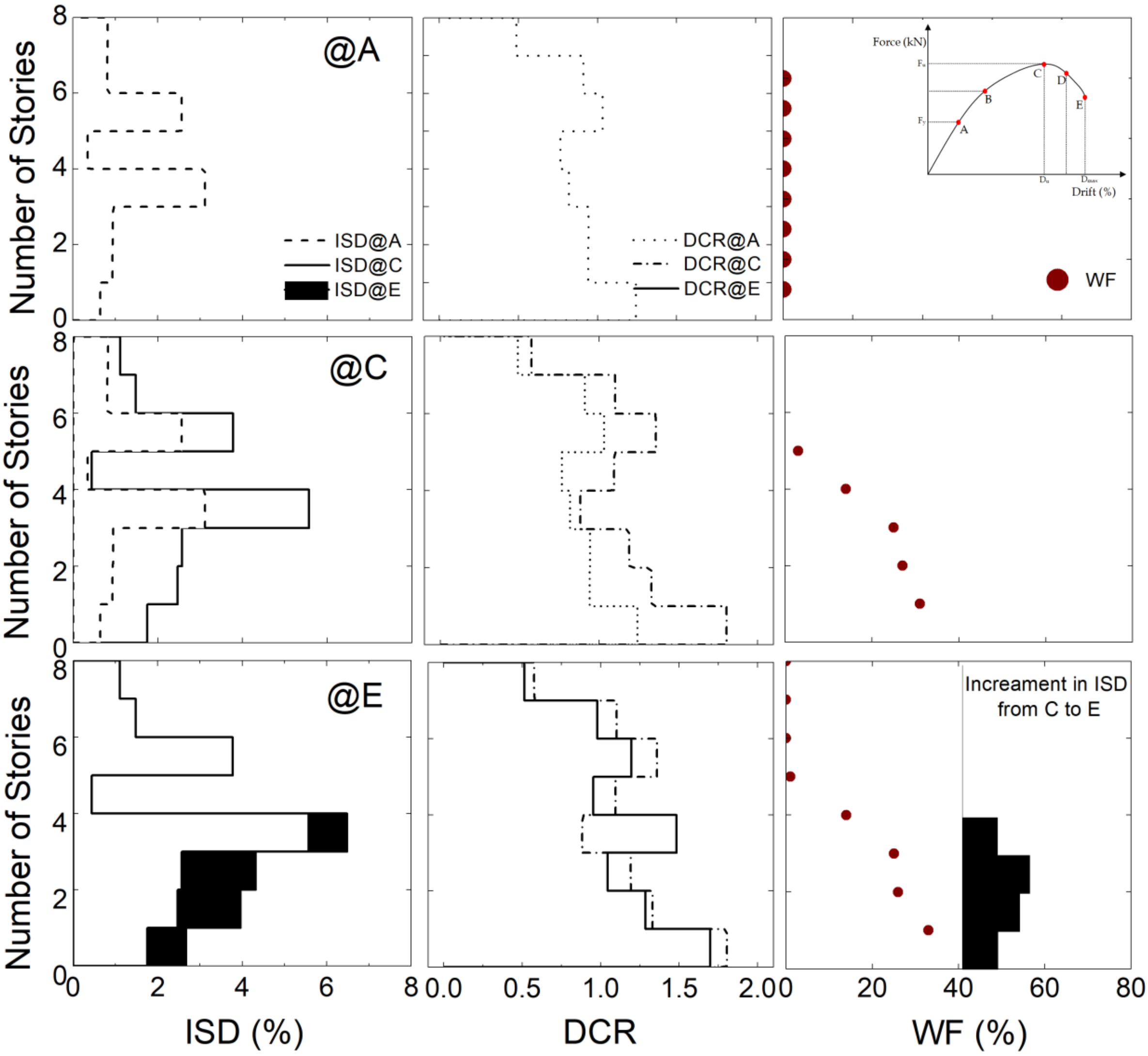

Figure 6.11: Interstorey drift, demand capacity ratio, and weighting factors at different stages of the Pushover curve in the P8 building

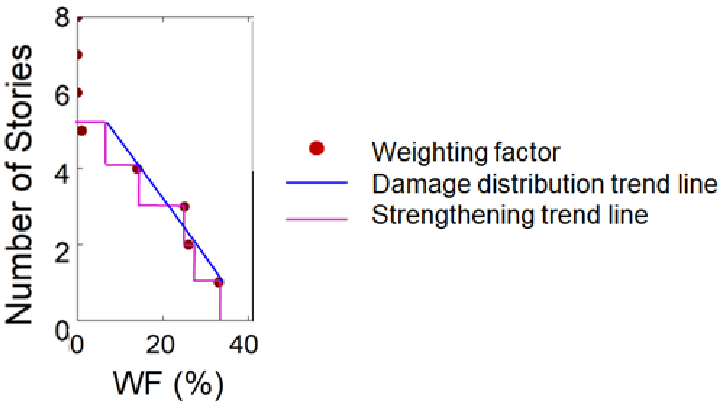

Figure 6.12: Strengthening pattern for P8 building

6.1.4 Storey-wise damage progression P10

The damage contribution of each storey for the P10 building is tabulated in Table 6.8. The Building deflection profile is plotted in Figure 6.14 to compute ISD. To understand damage distribution, ISD at stages A, C, and E are computed and plotted along with the DCR of the exterior right column in Figure 6.15.

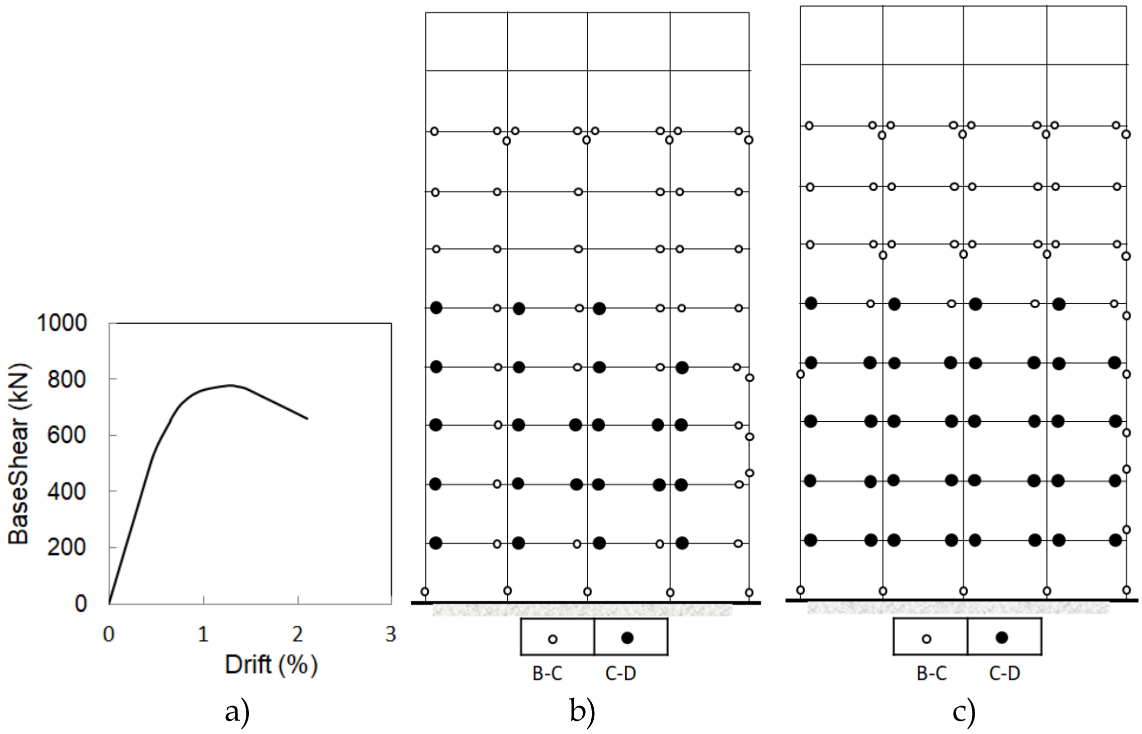

Figure 6.13: Pushover analysis of a P10 building along with hinge states in stages C and E

An increment in ISD in stage C is observed in almost all stories. As DCR increased in all stories, a little damage in the bottom seven stories is observed. Increment in ISD from stage C to stage E is observed in the bottom four stories and the sixth, seventh, and eighth storey as shaded in black in stage E of Figure 6.15. From stage C to E, as lateral load increased, DCR reduced in the bottom four stories. Demands redistributed to the fifth and sixth storey.

Table 6.8: Damage contribution of each storey in each stage of the pushover curve of the P10 building.

Damage	**A** **0.001%**	**B** **2.6%**	**C** **43%**	**D** **73%**	**E** **100%**
Tenth Storey	-	-	-	-	-

Ninth Storey	-	-	-	-	-
Eight Storey	-	-	1	1	1
Seventh Storey	-	-	3	3	3
Sixth Storey	-	0.3	3	3	3
Fifth Storey	-	0.2	4	5	6
Fourth Storey	-	0.4	7	10	13
Third Storey	-	0.6	8	14	19
Second Storey	-	0.7	8	16	20
First Storey	0.001	0.4	9	21	35

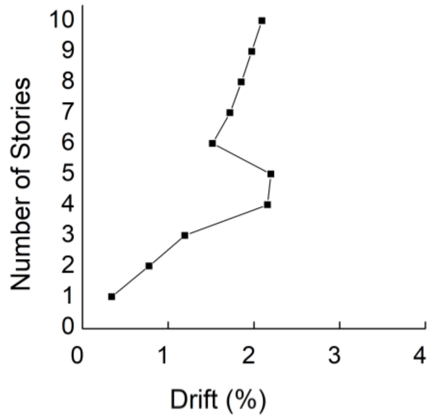

Figure 6.14: Deflection profile of P10 building

The reduction in DCR is due to the damage in the beam members, as all the beam members get damaged up to the fourth storey (Figure 6.13 (c)), and less restraint is provided to the columns. Damaged beams lead to the increased flexibility of the columns, and fewer moments are attracted to these stories on redistribution of moments. DCR reduction in the bottom four stories is accompanied by a huge increment in ISD from C to E, as shaded in black in Figure 6.15. ISD values are higher because of the damaged beams and more flexible columns. Further, as moments got redistributed to upper stories, ISD increment is also observed at the sixth and seventh storey. However, both moment redistribution and ISD increment are less. Similarly, damage contribution is observed from the same stories where ISD increment is observed. There is a huge damage contribution from the bottom four stories and then less contribution from the fifth, sixth, seventh, and eighth storey. Damage has started progressing upwards in Precode buildings from this height, however, the amount is less. In the P10 building, major damage distribution is in the bottom stories, with a maximum contribution of damage from the first storey and minimum significant damage at 80% height of the building. The weighting factor is same as the damage contribution of each storey. Therefore, the first storey is the highest weighted storey to affect the health of the building.

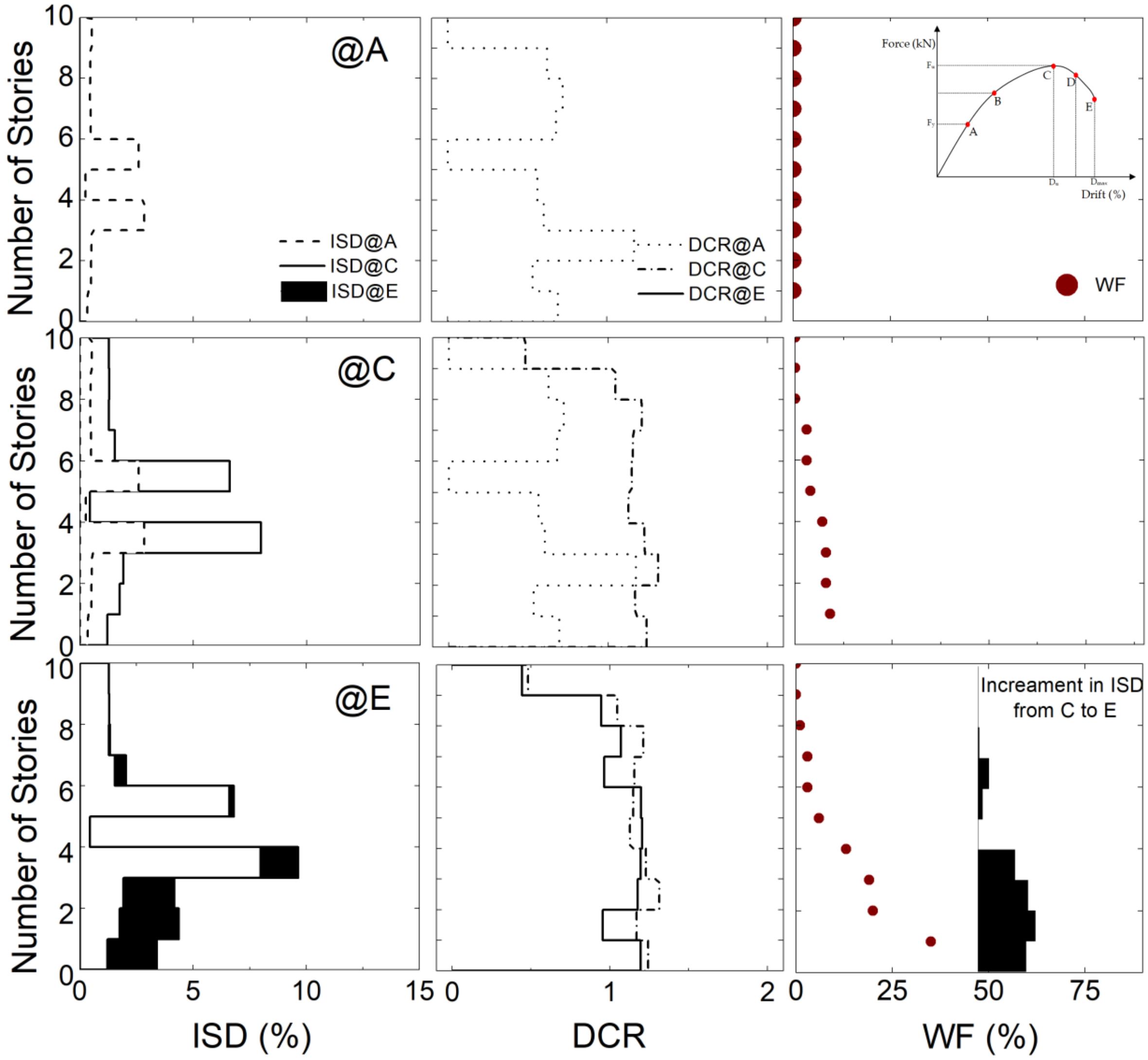

Figure 6.15: Interstorey drift, demand capacity ratio, and weighting factors at different stages of the Pushover curve in the P10 building

Strengthening activities are proposed in line with the damage weights. Zone 1 is defined earlier as stories from the bottom up to one storey above the mid-height of the building. However, in this case, the damage is progressing higher than the Zone 1 upper limit. Therefore, zone 2 is defined as the rest of the stories up to 90% height of the building. Stepped strengthening is proposed in Zone 1 and Zone 2, as shown with a pink line in Figure 6.16. This shall be done sequentially as per the base shear requirement of that area. If the updated capacity after the first storey strengthening is less than the base shear, strengthening shall be done at the next storey. And the same procedure shall continue until the updated capacity of the strengthened building is more than the base shear requirement.

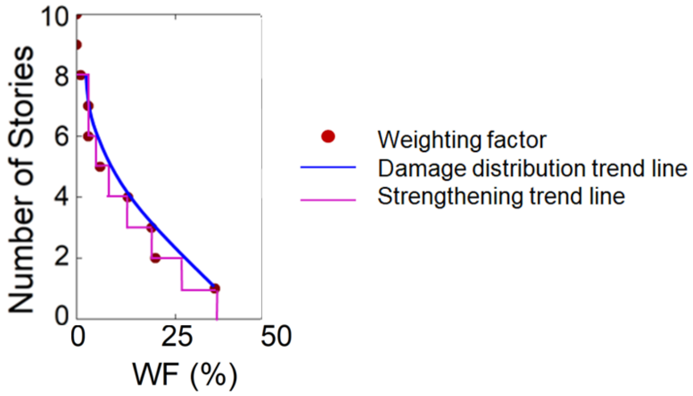

Figure 6.16: Strengthening pattern for P10 building

6.1.5 Discussions

Modal participation factors of each building are tabulated in Table 6.9. The contribution of the first mode is 86% in 4-storey buildings and 79% in 10-storey buildings, as tabulated in Table 6.9. The contribution of higher modes increased from 14% to 21% as the height of the building increased from P4 to P10. Therefore, validating the damage shift to upper stories as the number of stories increased. Therefore, it has been demonstrated that weighting factors cannot be associated with a single pattern like uniform, triangular, and nonlinear distribution along the height of the building. The distribution pattern of weighting factors is parabolic, and the shape of the parabola changes with the increasing number of stories.

Table 6.9: Modal Participation Ratio for type P buildings

	P4	P6	P8	P10
Mode 1	**86.437**	**83.078**	**80.646**	**79.08**
Mode 2	**9.541**	**9.756**	**10.056**	**10.3**
Mode 3	2.813	3.639	3.948	**4.30**
Mode 4	0.680	1.867	1.898	1.85
Mode 5		0.931	1.419	1.45
Mode 6		0.274	0.620	0.9
Mode 7			0.739	0.6
Mode 8			0.221	0.40

6.2 Effect of Storey Height

To study the effect of storey height variation in storey-wise damage and weightage distribution, the P6 building is considered with variable storey heights ranging from 3m to 4.5m. Damage contribution is computed at each stage A, B, C, D, and E. The damage contribution at yielding stage A is tabulated in Table 6.10 and indicates that damage started on the same floor in all buildings. Damage contributions at stage B & C as mentioned in Table 6.11 and Table 6.12, highlights similar damage in four stories. It is observed that the damage distribution in stories remains almost the same. Table 6.13 & Table 6.14 present damage at stages D & E, and it is observed that damage distribution remains the same even in later stages of pushover analysis. Therefore, different storey heights in the buildings do not affect the damage distribution and weighting factors.

Table 6.10: Damage contribution at stage A in the P6 building with increasing storey height

Damage	**3m** **0.001%**	**3.5m** **0.001%**	**4m** **0.001%**	**4.5m**
Sixth Storey	-	-	-	-
Fifth Storey	-	-	-	-
Fourth Storey	-	-	-	-
Third Storey	-	-	-	-
Second Storey	0.001	0.001	0.001	0.001
First Storey	-	-	-	-

Table 6.11: Damage contribution at stage B in the P6 building with increasing storey height

Damage	**3m** **3%**	**3.5m** **2.5%**	**4m** **1.7%**	**4.5m** **1.2%**
Sixth Storey	-	-	-	-
Fifth Storey	-	-	-	-
Fourth Storey	0.1	-	-	-
Third Storey	0.8	0.2	0.3	0.1
Second Storey	1.2	1.7	0.8	0.7
First Storey	0.9	0.6	0.6	0.4

Table 6.12: Damage contribution at stage C in the P6 building with increasing storey height

Damage	**3m** **61%**	**3.5m** **64%**	**4m** **62%**	**4.5m** **65%**
Sixth Storey	-	-	-	-
Fifth Storey	-	-	-	-
Fourth Storey	4	2	2	2
Third Storey	13	13	13	12

Second Storey	18	20	21	22
First Storey	26	29	26	29

Table 6.13: Damage contribution at stage D in the P6 building with increasing storey height

Damage	**3m** **83%**	**3.5m** **91%**	**4m** **83%**	**4.5m** **85%**
Sixth Storey	-	-	-	-
Fifth Storey	-	-	-	-
Fourth Storey	4	2	2	2
Third Storey	17	16	16	15
Second Storey	25	33	28	29
First Storey	37	40	37	39

Table 6.14: Damage contribution at stage E in the P6 building with increasing storey height

Damage	**3m** **100%**	**3.5m** **100%**	**4m** **100%**	**4.5m**
Sixth Storey	-	-	-	-
Fifth Storey	-	-	-	-
Fourth Storey	3	2	2	1
Third Storey	21	20	20	18
Second Storey	28	31	31	33
First Storey	47	48	46	47

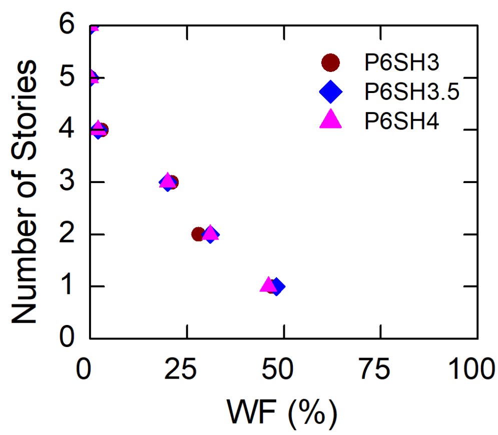

Figure 6.17: Effect of storey height variation on storey weightage in stage E

The same numbers are plotted in Figure 6.17 to study the damage distribution pattern. It is observed that damage distribution in all stories remains the same even if the storey height increases. Therefore, the highest weighted stories and strengthening proposals' conclusions remain the same in different storey heights.

6.3 Summary

The weightage of stories in global damage is computed by calculating the energy dissipated by each member in the storey using the area under the moment rotation curve. The effect of increase in the number of stories and increase in storey height on storey weights is studied in this chapter. Four buildings P4, P6, P8, and P10, are analyzed to study variable axial load on columns by increasing the number of stories. A huge increment in interstorey drift from stage C to stage E in the bottom stories is observed in all buildings. As height increases to P10, along with a huge ISD increment in bottom stories, a small ISD increment is observed in upper stories also (Figure 6.15). Damage distribution is observed in corresponding stories with a parabolic curve. It is observed that with increasing axial load on columns, the shape and extent of parabolic damage distribution keep on changing. For low axial loads, damage distribution observed is a convex parabola with maximum weightage of damage at the first storey, as shown in Figure 6.4. As axial load increased, the convex shape of damage distribution in P4 became similar to the straight line in P6 and P8 (Figure 6.18). As the axial load increased further in P10, the parabola started extending upwards up to eight storey; however, the maximum weightage of damage is still at the bottom-storey (Figure 6.18). Damage distribution started shifting to upper stories. Unlike concave parabolic damage with maxima at mid-height in G10, the parabola in P10 is convex with maxima at the bottom. Precode buildings are code-designed, and beams have huge energy dissipation capacity due to ductile detailing. The damage started shifting to upper stories due to flexible bottom stories and changes in modal participation ratios. However, bottom-storey beams still have capacity left and can contribute to dissipating more energy. Therefore, along with the initiation of damage shift to upper stories, bottom stories also contribute to energy dissipation. This led to huge damage weightage in bottom stories and a little shift of damage to upper stories. Therefore, the convex shape of damage with maxima at the first storey in P10 instead of concave with maxima at mid-height in G10 is observed.

To study the second parameter, i.e., the effect of variable storey height on damage distribution and strengthening proposals, four P6 buildings with storey heights of 3m, 3.5m, 4m, and 4.5m are designed and analyzed. It is observed that the same number of stories are damaged when the storey height of the building is increased. The quantity of the damage remains almost the same. Therefore, damage distribution and the highest weighted storey are not affected by varying storey height of the precode building of IS 1893.

Strengthening is proposed zone-wise based on damage distribution in the building. For studied buildings P4, P6 and P8, irrespective of storey height, stepped strengthening is proposed in zone 1 and shall be done sequentially in regular RC framed structures (Figure 6.4). In P10, strengthening is proposed in both Zone 1 and Zone 2, which shall be done in a sequential manner. If the updated capacity is less than the base shear, a further reduced amount of strengthening shall be done.

Therefore, it is demonstrated that damage distribution can be associated with a single type of distribution in selected precode buildings. It is either a convex parabolic or straight line with maxima at the first storey; however, the upper limit of damage changes with building height. In P4, P6 and P8 buildings, damage distribution is up to one storey above the mid-height of the building and in 10 storey, it extends to 80% height of the building. Strengthening is done in zone 1 in P4, P6 and P8 stories and in zone 1 and zone 2 in P10.

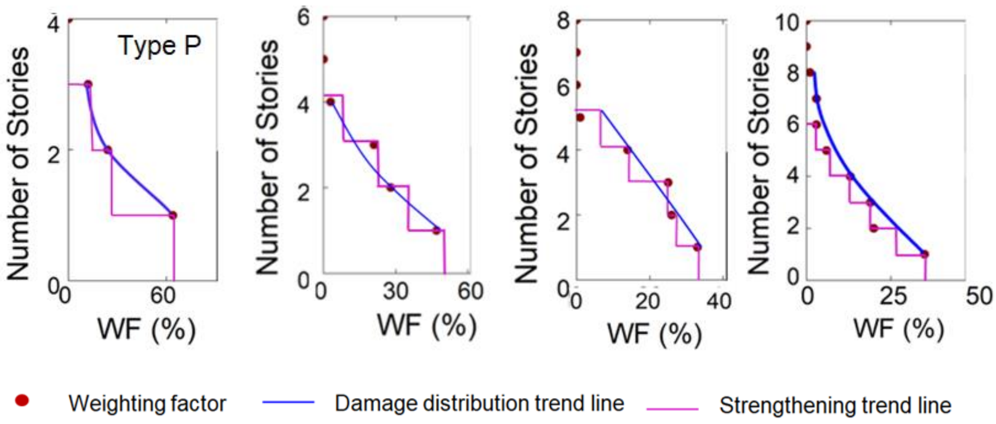

Figure 6.18: Summary of damage weights distribution and proposed strengthening scheme in Type P buildings

7 PROPOSED SEQUENCE OF WEIGHTING FACTORS

A proposal for the sequence of strengthening is made from observations from damage distribution and computed weighting factors at each storey and within each storey among exterior and interior columns. The sequence of strengthening according to decreasing values of weighting factors for Type G and Type P buildings is mentioned in Figure 7.1 and Figure 7.2. Sequence 1 represents the highest weighted member in a building, and sequence 2 represents the members with the next weighted member in descending order. Similarly, all sequence numbers are allotted as per the decreasing weightage. This sequence shall assist in strengthening different types of regular bare-frame RCC MRF buildings. Strengthening shall start with all the members with sequence 1. The updated capacity of the building shall be checked with the base shear requirement in that area. If the updated capacity is less than the base shear, strengthening shall be done at members with sequence number 2. Again, updated capacity shall be compared with the base shear of that area. This shall be repeated until the updated capacity of the building exceeds the base shear requirement in that area.

In Figure 7.1 a), in type G building, all exterior columns are strengthened from bottom to top at once to give a peripheral stiffening, which triggers the redistribution of forces and redirects a significant amount of forces to beams, as seen from NLTH in chapter 3. In the next step, storey-wise strengthening shall start with strengthening the first storey's interior columns and further beams. In subsequent steps, storey-wise strengthening shall continue up to one storey above the mid-height of the building, as concluded in Chapter 5. In Figure 7.1 b) and c), the same sequence starting from exterior column strengthening from bottom to top is proposed, followed by storey-wise strengthening of columns and beams. In the G10 building, since no special significance of exterior columns is concluded, interior and exterior columns are strengthened together, as shown in Figure 7.1 d). As per the conclusions in G10, all stories from the bottom to one storey above the mid-height of the building have the highest weightage. Therefore, all columns up to the sixth storey are strengthened in one step and beams in the second step. Further, storey-wise strengthening of the upper stories shall continue with columns and beams up to 90% of the height of the building.

Due to no special significance of exterior and interior columns and stepped strengthening proposals in precode buildings from the ground up to one storey above the mid-height of the building, strengthening sequences are proposed in Figure 7.2 a), b), and c). Strengthening of exterior and interior columns is done in a single step, and storey-wise weights are followed for the rest of the members. However, in P10, building damage shifted to upper stories in the same pattern;

therefore, a strengthening sequence is proposed up to 90% of the height of the building, as shown in Figure 7.2 d).

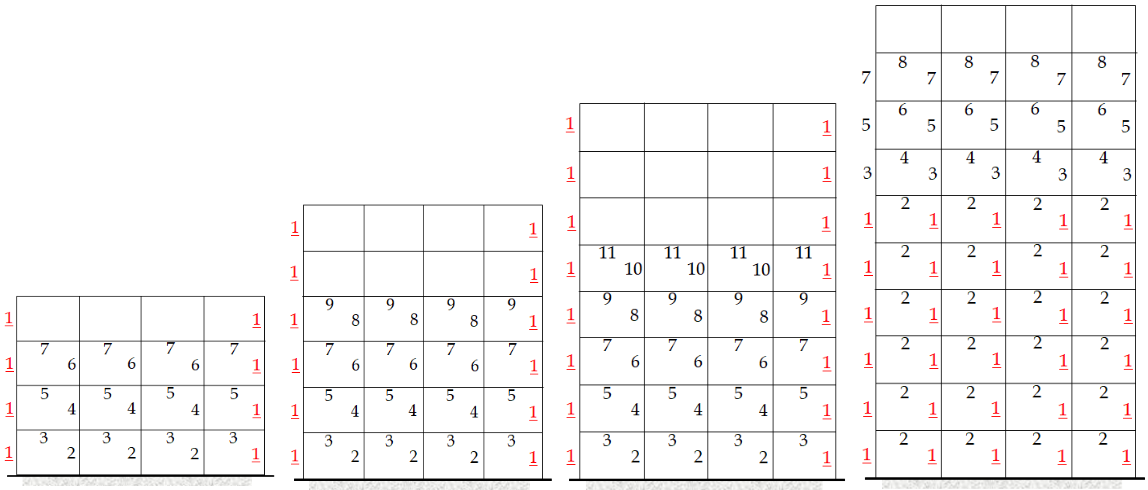

a) G4 b) G6 c) G8 d) G10

Figure 7.1: Proposed strengthening sequences for Type G buildings with storey heights 3m to 4.5m

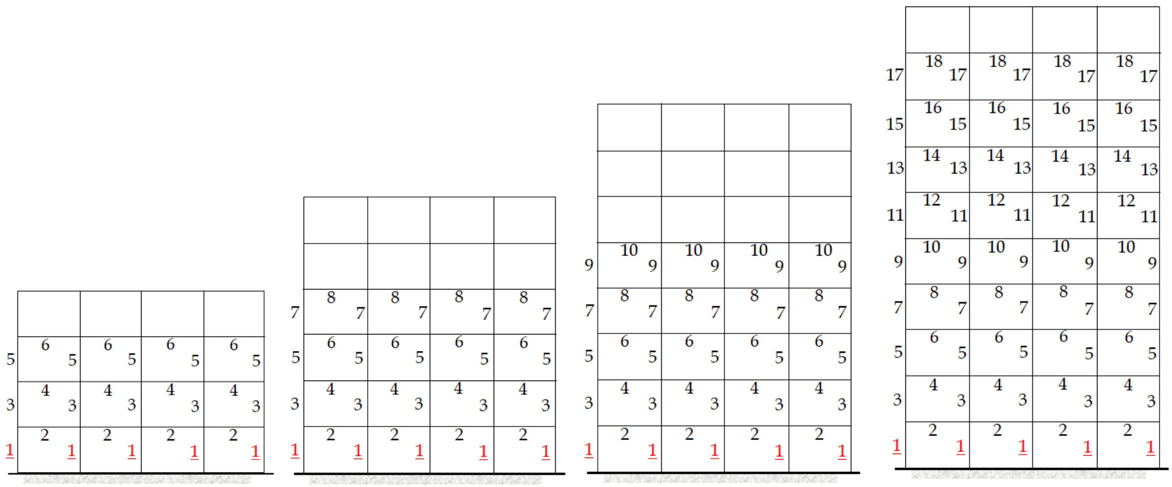

a) P4 b) P6 c) P8 d) P10

Figure 7.2: Proposed strengthening sequences for Type P buildings with storey heights 3m to 4.5m

The sequence of strengthening activities as per the weighting factors in descending order is proposed. After every sequential step of strengthening, base shear shall be compared with the updated capacity curve to check whether further strengthening is required.

8 SUMMARY, CONCLUSION AND FUTURE WORK

8.1 Summary

The literature shows that the Energy Weighting Factor proposed by Park and Ang is good and well-calibrated for Park and Ang local damage index only. However, it does not work well with local energy-based indices. Other weighting factors proposed in the literature are TSWF and GLWF, which are based on triangular-shaped distribution from the bottom to the top of the building, and tributary gravity load has been used with energy-based local indices. However, there are some limitations for example, damage distribution is considered linearly decreasing from bottom to top, and importance of a member as per its location within the storey is assumed.

Therefore, damage weighting factors are computed in this study. Energy models are used to quantify damage on both a local and global scale. Weights have been calculated for gravity load-designed structures, referred to as Type G, and precode buildings of IS 1893, referred to as Type P, using nonlinear static analysis. Exterior and interior column weights and storey weights are computed. Variations of axial load on columns and storey height have been studied to comprehend their impact on weightage distribution.

The study demonstrated that the distribution of weighting factors varies in shape and location along the height of the building as the number of stories increases. The highest weighted stories have been identified in all cases, and based on the observations strengthening solution is proposed. Also, a sequence of members in descending order of weights is proposed to assist in strengthening activities.

8.2 Conclusion

1. In gravity load-designed buildings up to the eighth storey, exterior columns have higher weightage than interior columns, irrespective of storey height. However, in precode buildings of IS 1893, weights are comparable for exterior and interior columns.

2. Damage distribution is parabolic in shape in Type G and Type P buildings. The convex shape of the parabola in low-rise buildings transitions to a straight line as the height of the building increases up to eight stories, with maxima at the first storey and minima at the mid-height of the building. Therefore, the highest weightage is at the first storey in Type P and Type G buildings.

However, in G10, damage propagates to upper stories as a concave parabola with maxima in middle stories. Therefore, the highest weighted stories are all the stories from the bottom till one storey above the mid-height of the building.

Furthermore, in P10, damage propagates to upper stories as a convex parabola with maxima at the first storey and minima at 80% height of the building, where the first storey is the highest weighted storey.

3. Strengthening is proposed zone-wise as per the highest weighted members. Zone 1 covers the first storey up to one storey above the mid-height of the building, and zone 2 includes additional upper stories up to 90% of the building's height. In all buildings of both Type G and P up to eight stories, stepped strengthening is proposed sequentially in Zone 1. In ten-storey buildings where damage propagated to upper stories, strengthening is done in both Zone 1 and Zone 2. In P10, stepped strengthening is done sequentially in both zones. In G10, where concave damage distribution is observed, the same amount of strengthening in Zone 1 is mandatory in a single sequence. Further stepped strengthening is done sequentially in Zone 2. Wherever stepped strengthening is recommended, it must be carried out sequentially following the base shear requirement of that area after every step.

4. Sequence of weighting factors in descending order is proposed in Figure 7.1 and Figure 7.2, which shall assist decision-making in strengthening activities. Strengthening shall start with all members with sequence 1. To determine if the next strengthening sequence is necessary, updated capacity after each strengthening step shall be computed and checked with the base shear of that area.

8.3 Limitations

1. Conclusions are based on the behavior of bare frame regular buildings only.

2. These weightages are for the case when members failed in flexure. If members are shear critical, damage distribution would be very different and hence the weightages and strengthening sequences are subjected to change.

3. As beam column joints are not modelled, they may be the weak links.

8.4 Future Work

1. For recommendations and guidelines regarding strengthening existing regular RCC MRF buildings in Indian Standard codes, further studies are required to convert these findings to generalized parabolic equations for damage distribution. For this, machine learning algorithms can be employed.

2. Damage type from flexure, axial and shear forces may be studied with different concrete grades.

3. Three-dimensional modelling shall be done to distinguish the weights of corner and perimeter columns.

4. The same study shall be done for infill buildings of type G and Type P buildings with storey height and axial load variation.

5. Experimental work can be planned to demonstrate these analytical findings.

9 REFERENCES

Akiyama, H. (1985), *Earthquake-Resistant Limit State Design for Buildings*. University of Tokyo Press, Tokyo, Japan.

Akiyama, H. and Kato, B. (1980), "Energy Concentration of Multi-Story Buildings.", in *The 7th World Conference on Earthquake Engineering*, 553–560.

ASCE/SEI-7-16 (2017), *Minimum Design Loads and Associated Criteria for Buildings and Other Structures*. https://doi.org/10.1007/978-3-540-44822-8_5.

ASCE/SEI 41-17 (2017), *Seismic Evaluation and Retrofit of Existing Buildings*, *Seismic Evaluation and Retrofit of Existing Buildings*. https://doi.org/10.1061/9780784414859.

Banon, H., Biggs, J.M. and Irvine, H.M.A.X. (1980), *Prediction of Seismic Damage in Reinforced Concrete Frames*. Cambridge, U.K.

Bazan, M. and Sasani, M. (2004), "A new damage model for reinforced concrete elements", in *13th World Conf. On Earthquake Engineering*. Vancouver.

Boonmee, C., Rodsin, K. and Sriboonma, K. (2018), "Gravity Load Collapse Behavior of Nonengineered Reinforced Concrete Columns", *Advances in Civil Engineering*. https://doi.org/10.1155/2018/9450978.

Bosco, M., Ghersi, A. and Marino, E.M. (2009), "On the evaluation of seismic response of structures by nonlinear static methods", *Earthquake Engineering & Structural Dynamics*, **38**(13), 1465–1482. https://doi.org/10.1002/eqe.

Bracci, J.M. *et al.* (1989), "Deterministic Model for Seismic Damage Evaluation of Reinforced Concrete Structures", *National Center for Earthquake Engineering Reasearch, NCEER-89-0033* [Preprint].

Caltech (1971), *The San Fernando Earthquake: A report from Caltech's Earthquake Engineers*. http://calteches.library.caltech.edu/2849/1/earthquake.pdf.

Cao, V. V. *et al.* (2014), "A new damage index for reinforced concrete structures", *Earthquake and Structures*, **6**(6), 581–609. https://doi.org/10.12989/eas.2014.6.6.581.

Chung, Y.S., Shinozuka, M. and Meyer, C. (1988), "Automated Seismic Design of Reinforced Concrete Buildings", *National Center for Earthquake Engineering Research, NCEER-88-0024* [Preprint].

CSI (2016), "SAP2000 Integrated Software for Structural Analysis and Design", *Computers and Structures Inc* [Preprint]. Berkeley, California, USA.

Deger, Z.T. and Sutcu, F. (2017), "Evaluation of Earthquake Input Energy Distribution in an RC Building for an Energy-Based Seismic Design Approach", in *16th World Conference on Earthquake Engineering, Santiago, Chile*, 269.

Dhir, P.K., Davis, R. and Sarkar, P. (2018), "Safety Assessment of Gravity Load–Designed Reinforced Concrete–Framed Buildings", *ASCE-ASME Journal of Risk and Uncertainty in Engineering Systems, Part A: Civil Engineering*, **4**(2), 1–10. https://doi.org/10.1061/ajrua6.0000955.

Diaz, S.A. *et al.* (2017), "Energy damage index based on capacity and response spectra", *Engineering Structures*, **152**, 424–436. https://doi.org/10.1016/j.engstruct.2017.09.019.

DiPasquale, E. and Cakmak, A.S. (1987), "Detection of seismic structural damage", *National Center for Earthquake Engineering Research* [Preprint].

Dowell, E.H. (1979), "On Some General Properties of Combined Dynamical Systems", *Joural of Applied Mechanics*, **46**(3), 206–209.

Esper, P. and Tachibana, E. (1998), "Lessons from the Kobe earthquake", *Geological Society Engineering Geology Special Publication*, **15**(October 1998), 105–116. https://doi.org/10.1144/GSL.ENG.1998.015.01.11.

FEMA (2018), *Seismic Performance Assessment of Buildings Volume 1 - Methodology, P-58-1, Federal Emergency Management Agency, Washington, DC*. California. https://doi.org/10.4231/D3ZW18S8N.

Ghobarah, A., Abou-Elfath, H. and Biddah, A. (1999), "Response-based damage assessment of structures", *Earthquake Engineering and Structural Dynamics*, **28**(1), 79–104. https://doi.org/10.1002/(SICI)1096-9845(199901)28:1<79::AID-EQE805>3.0.CO;2-J.

Ghosh, S.K. (1995), "Observations on the performance of structures in the Kobe earthquake of January 17, 1995", *PCI Journal*, **40**(2), 14–22. https://doi.org/10.15554/pcij.03011995.14.22.

Halder, L. and Paul, S. (2016), "Seismic Damage Evaluation of Gravity Load Designed Low Rise RC Building Using Non-linear Static Method", *Procedia Engineering*, **144**, 1373–1380. https://doi.org/10.1016/j.proeng.2016.05.167.

Hall, J.F. (2018), "On the descending branch of the pushover curve for multistory buildings", *Earthquake Engineering and Structural Dynamics*, **47**(3), 772–783. https://doi.org/10.1002/eqe.2990.

Haselton, C.B. and Deierlein, G.G. (2007), "Assessing Seismic Collapse Safety of Modern Reinforced Concrete Moment-Frame Buildings", *PEER Report 2007/08, Pacific Earthquake Engineering Research Centre* [Preprint]. http://myweb.csuchico.edu/~chaselton/Website_Files/Publications/Pub_Dissertation_PEERReport_Haselton.pdf.

Housner, G.W. (1956), "Limit Design of Structures to Resist Earthquakes", in *The 1st World Conf. Of Earthquake Engineering*. Berkeley, California.

Humar, J.M., Lau, D. and Pierre, J.R. (2001), "Performance of buildings during the 2001 Bhuj earthquake", *Canadian Journal of Civil Engineering*, **28**(6), 979–991. https://doi.org/10.1139/l01-070.

Ibarra, L.F. and Krawinkler, H. (2005), "Global Collapse of Frame Structures under Seismic Excitations", *PEER Report 152, John A. Blume Earthquake Engineering Centre*, 1–324.

IITM and SERC (2005), *Seismic evaluation and retrofit of Multi-storeyed RC buildings, Department of Science and Technology*. Chennai, India.

Inel, M. and Ozmen, H.B. (2006), "Effects of plastic hinge properties in nonlinear analysis of reinforced concrete buildings", *Engineering Structures*, **28**(11), 1494–1502. https://doi.org/10.1016/j.engstruct.2006.01.017.

IS 15988:2013 (2013), *Seismic Evaluation and Strengthening of Existing Reinforced Concrete Buildings - Guidelines*. New Delhi, India.

Jain, S.K. (1998), "Indian earthquakes: An overview", *Indian Concrete Journal*, **72**(11), 555–561. https://www.iitk.ac.in/nicee/readings/paper4.pdf.

Jennings, P.C. (1997), "Enduring Lessons and Oppurtunities Lost from the San Fernando Earthquake of February 9, 1971", *Earthquake Spectra*, **13**(1), 25–44.

Jiang, H. *et al.* (2015), "Seismic damage assessment of RC members by a modified Park-Ang model", *Advances in Structural Engineering*, **18**(3), 353–364. https://doi.org/10.1260/1369-4332.18.3.353.

Kayal, J.R. (2008), *Microearthquake Seismology and Seismotectonics of South Asia*. Springer.

Kircher, C.A., Whitman, R. V. and Holmes, W.T. (2006), "HAZUS earthquake loss estimation methods", *Natural Hazards Review*, **7**(2), 45–59. https://doi.org/10.1061/(ASCE)1527-6988(2006)7:2(45).

Kunnath, S.K., Reinhorn, A.M. and Lobo, R.F. (1992), "IDARC Version 3.0: A Program for the Inelastic Damage Analysis of Reinforced Concrete Structures", *National Center For Earthquake Engineering Research Centre, NCEER-92-0022* [Preprint].

Liel, A.B., Haselton, C.B. and Deierlein, G.G. (2011), "Seismic Collapse Safety of Reinforced Concrete Buildings. II: Comparative Assessment of Nonductile and Ductile Moment Frames", *Journal of Structural Engineering*, **137**(4), 492–502. https://doi.org/10.1061/(asce)st.1943-541x.0000275.

Maeda, M. and Kang, D.E. (2009), "Post-earthquake damage evaluation of reinforced concrete buildings", *Journal of Advanced Concrete Technology*, **7**(3), 327–335. https://doi.org/10.3151/jact.7.327.

Mahboubi, S. and Shiravand, M.R. (2019), "Proposed Input Energy-Based Damage Index for RC Bridge Piers", *Journal of Bridge Engineering*, **24**(1). https://doi.org/10.1061/(ASCE)BE.1943-5592.0001326.

Mander, J.B., Priestley, M.J.N. and Park, R. (1983), "Behaviour of Ductile Hollow Reinforced Concrete Columns.", *Bulletin of the New Zealand National Society for Earthquake Engineering*, **16**(4), 273–290. https://doi.org/10.5459/bnzsee.16.4.273-290.

Mander, J.B., Priestley, M.J.N. and Park, R. (1988), "Theoretical Stress-Strain Model for Confined Concrete", *J. Struct. Eng*, **114**(8), 1804–1826.

Massumi, A. and Moshtagh, E. (2013), "A new Damage Index for RC buildings based on variations of nonlinear Fundamental Period", *The Structural Design of Tall and Special Buildings*, **22**, 50–61. https://doi.org/10.1002/tal.

Moinfar, A.A. and Naderzadeh, A. (1990), "An immediate and preliminary report on the manjil, iran earthquake of 20 june 1990", *Bulletin of the New Zealand Society for Earthquake Engineering*, **23**(4), 254–283. https://doi.org/10.5459/bnzsee.23.4.254-283.

Murty, C.V.R. *et al.* (2016), "Twin 2015 Nepal Earthquakes : Concerns toward Earthquake Safety of Buildings", in *6th International Conference on Recent Advances in Geotechnical Earthquake Engineering and Soil Dynamics*, Greater Noida, India.

Newmark, N.M. and Rosenblueth, E. (1974), *Fundamental of Earthquake Engineering*. Prentice Hall.

Niharika, T. and Ramancharla, P.K. (2020), "Performance Assessment of Upper Stories in an Open Ground Storey Building With Retrofitted Ground Storey", in *17th World Conference on Earthquake Engineering, 17WCEE*.

Parisi, F., Scalvenzi, M. and Brunesi, E. (2019), "Performance limit states for progressive collapse analysis of reinforced concrete framed buildings", *Structural Concrete*, **20**(1), 68–84. https://doi.org/10.1002/suco.201800039.

Park, Y.J. and Ang, A.H.-S. (1985), "Mechanistic seismic damage model for reinforced concrete", *Journal of Structural Engineering (United States)*, **111**(4), 722–739.

https://doi.org/10.1061/(ASCE)0733-9445(1985)111:4(722).

Park, Y.J., Ang, A.H.-S. and Wen, Y.K. (1987), "Damage-Limiting Aseismic Design of Buildings.", *Earthquake Spectra*, **3**(1), 1–26. https://doi.org/10.1193/1.1585416.

Pinho, R. *et al.* (2013), "Evaluation of nonlinear static procedures in the assessment of building frames", *Earthquake Spectra*, **29**(4), 1459–1476. https://doi.org/10.1193/100910EQS169M.

Poljanšek, K. and Fajfar, P. (2008), "A New Damage Model for the Seismic Damage Assessment of Reinforced Concrete Frame Structures", in *The 14th World Conference on Earthquake Engineering*. Beijing.

Popov, E.P. (1987), "Observations on the Me Mexico earthquake of 19 September 1985", *Engineering Structures*, **9**(2), 74–83. https://doi.org/10.1016/0141-0296(87)90001-0.

Powell, G.H. and Allahabadi, R. (1988), "Seismic damage prediction by deterministic methods: Concepts and procedures", *Earthquake Engineering & Structural Dynamics*, **16**(5), 719–734. https://doi.org/10.1002/eqe.4290160507.

Rai, D.C. *et al.* (2016), "Reconnaissance of the effects of the M7.8 Gorkha (Nepal) earthquake of April 25, 2015", *Geomatics, Natural Hazards and Risk*, **7**(1), 1–17. https://doi.org/10.1080/19475705.2015.1084955.

Rehman, K. *et al.* (2016), "Analysis of the devastating Kashmir earthquake 2005 aftershocks", *Arabian Journal of Geosciences*, **9**(5). https://doi.org/10.1007/s12517-016-2418-6.

De Risi, M.T. *et al.* (2022), "Modelling and Seismic Response Analysis of Italian pre-code and low-code Reinforced Concrete Buildings. Part I: Bare Frames", *Journal of Earthquake Engineering*, **27**(6), 1–32. https://doi.org/10.1080/13632469.2022.2074919.

Rodrigues, H. *et al.* (2018), "Influence of seismic loading on axial load variation in reinforced concrete columns", *Advances in Civil and Architectural Engineering*, **9**(16), 37–49. https://doi.org/10.13167/2018.16.4.

Rodriguez-Gomez, S. and Cakmak, A.S. (1990), "Evaluation of Seismic Damage Indices For Reinforced Concrete Structures", *National Center for Earthquake Engineering Reasearch, NCEER-90-0022* [Preprint].

Rodriguez, M.E. and Padilla, D. (2009), "A damage index for the seismic analysis of reinforced concrete members", *Journal of Earthquake Engineering*, **13**(3), 364–383. https://doi.org/10.1080/13632460802597893.

Roufaiel, B.M.S.L. and Meyer, C. (1987), "Reliability Of Concrete Frames Damaged By Earthquakes", *Journal of Structural Engineering*, **113**(3), 445–457.

Roy, N. *et al.* (2002), "The Gujarat earthquake (2001) experience in a seismically unprepared area: Community hospital medical response", *Prehospital and Disaster Medicine*, **17**(4), 186–195. https://doi.org/10.1017/S1049023X00000480.

Saatcioglu, M., Ghobarah, A. and Nistor, I. (2005), "Effects of the December 26 , 2004 Sumatra Earthquake and", *ISET Journal of Earthquake Technology*, **42**(457), 79–94.

Santhi, H.M., Samuel Knight, G.M. and Muthumani, K. (2005), "Evaluation of Seismic Performance of Gravity Load Designed Reinforced Concrete Frames", *Journal of Performance of Constructed Facilities*, **19**(4), 277–282.

https://doi.org/10.1061/(asce)0887-3828(2005)19:4(277).

Shiradhonkar, S.R. and Sinha, R. (2017), "A Capacity-Based Global Seismic Damage Index for Reinforced Concrete Frame Buildings", *The 16th World Conference on Earthquake Engineering*, Paper No. 160.

Sreejaya, K.P. *et al.* (2022), "Seismic hazard map of India and neighbouring regions", *Soil Dynamics and Earthquake Engineering*, **163**(August), 107505. https://doi.org/10.1016/j.soildyn.2022.107505.

Surana, M., Singh, Y. and Lang, D.H. (2017), "Seismic Characterization and Vulnerability of Building Stock in Hilly Regions", *Natural Hazards Review*, **19**(1), 1–16. https://doi.org/10.1061/(asce)nh.1527-6996.0000275.

Toksoz, M.N. *et al.* (1999), "Izmit (Turkey) Earthquake of 17 August 1999: First Report", *Seismological Research Letters*, **70**(6), 669–679. https://doi.org/10.1785/gssrl.70.6.669.

Uang, C.-M. and Bertero, V.V. (1988), "Use of energy as a design criterion in earthquake-resistant design", *Earthquake Engineering Research Center*, **88**, 18.

UÇAR, T. and MERTER, O. (2018), "Hysteretic Energy Demand in SDOF Structures Subjected to an Earthquake Excitation: Analytical and Empirical Results", *Journal of Natural and Applied Sciences*, **22**(2), 364–374. https://doi.org/10.19113/sdufbed.84512.

Vimala, A. and Kumar, R.P. (2014), "Expended energy based damage assessment of RC bare frame using nonlinear pushover analysis", in *Urban Safety of Mega Cities in Asia*, 47–56.

Wang, M.L. and Shah, S.P. (1987), "Reinforced concrete hysteresis model based in damage concept", *Earthquake Engineering and Structural Dyanmics*, **15**(8), 993–1003.

Yunfei, H. *et al.* (1986), "The Experimental Study of a Two-Bay Three Story Reinforced Concrete Frame Under Cyclic Loading", in *Proceedings of the 8 th Symposium on Earthquake Engineering, Roorkee, India*.

Zhao, B., Taucer, F. and Rossetto, T. (2009), "Field investigation on the performance of building structures during the 12 May 2008 Wenchuan earthquake in China", *Engineering Structures*, **31**(8), 1707–1723. https://doi.org/10.1016/j.engstruct.2009.02.039.